111-[illegible]
33579
p 133

NASA Contractor Report 187575

# EFFECT OF THERMAL EXPOSURE, FORMING, AND WELDING ON HIGH-TEMPERATURE, DISPERSION-STRENGTHENED ALUMINUM ALLOY: Al-8Fe-1V-2Si

J.R. Kennedy

GRUMMAN CORPORATE RESEARCH CENTER
Bethpage, New York

Contract NAS1-18533 Extension
August 1991

([illegible]) [illegible] THERMAL
[illegible], FORMING, AND WELDING ON
HIGH-TEMPERATURE, [illegible]-STRENGTHENED
ALUMINUM ALLOY: Al-[illegible]-1V-2Si Final Report,
May [illegible] - Jun. 1991 (Grumman Aerospace
N91-[illegible]
Unclas
G3/26 [illegible]

National Aeronautics and
Space Administration

Langley Research Center
Hampton, Virginia 23665-5225

**Report RE-787**

# Effect of Thermal Exposure, Forming, and Welding on High-Temperature, Dispersion-Strengthened Aluminum Alloy: Al-8Fe-1V-2Si

**August 1991**

by

J.R. Kennedy

Grumman Corporate Research Center
Bethpage, New York 11714-3580

Final Report on
Contract NAS1-18533 Extension

for

National Aeronautics and Space Administration
Langley Research Center
Hampton, VA 23665-5225

NASA Contractor Report 187575

Approved by: Richard DeIasi
Richard DeIasi, Director
Corporate Research Center

THIS PAGE INTENTIONALLY LEFT BLANK

# PREFACE

This technical report covers the work performed under Contract NAS1-18533. This research was funded by the Langley Research Center of the National Aeronautics and Space Administration (NASA), Hampton, VA. The program was conducted under the technical direction of Mr. Dick Royster of the Metallic Materials Branch in the Materials Division of the NASA Langley Research Center.

The work presented here was performed during the period May 1989 to June 1991 by Grumman Corporation (Bethpage, NY) and the Allied-Signal Corporation (Morristown, NJ).

The materials fabrication and degassing operations were performed by the Alloy Development group of the Metals and Ceramics Laboratory within the Corporate Technology section of Allied-Signal Inc. The evaluation of the effects of thermal exposure on mechanical properties, forming, and welding was performed by the Structural Materials group of the Grumman Corporate Research Center.

Program Principal Investigator: Mr. J. Kennedy (Initially Dr. E. Ting)
MS: A02-26
Grumman Corporate Research Center
Bethpage, New York 11714

Allied-Signal Principal Investigator:.................................. Dr. P. S. Gilman
Allied-Signal Co-investigators:............................................ Dr. M. S. Zedalis, Dr. D.J. Skinner and Dr. J. M. Peltier

Contributors (Allied-Signal):............................................. M. Rodriguez, J. Gleason, C. Calderone, A. Testa and D. Timan

Contributors (Grumman):
  Corporate Research Center:............................................. Dr. P. Adler, H. Baker, G. Busch, J.Dinkel, Dr. E. Ting and T.Williams, Jr.
  Engineering - Structural Sciences:................................. R. Friedman
  Test and Evaluation - Structural Test:............................ R. Schwarz
  Manufacturing Technology-Materials Engineering....... A. Sinowitz, A. Rava
  Manufacturing Engineering - Forming:........................... S. Maria, L. Morgan, J. Newman
  Manufacturing - Welding Engineering:............................ P. Dent, R. Simonds, W. Sisco
  Manufacturing Engineering - Mechanical Fastening:.... J. Fusco, D. Noonan, R. Bellew

THIS PAGE INTENTIONALLY LEFT BLANK

# ABSTRACT

The feasibility of applying conventional hot forming and welding methods to high-temperature aluminum alloy, Al-8Fe-1V-2Si (FVS812), for structural applications and the effect of thermal exposure on mechanical properties were determined. FVS812 (AA8009) sheet exhibited good hot forming and resistance welding characteristics. It was brake formed to 90° bends (0.5T bend radius) at temperatures ≥390°C (730°F), thus indicating the feasibility of fabricating basic shapes, such as angles and zees. Hot forming of simple contoured-flanged parts was demonstrated. Resistance spot welds with good static and fatigue strength at room and elevated temperatures were readily produced. Extended vacuum degassing during billet fabrication reduced porosity in fusion and resistance welds. However, electron beam welding was not possible because of extreme degassing during welding, and gas-tungsten-arc welds were not acceptable because of severely degraded mechanical properties. The FVS812 alloy exhibited excellent high-temperature strength stability after thermal exposures up to 315°C (600°F) for 1000 h. Extended billet degassing appeared to generally improve tensile ductility, fatigue strength, and notch toughness. But the effects of billet degassing and thermal exposure on properties need to be further clarified. The manufacture of zee-stiffened, riveted, and resistance-spot-welded compression panels was demonstrated.

THIS PAGE INTENTIONALLY LEFT BLANK

# CONTENTS

PRECEDING PAGE BLANK NOT FILMED

THIS PAGE INTENTIONALLY LEFT BLANK

## ILLUSTRATIONS

## ILLUSTRATIONS

ILLUSTRATIONS

# ILLUSTRATIONS

# TABLES

# TABLES

## 1. INTRODUCTION

The newly emerging dispersion-strengthened, high temperature aluminum (HTA) alloys have great potential for application to the development of advanced aerospace vehicles (1, 2, 3, 4, 5). Although conventional aluminum alloys have excellent strength-to-weight ratios, they are restricted to a maximum service temperature of less than 180°C (356°F) because of limited thermal stability. The Al-Fe-V-Si alloys derive their strength from the interaction of dislocations and an intermetallic dispersoid strengthening phase formed during rapid solidification, and are thermally stable up to approximately 400°C (752°F). Combined with compatible, low cost forming and joining fabrication methods, HTA alloys could double the useful temperature range of conventional aluminum alloys and, given their low density, could compete with titanium alloys for advanced design applications up to 150-300°C (300 to 600°F). However, since these alloys are susceptible to dispersoid coarsening during exposure to temperatures ≥ 500°C (930°F), the choice of fabrication method will be dictated by its effect on dispersoid stability. Thus, the effect of thermal exposure on dispersoid stability and mechanical properties are critical issues.

The overall objective of this research was to evaluate the feasibility of applying advanced and conventional forming and joining methods to rapidly solidified, dispersion-strengthened Al-Fe-V-Si alloys for elevated temperature applications. Previously, it was demonstrated that these alloys could not be superplastically formed and that diffusion bonding was possible only at temperatures ≥ 600°C (1112°F), where rapid dispersoid coarsening led to degraded mechanical properties (6). A summary of that work is presented in the Background Section of this report. The objective of the current work was to evaluate conventional hot forming and welding methods for application to the Al-Fe-V-Si alloy system. The FVS812 alloy, Al-8Fe-1V-2Si (AA8009) was selected for this purpose. This work establishes basic forming and joining parameters, determines their effects on mechanical behavior, and determines the effect of thermal exposure on material behavior.

THIS PAGE INTENTIONALLY LEFT BLANK

## 2. PROGRAM PLAN

### 2.1 ALLOY SELECTION

The Allied FVS812 (AA8009) alloy, with 27 % volume fraction of dispersoids, was selected for the mechanical property, forming, and welding studies in this work. It is the most developed alloy within the Al-Fe-V-Si system and represents an excellent combination of strength, ductility, stiffness and toughness. The alloy was fabricated using the rapid solidification approach developed at Allied-Signal. Fabrication included vacuum hot-degassing, extrusion, and hot rolling into sheet. Two conditions representing different levels of degassing were produced and the effect of time and temperature on degassing were determined.

### 2.2 MECHANICAL PROPERTIES

Mechanical property baseline data for FVS812 (AA8009) sheet were determined using conventional tests at selected temperatures and times. Material was subjected to various thermal exposure conditions before and during testing which included: uniaxial tension and compression, baseline stress-life (S-N) fatigue behavior, and Kahn notch toughness. The effect of vacuum degassing, strain rate, and welding were evaluated. Thermal exposure included 100 and 1000 h at 200°C (400°F) and 315°C (600°F).

### 2.3 FORMING

Since the high strength and relatively low ductility of FVS 812 (AA8009) seriously limits cold formability, hot forming studies were conducted at temperatures up to 500°C (930°F). Forming conditions to establish processing parameters for fabricating simple shapes, such as angles, zees and channels, were identified by conducting bend tests at room and elevated temperatures to determine minimum bend radii and springback characteristics. The ability to hot form complex parts was explored. The effect of moderate temperature forming cycles on dispersoid stability and final mechanical properties was determined by microstructural observation and mechanical testing.

### 2.4 JOINING

The weldability of Al-Fe-V-Si alloys depends on gas evolution and dispersoid stability during welding. Therefore, the effect of contaminants on welding behavior was investigated for two billet degas conditions, representing standard and extended vacuum degassing treatments. The effect of weld thermal exposure on coarsening or melting of the strengthening dispersoids during welding was determined for electron beam (EB) welding, gas-tungsten-arc (GTA) and resistance spot welding (RSW). Resistance spot welding is of interest for non-fatigue critical applications for the Advanced Launch System and High Speed Civilian Transport programs. This work explored the weldability of FVS812 (AA8009) and established baseline joint design parameters. The extent of property degradation as a result of such temperature exposures was characterized.

## 2.5 COMPONENT DEMONSTRATION

The fabrication of two zee-stiffened FVS812 alloy compression panels (one riveted and the other resistance spotwelded) was demonstrated. These panels, along with a baseline 2024 aluminum alloy panel, will be tested at room temperature at NASA LaRC.

## 3. BACKGROUND

This section of work (under Contract NAS1-18533) was performed during the period from November 1987 to March 1989 at the Grumman Corporate Research Center, Bethpage, NY and the Allied-Signal Corporate Technology Center, Morristown, NJ (6). The objective was to investigate the SPF and DB behavior of the Al-Fe-V-Si alloy system and to evaluate the effect of such processing on microstructure and mechanical properties. The effects of dispersoid volume fraction, dispersoid size, elevated temperature exposure, deformation rate, and bonding pressure were evaluated. Significant results and conclusions of that work are summarized below.

Alloy designations and dispersoid volume fractions are as follows: FVS301 (8%), FVS611 (16%), FVS812 (27%), FVS1212 (36%).

### 3.1 ALLOY AND MICROSTRUCTURE

The Al-Fe-V-Si system of dispersion-strengthened alloys derive their strength from the interaction of insoluble particles and dislocations and are based on the formation of ternary and/or quaternary intermetallics with a symmetrical lattice (7, 8, 9, 10). The intermetallic dispersoid phase that strengthens the Al-Fe-V-Si alloys has a general composition close to Al13(Fe,V)3Si (11) and has significantly more thermal stability than the precipitates found in conventional age-hardening aluminum alloys.

Typically, the ultra-fine grain size systematically decreased with increasing dispersoid volume fraction. Grain size ranged from 1.25 μm for alloy FVS301 to about 0.3 μm for FVS1212. After hot rolling, grain size was not significantly different from that of the extrusion, suggesting that the dispersoids were very effective at pinning grain boundaries. The dispersoids consisted of fine $Al_{13}$ $(Fe,V)_3Si$ particles. In the as-extruded condition, the dispersoids were under 50 nm and size-independent of volume fraction. In the higher volume fraction alloys, the dispersoids tended to be positioned at grain and/or subgrain boundaries. In the sheet condition, dispersoid size increased due to rolling, most notably in low dispersoid volume fraction alloys. An increase in dispersoid size will ultimately reduce mechanical strength due to reduced dislocation interaction. In general, the maximum dispersoid size achieved after rolling was approximately less than 100 nm.

### 3.2 MECHANICAL PROPERTIES

In the extruded alloys, tensile strength increased and ductility decreased with increasing dispersoid content. A minimum in elongation at intermediate temperatures (150°C (302°F)) is attributed to solute drag(11). In sheet form, room temperature tensile strength decreased with rolling temperature and increased with dispersoid content, as shown in Table 1. When tested at 200 and 315°C (392 and 600°F), the higher dispersoid volume fraction alloys result in relatively higher strengths and lower elongations. These alloys do not exhibit significant strain hardening, but, instead, the engineering stress gradually decreases as a result of localized necking preceding failure. There was essentially no effect of a 120 h exposure at 400°C (750°F) on the properties of any of the extruded alloys. FVS0812 exhibits insignificant variations in tensile properties following 120 h or 504 h at 400°C (750°F ) and 120 h at 455°C (850°F). Following 120 h at 510°C (950°F) the yield and tensile strengths of FVS0812 have been reduced by almost 10% and the elongation by nearly 50%. The modulus of the alloys increased with dispersoid volume fraction, but not linearly. The modulus for FVS812 was 12.3 mpsi (85 GPa). Fatigue crack growth rates for extruded FVS0611 and FVS0812 in the L-T and T-L orientation appear to be comparable. Fracture toughness is higher in the L-T orientation for the FVS611 (16 v/o) and FVS0812 (27 v/o) extrusions. The lower T-L toughness is associated with prior particle boundaries from the powder metallurgy fabrication process(12).

**Table 1 Average Room Temperature Tensile Strength (Long.) of Al-Fe-V-Si Sheet as a Function of Rolling Temperature**

| Alloy/°C (°F) | Strength 0.2 Yield MPa(ksi) | UTS MPa(ksi) | Elong. % |
|---|---|---|---|
| FVS301/300(572) | 172 (25.0) | 203 (29.5) | 19.1 |
| FVS301/400(752) | 133 (19.3) | 180( 26.1) | 27.0 |
| FVS301/500(932) | 104 (15.1) | 148 (21.5) | 30.7 |
| FVS611/300(572) | 298 (41.9) | 317 (45.9) | 17.6 |
| FVS611/400(752) | 212 (30.7) | 248 (36.0) | 9.5 |
| FVS611/500(932) | 116 (16.8) | 181 (26.2) | 27.7 |
| FVS812/300(572) | 430 (62.4) | 454 (65.8) | 13.3 |
| FVS812/400(752) | 392 (56.8) | 416 (60.3) | 17.4 |
| FVS812/500(932) | 271 (39.3) | 342 (49.6) | 18.0 |
| FVS1212/300(572) | 500 (72.5) | 530 (76.9) | 9.4 |
| FVS1212/400(752) | 482 (69.9) | 503 (73.0) | 12.1 |
| FVS1212/500(932) | 413 (59.9) | 448 (65.0) | 13.3 |

### 3.3 SUPERPLASTIC EVALUATION

Superplastic deformation of the Al-Fe-V-Si alloys was not possible due to effective pinning of grain boundaries by dispersoids. Overall, the Al-Fe-V-Si alloys showed little or no strain rate sensitivity at strain rates between $1x10^{-6}$ and 0.10 $s^{-1}$ at temperatures under approximately 550°C (1022°F). At strain rate sensitivity (m) values significantly less than 0.3, the Al-Fe-V-Si alloys can not be considered superplastic. Elongations after deformation at 500 and 600°C (932 and 1112°F) under the slow strain rates ($<2x10^{-3}s^{-1}$) were approximately 40% or less. There was little change in grain size but dispersoid coursening was observed, as discussed below. Localized superplasticity was observed in the form of fine ligaments at the fracture surface, which suggested deformation according to the core and mantle mechanism (13). Failure at very low strain rates is likely due to diffusion controlled void formation (cavitation).

Higher strain rates ($> 2x10^{-3}$ $s^{-1}$) resulted in significant increases in elongation (up to 325 % at temperatures ≈ 600°C (1112°F). At these temperatures, the effect of dispersoids was less significant, as deformation became more matrix diffusion controlled. This suggests that thermally induced dislocation climb through vacancy diffusion is operative (14). At temperatures ≤ 600°C (1112°F), however, strain rate had very little effect on strength and elongation. The alloys exhibited a small strain rate sensitivity at temperatures ≈ 600°C (1112°F) under strain rates between 0.01 and 0.10 s-1 . The highest average m value was approximately 0.13.

At temperatures ≥ 600°C (1112°F), rapid coarsening of the dispersoids and their transformation to primary $Al_3Fe$ resulted in significant degradation of mechanical properties. Furthermore, the coarsening was amplified by strain during the deformation process. At temperatures below 500°C (932°F), strain-enhanced coarsening was also observed to a lesser degree. Non-strain induced coarsening was significantly less at 500°C (932°F) as compared to 600°C (1112°F). After deformation at temperatures above 500°C (932°F) there was no increase in grain size, and, in some cases, a reduction, which.may be indicative of recrystallization during deformation. Grain size in the deformed samples was very similar to the as-received grain size. Deformation at 600°C (1112°F) resulted in more strain enhanced coarsening of the dispersoid phase in the region nearer the break than in the region away from the break, where the particles were similar to the as-received size. Also, coarse, needle-like $Al_3Fe$ particles formed in the matrix as a result of thermal exposure during deformation.

The presence of these needles and/or excessively coarse silicide dispersoids will severely degrade the material's mechanical properties. The properties of the Al-Fe-V-Si alloys can be retained only if the microstructure of the alloys can be preserved during thermomechanical processing. Generally, tensile properties are not degraded after short exposures at 500°C (932°F) up to 4 h.

## 3.4 DIFFUSION BONDING EVALUATION

Bonding was not achieved in any of the Al-Fe-V-Si alloys at temperatures below 600°C (1112°F) and pressures up to 6.9 MPa (1000 psi). They require a homologous temperature greater than 0.95 for bonding, which is similar to 7475 Al alloy. For the creep resistant Al-Fe-V-Si alloys, very high temperatures are required to reduce the "flow" stress to a level that is compatible with conventional gas pressure diffusion bonding. At these temperatures, the accompanying coarsening of strengthening dispersoids and resultant losses in the properties are unfortunate by-products.

Diffusion bonding of the Al-Fe-V-Si alloys was possible at temperatures at or above 600°C (1112°F), but significant reduction in the alloy strength occurred due to rapid coarsening of the dispersoids and the formation of large needle-like $Al_3Fe$ particles. Microscopic examination indicated that the dispersoids are thermally stable up to a homologous temperature of 0.75 or approximately 500°C (932°F). Once significantly coarsened, the shear strength of the diffusion bonds was mainly determined by the matrix strength which was 69-103 MPa (10-15 ksi).

Dissimilar diffusion bonds between the Al-Fe-V-Si alloys and fine-grained, superplastic 7475 aluminum alloy were produced at 516°C (960°F) for short times and low pressures. Bonds with shear strengths up to 90% that of the Al-Fe-V-Si base metals were attained. The excellent dissimilar bonds were limited by lower than expected base metal shear strength and compositional gradients due to interfacial diffusion. The fine grain size of the Al-Fe-V-Si alloys enhanced diffusion bonding by reducing bonding time and pressure.

# 4. EXPERIMENTAL PROCEDURE

## 4.1 ALLOY PRODUCTION

Allied-Signal Inc., as a subcontractor to Grumman, supplied the high-temperature aluminum alloy FVS812 (new designation: AA 8009) as nominally 1.6 mm x 610 mm x 1219 mm (0.063 in. x 24 in. x 48 in.) wide sheet produced under:

- Standard commercial conditions
- Extended degassing sequence for the purpose of reducing the hydrogen level in the material in order to improve the weldability of the alloy.

FVS812, which has 27 volume percent of silicide dispersoids, was rapidly solidified using planar flow casting and ribbon comminution technology developed at Allied-Signal. FVS signifies the iron (Fe), vanadium (V), and silicon (Si) components; the digit(s) representing the approximate weight percent (rounded to an integer) of Fe, V, and Si in the alloy respectively. The following is a summary of the processing and fabrication of the sheet material supplied in this program.

***<u>Rapid Solidification</u>***. The alloy was solidified at cooling rates in excess of 106K $s^{-1}$ using the planar flow casting technique, which produces ribbon approximately 5 cm (2 in.) wide and 25 μm thick. The ribbons were then comminuted into -60 mesh (<250 μm) powder prior to being vacuum hot pressed into 11.5 cm (4.5 in.) diameter billets.

For Lot No. 89A096, 89A110 and 89A115 billets, the FVS812 (AA8009) powder-planar-flow casting was produced in the laboratory-size 4.5 kg (100 lb.) batch caster which produced all of the FVS812 alloy that was commercially supplied prior to January 1990. The material produced for these billets met the stringent chemistry requirements established through the commercial programs.

For the latter Lot No. 90A335 and 90A340 billets, the powder-planar flow casting was produced in the Allied High Temperature Aluminum Plant's 45 kg (1000 lb.) caster from which all FVS812 (AA 8009) is now cast. The casting conditions employed in the large caster are essentially identical to those used in the laboratory caster. The main difference is the larger batch size and the establishment of improved quality requirements of the cast material which assures a more consistent product. This accounts for the better uniformity in properties of sheet produced from these billets. The chemical compositions for each lot of material are summarized in Table 2. The high oxygen content measured in Lot No. 90A340 is most likely due to small leak in the system during degassing, which resulted in increased hydration of the aluminum powder and subsequently, higher hydrogen and oxygen after consolidation.

**Table 2 Chemical Composition of Experimental FVS 812 Alloys**

| | | Composition (weight %) | | | | |
|---|---|---|---|---|---|---|
| Alloy-Lot# | Degas Time, h | Al | Fe | Si | V | O |
| 89A96 | 2 | 88.3 | 8.6 | 1.8 | 1.3 | 0.112 |
| 89A110 | 2 | 88.4 | 8.5 | 1.8 | 1.3 | 0.157 |
| 89A115 | 20 | 88.3 | 8.6 | 1.8 | 1.3 | 0.139 |
| 90A335 | 2 | 88.2 | 8.6 | 1.8 | 1.4 | 0.107 |
| 90A340 | 20 | 88.6 | 8.4 | 1.8 | 1.2 | 0.386 |

Degas time: 1.5 h nominally referred to as 2 h in this report.

***Billet Production***. All of the down stream processing of the billets was identical except that the powder for billets 89A115 and 90A340 were degassed for 20 hours rather than the standard 1.5 hours (nominally referred to as 2 h degas in this report).

The degassing and vacuum hot pressing parameters are summarized in Table 3. The differences in vacuum pressures during degassing are indicative of system leaks . Since temperature and time are held constant during the degassing cycle , the differences in vacuum pressure reflect how well the system was sealed for a particular batch. Based on these results and internal studies at Allied-Signal, modifications to vacuum seals and standard operation practice have resulted in improved typical vacuum levels at which degassing is performed. Currently, the typical vacuum is about $1\times10^{-6}$ torr and hydrogen levels in standard degassed material are about 2.3 ppm (15).

After degassing treatments, hydrogen concentrations were measured by LECO Corporation using a Model RH402 Hydrogen Analyzer. A clean five gram pin sample, 8.5 mm (0.335 in.) x sheet thickness, was heated in vacuum at 60% full power for approximately 15 s. Hydrogen content was determined by integrating the signal over 100 seconds. The amount of hydrogen measured in this step is termed "surface hydrogen", since the heating cycle raises the temperature of the sample but does not result in melting. The exact temperature reached by the sample is not known. Once surface hydrogen was determined, the sample was then melted by applying higher power. The sample was held in the molten state for approximately 60 s and "bulk hydrogen" was determined by integrating the signal over 100 seconds. "Total hydrogen" is the combination of surface and bulk hydrogen levels. Hydrogen levels for FVS812 alloys are summarized in Table 4.

**Table 3 FVS812 Alloy Billet Processing Data**

| Billet I.D.# | Billet Dimensions Dia., cm (in) | L, cm (in) | Wt., kg (lb) | Degas Time, h | Degas Vacuum, torr | Extrusion Temp., °C (°F) |
|---|---|---|---|---|---|---|
| 90A335 | 25(10.0) | 41 (16.4) | 58 (127) | 1.5 | 2x10-4 | 416 (717) |
| 90A340 | 25(10.0) | 43 (17.0) | 61 (134) | 20 | 1.5x10-4 | 416 (717) |
| 89A115 | 25 (10.0) | 42 (16.8) | 59 (129) | 20 | 2.2x10-6 | 416 (717) |
| 89A096 | 27 (10.8) | 39 (15.6) | 61 (134) | 1.5 | 3x10-4 | 427 (737) |
| 89A110 | 25 (10.0) | 42 (16.8) | 58 (128) | 1.5 | 1x10-3 | 427 (737) |

Degas temp.: 350°C (662°F)
Degas time:1.5 h nominally referred to as 2 h in this report.
Rolling temp.: 343°C (645°F)
Extrusion Size: 4 x 20 cm (1.6 x 7.9 in.)
Extruded at International Light Metals, Torrance, CA

***Extrusion***. All of the billets were extruded at International Light Metals, Torrance, CA. They were extruded from nominally 26 cm (10.25 in.) diameter, the size of the extrusion liner, to a 44 mm x 203 mm (1.75 in. x 8 in.) rectangular cross section, an extrusion ration of 5.9:1. The extrusions from billets 89A096, 89A110 and 89A115 were improperly lubricated, which caused a loss of material available to be hot rolled. This is the reason that billets 90A335 and 90A340 were added to the program.

**Table 4 Hydrogen Levels for FVS812 Alloys**

| Alloy-Lot# | Degas Time,h | Hydrogen Content (wppm) Surface | Bulk | Total |
|---|---|---|---|---|
| 89A96 | 2 | 0.3 | 3.0 | 3.3 |
| 89A115 | 20 | 0.2 | 2.4 | 2.6 |
| 90A335 | 2 | 0.2 | 2.4 | 2.8 |
| 90A340 | 20 | 0.2 | 5.7 | 5.9 |

***Hot Rolling***. All of the hot rolling was performed at the Kaiser Center for Technology, Pleasanton, CA. Five heats of the alloy were produced, which represented a standard degas time of 1.5-h (nominal 2 h) and an extended degas time of 20 h. FVS 812 processing data is presented in Table 3. The extruded billets were sectioned to lengths up to 64 cm (25 in.) long. Pieces that were less than 64 cm (25 in.) long were longitudinally hot rolled to approximately 64 cm (25 in.) long. All of the pre-forms were then crossed-rolled to a thickness of 1.6 mm (0.063 in.). The rolling preforms were preheated to 343°C (650°F) prior to hot rolling. The pieces were deformed approximately 15% per pass and were reheated after each pass to keep the temperature as constant as possible. Graphite lubrication was used during rolling. When the correct thickness was achieved, the hot rolled sheets were sheared to the final dimensions, 1.6 mm x 610 mm x 1219 mm (0.063 in x 24 in. x 48 in.), prior to shipment to Grumman.

In general the surface quality of the sheet was good, but the overall flatness was poor and varied due to the use of a small rolling mill. The sheets were considered to be excessively wavy such as to require a flattening heat treatment procedure prior to fabrication of the zee-stiffened compression test panels. This is an area in need of further improvement.

### 4.2 MICROSTRUCTURE EXAMINATION

Light microscopy samples were mechanically polished to a one micron finish and etched in Keller's reagent prior to examination on a Leitz MM6 metallograph. Hardness measurements were made using conventional Wilson/Rockwell (Rb) or Wilson/Knoop testing machines. Scanning electron microscopy with energy dispersive x-ray spectrography (SEM/EDAX) analysis was performed on an Amray 1000 scanning electron microscope.

### 4.3 MECHANICAL TESTING

***Tensile***. Tensile tests were performed on samples prepared from rolled 89A096, 89A115, 90A335, and 90A340 (Lot No. 96, 115, 335 and 340) aluminum alloy sheet, according to ASTM Specification B557, E8 and E21. Baseline data was obtained from 2219-T62, and 2024-T81 aluminum alloy sheet loaded in the longitudinal, L, direction. Tests on the high temperature aluminum alloys were conducted in the longitudinal, L, and transverse, T, directions. The effects of thermal exposure on FVS 812 were investigated by heating samples at 200°C and 315°C, and for 100 and 1000 hours. The tensile test specimen geometry conformed to ASTM B557 and E8 for subsize tensile specimens (Fig. 1). Tensile properties were obtained for these materials in air at room temperature, and at 315°C in air using an ATS Series 3210 oven.

Tensile tests were performed on an MTS Model 810 servo-hydraulic material test system. Analog and digital load/strain data were obtained for each sample. Load was measured using a calibrated 89 kN (20 kip) load cell and strain was measured with a calibrated 12.7 mm (0.5 in.) gage length extensometer. During room temperature testing, the strain extensometer was attached directly to the test specimens, and at elevated temperature a sliding extension fixture to locate the extensometer out of the heated zone was used in conjunction with the ATS Series 3210 oven. The analog data was recorded on a

Houston Instruments Model 2000 X-Y Recorder. Digital data from the MTS Model 458 Controller was recorded and processed on a Wells American computer through an MTS Model 459.16 interface. Unless specified, a strain rate of 0.001 inches per inch per second was used. Strain rates as high as 10 inches per inch per second were used on selected samples. Typically, two tests per condition were conducted.

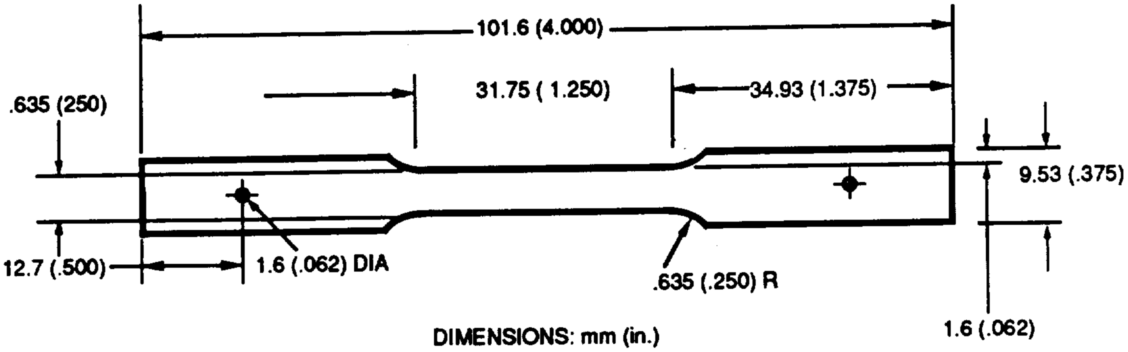

Fig. 1 Subsize Tensile Specimen

**Compression.** Test coupons, 1.6 mm (0.063 in.) by 16 mm (0.625 in.) by 66 mm (2.6 in.) in size, were machined for compression testing. The specimens were installed in a Montgomery-Templin compression jig and the tests were conducted at room temperature, as per ASTM E9-81, "Compression Testing of Metallic Materials at Room Temperature" using a 60 KIP Tinius Olsen Electro-Matic universal testing machine in conjunction with two MTS extensometers.

**Toughness (Kahn Tear Test).** Kahn Tear tests were performed on samples prepared from rolled 89A096 (Lot 96) and 89A115 (Lot 115) aluminum alloy sheet, in accordance with established practices (16, 17, 18). Baseline data was determined from 2219-T62 and 2024-T81 aluminum alloy sheet. Test specimens were prepared with the rolling direction either parallel to the load (L-T) or normal to the load (T-L). The effect of thermal exposure was investigated by heating samples at 200°C and 315°C in air for 100 and 1000 hours. The test specimens conformed to the geometry shown in Fig. 2.

The Kahn Tear tests were performed under ambient conditions at room temperature on an MTS Model 943-80 servohydraulic test system. Analog and digital load/displacement data was obtained for each sample. The analog data was recorded on a Houston Instruments Model 2000 X-Y Recorder. The digital data was acquired at 0.2 second intervals through the MTS system. All tests were conducted at a constant crosshead speed of 2.5 mm/min. (0.1 inches/minute) and utilized the 12.7 mm (0.5 in.) displacement range. The tests were considered complete at 12.7 mm (0.5 in.) crosshead displacement (Note: at 12.7 mm displacement the residual tensile load was less than 5 lbs force although most test specimens had not completely parted). A Gaertner 20X microscope was set up on the test machine to view crack initiation, and a mark was placed on the analog record at the point at which crack was first observed. This mark was used to verify crack initiation displacement during post test processing to calculate crack initiation energy and crack propagation energy. Crack initiation energy and crack propagation energy were calculated by integrating the numerical data from start to crack initiation, and from crack initiation to test completion respectively.

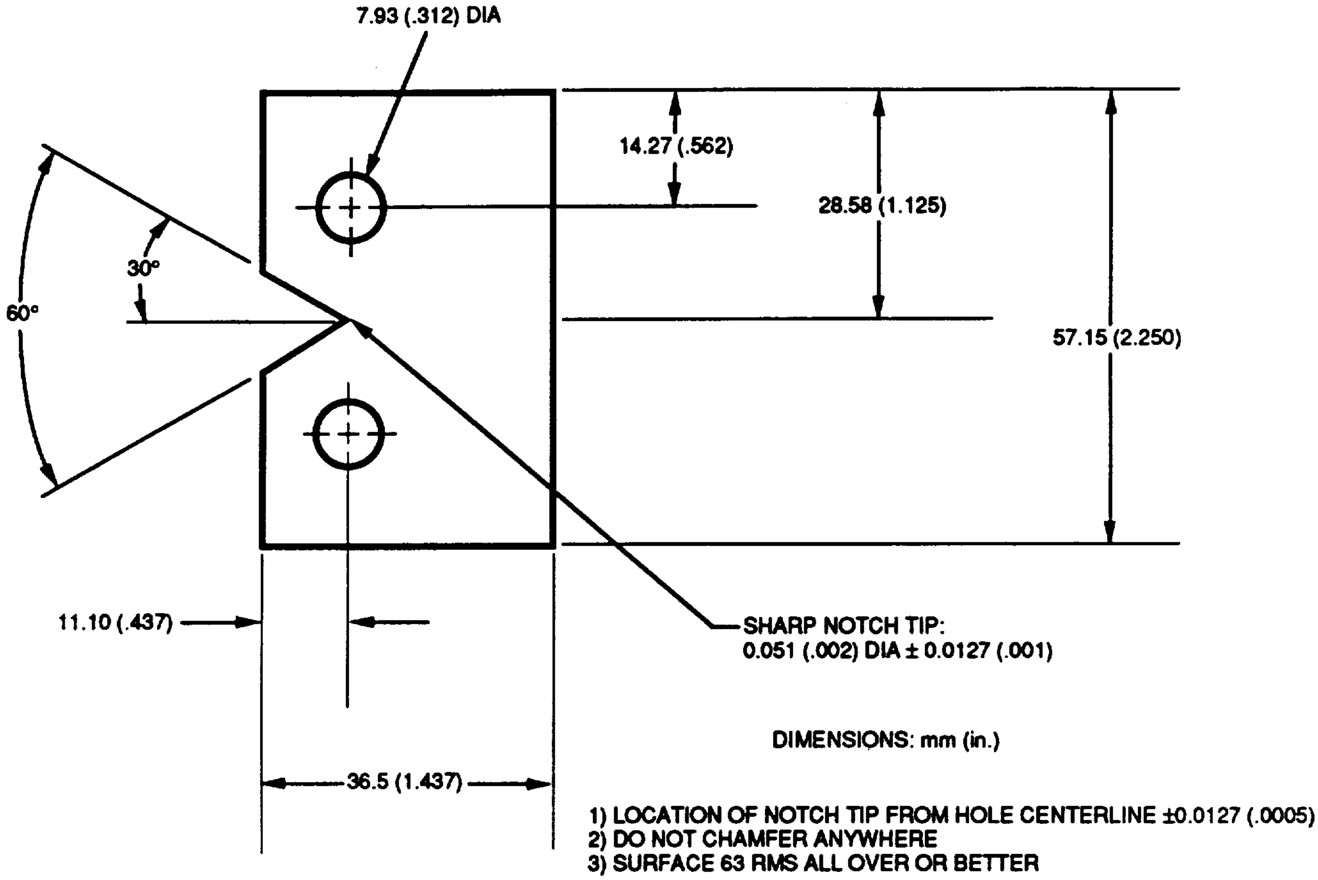

Fig. 2 Kahn Tear-Test Specimen

***Fatigue.*** Fatigue stress-life (S-N) tests were performed on samples prepared from rolled 89A096 (Lot 96)and 89A115 (Lot 115) aluminum alloy sheet, according to ASTM-E466. Comparison data was obtained for 2024-T81 aluminum alloy. Test specimens were prepared for loading in both the L and T directions. The effect of thermal exposure on fatigue life was investigated by soaking samples at 315°C for 100 hours. The test specimens conformed to the geometry shown in Fig. 3. Testing was performed in accordance with ASTM E466-82. S/N data was acquired at both room temperature and at two elevated temperatures: 200°C and 315°C (392°F and 600°F). Most tests were replicated and all were conducted in air under ambient conditions. Constant amplitude testing was performed at a minimum-to-maximum load ratio (R) of 0.1. These tests were conducted at cycling rates in the range of 1.5 Hz - 15 Hz.

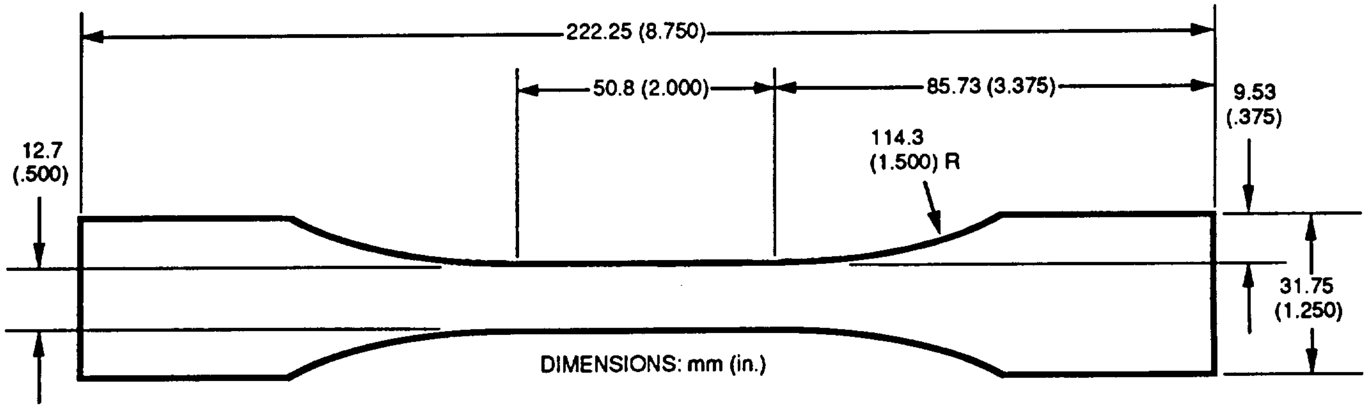

Fig. 3 Fatigue Test Specimen

### 4.4 FORMING

***Minimum Bend Radius***. To determine minimum bend radius, tests were conducted on an existing standard "Vee-type "test die (ST-6010) with a 90° fixed bend angle and varying bend radii on the male punch (Fig. 4). The radius varied every 56 mm (2.2 in.). The radii included the following sizes: 0.79 mm (0.031 in.), 1.19 mm (0.047 in.), 2.38 mm (0.093 in.), 3.18 mm (0.125 in.), 3.57 mm (0.141 in.), 4.76 mm (.188 in.). Bending was conducted such that the bend-line was either parallel, perpendicular, or diagonal (45°) to the sheet rolling direction. The sample parts were 1.6 mm (.063 in.) thick by 51 mm (2.0 in.) wide by 76 mm (3.0 in.) long and were brush-coated with boron nitride suspended in toluene prior to forming. Six parts were formed at a time. Once the parts were set in place, the hot press was closed until the punch just made contact with the parts to be formed. The protective curtains were drawn to insure better heat retention and the press was held in this position for ten minutes to insure a proper heat soak. The press was then closed and held for two minutes, after which the parts were removed and allowed to air cool. Bending was conducted at temperatures ranging from room temperature up to 500°C (930°F). The temperature at each test was held to approximately ±12°C (±25°F). The tonnage used to form the parts was set at 5 tons, the lowest pressure used in production. The ram of the press traveled at approximately 3.4 mm/s (.132 in/s). Subsequent to bending, the parts were cleaned with a water rinse and inspected visually for cracks at the bend radius up to 20x magnification and then by dye-penetrant inspection (19).

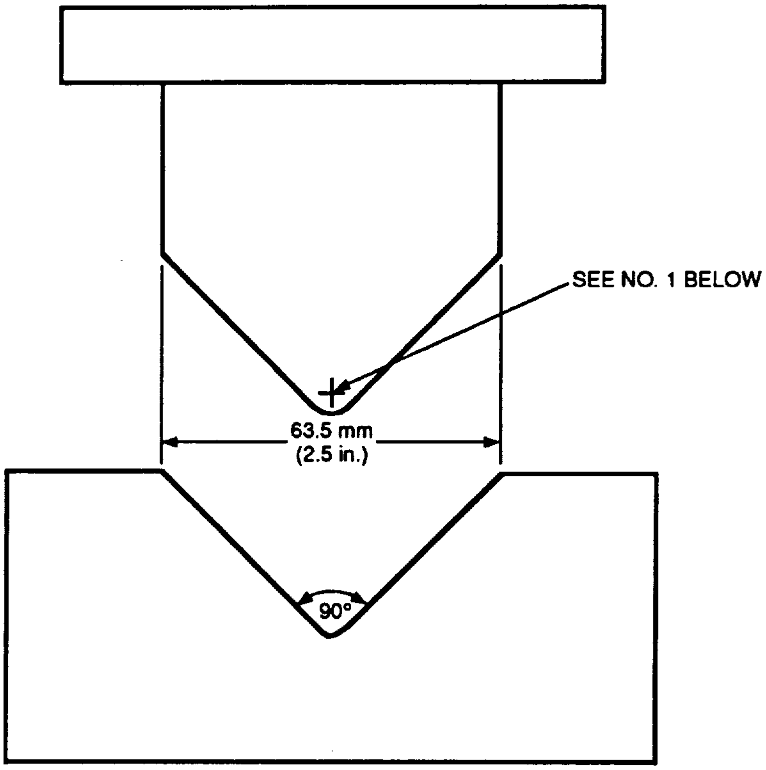

1) RADII: 0.79 mm (0.031 in.), 1.19 mm (0.047 in.)
2.38 mm (0.093 in.), 3.18 mm (0.125 in.)
3.57 mm (0.141 in.), 4.76 mm (0.188 in.)

2) RADII VARIES EVERY 56mm (2.2 in.)

3) RELIEF OF FEMALE DIE NOT SHOWN

Fig. 4 Vee-Test Punch and Die

***Hot-Formed Part with Contoured Flange.*** An existing die was used to evaluate hot wipe-forming of the FVS812 alloy-Lot 110 (2 h degas), 1.6 mm (0.063 in.) thick sheet. Normally, the die ( A51B27133-13/14-FPW)) is used to hot form "clips" of titanium alloy, Ti-6Al-6V-2Sn, as part of a nacelle frame-stiffener. Prior to forming, the parts were blanked and coated with boron nitride. Forming was conducted on a 300 ton Willi White hydraulic press, with heated platens and pressure pad cushion, at temperatures from 315°C (600°F) to 480°C (900°F) after various heating times ranging from 2-7 min. Forming speed was approximately 2.5 mm/s (0.1 in/s). After forming, the parts were inspected for shape and cracking.

***Hot-Formed Part: Pressure-Pad Draw Forming.*** An existing die was used to make a preliminary evaluation of draw forming of the FVS812 alloy. Normally, the hot die (C652-17P2A5498-1HFD#1) is used for forming titanium alloy, Ti-6Al-4V "support" pieces, 1.3 mm (0.050 in.) thick. Prior to forming, the parts were blanked and coated with boron nitride. Forming was conducted at 455-480°C (850-900°F ) on a 150 ton USI hydraulic press with a heated bolster plate, with punch speed estimated at 2.5 mm/s (0.1 in/s).

### 4.5 WELDING

***Fusion.*** Sheet materials 1.6 mm (.063 in.) thick were welded in both the standard process (Lot 96) and vacuum degassed form (Lot 115). Weld preparation for the EBW and GTA processes included machining of the butting edges, deoxidation in a nitric/chromic acid solution (per Mil-S-5002) and manual scraping of the joint area immediately prior to welding. Autogenous bead-on-plate and butt joints were made using machine gas- tungsten-arc-welding in the flat position. All welds were made using direct current electrode negative (DCEN) with helium shielding gas on the face (100CFH) and root (250 CFH) sides. An eight-foot long Jetline Welder with a Linde HW-500SS power supply was used with a 0.063 in. diameter tungsten electrode and No. 10 ceramic gas cup. Electron beam welds were made in the flat, horizontal and vertical positions in a Sciaky Model VX.3 electron beam welder, with a capability of 60KV and 500 ma under vacuum of $10^{-5}$ torr.

***Resistance Spot Welding.*** Initial parameter development was accomplished with 1.6 mm (.063 in.) thick samples of the standard alloy (Lot 96) processed using the normal pre-weld cleaning procedures (vapor degrease, alkaline clean, deoxidize in nitric/chromic acid, rinse, dry and wire brush immediately prior to welding). All welding was performed on a 100 kVA three phase frequency converter machine, capable of monitoring weld expansion versus time (which is an indication of heat buildup in the weld) and displaying the result graphically on a CRT display. Radiographic tests on welds were made to the requirements of Mil-W-6858D for Class A welds. Shear strength and consistency of the welds were determined according to the minimum requirements of Mil-W-6858D. Cross tensile-to-shear strength ratios, were tested to the Mil-W-6858 specification. Weld tests were performed on the standard and extended vacuum degassed alloys.

## 4.6 ZEE-STIFFENED COMPRESSION TEST PANELS

***Design and Analysis***. Three small-scale, zee-stiffened compression test panels were designed and fabricated:

- A baseline riveted panel with 2024-T62 aluminum zees and a 2024-T81 aluminum skin
- A riveted panel with FVS812 aluminum zees and skins
- A resistance spot-welded panel fabricated with FVS812 aluminum zees and skins.

The panels had the same nominal geometrical configuration, which was obtained by trial-and-error using the Grumman CURVPANL computer program and associated room temperature material properties. Compression loads were analyzed with the Grumman CURVPANL and YFUDGE computer programs.

***Fabrication.*** The zee-stiffened panels were fabricated by either riveting or resistance spot welding. All sheet-metal components were sheared from the as-received material and hand deburred by light filing. The FVS812 alloy -Lot 340 (20 h degas) was used to fabricate zee-stiffeners for the compression panels. The stiffeners were sheared into 57 mm (2.25 in.) by 216 mm (8.5 in.) blanks and were hot-formed on a Pacific Brake ( Model 200-12) with a heated platen. Air bending was conducted on 1.6 mm (0.063 in.) thick material, perpendicular to the sheet rolling direction, using a 2.4 mm (0.094 in.) radius die with the platen bed heated to 260°C (500°F). The parts were preheated to 480°C (900°F) for five minutes in a portable electric furnace adjacent to the press brake, prior to forming. After transferring the part from the furnace to the press brake, the actual forming temperature was measured to be 430-454°C (800-850°F). After forming, the parts were visually and dye-penetrant inspected for cracks.

Aluminum alloy 2024-0, 1.6 mm (0.063 in.) thick sheet was used to fabricate zee-stiffeners for the baseline riveted compression test panel. Forming was conducted parallel to the rolling direction at room temperature using a 2.4 mm (0.094 in.) radius die. Subsequently, the formed 2024-0 parts were heated to the T6 temper.

The riveted and the resistance spotwelded panels were constructed using standard manufacturing procedures. The holes for the rivets were drilled in the skin and stiffeners with high-speed cobalt drills. Monel countersunk rivets, 3.2 mm (0.125 in.) diameter (NAS 1200M4) were used to fasten both the FVS812 and 2024 Al panels. The engineering drawings for the panels are included in the appendix. Resistance welding parameters are presented in the Results and Discussion section. Details of the panel assemblies are given in the Appendix.

***Testing.*** Preparatory to testing, surface flatness and straightness measurements were made on each of the panels. The panels will be tested at room temperature under compressive loading at the NASA Langley Research Center structural test facility.

# 5. RESULTS AND DISCUSSION

## 5.1 ALLOYS

***Microstructure and Strength***. The average grain size and dispersoid size for these alloys is 0.36 μm and 42 nm, respectively (6). The nominal composition of the dispersoid particles is $Al_{13}(Fe,V)_3Si$. Distinct grain boundaries cannot be resolved by light microscopy, however, the flow pattern arising from the prior powder boundaries may be observed. Light micrographs of the microstructure of FVS812 alloy, Lot 96 (2 h degas) are shown in Fig. 5, which are typical for the other alloys in this program. X-ray (111) pole figure indicate that these alloys exhibit only a weak fcc texture versus conventional ingot Al base alloys following similar thermomechanical processing (6). Dispersoid coarsening rates at 315°C (600°F) are of the order of $10^{-27}$ $mm^3/h$ and are considered negligible (11, 20).

Room temperature tensile properties for the FVS812 sheet used in this program are compared in Fig. 6 ( The data are presented in Tables A-1, A-2, and A-3). In general, the sheet was isotropic with respect to strength, with no apparent effects of degassing. Higher transverse elongation was typically observed but there is no apparent effect of degassing.

***Effect of Degassing on Hydrogen Content***. The results of degassing treatments described above are presented in Table 4. After 20 h extended degassing, the total hydrogen content was reduced by approximately 20% in the Lot 115 material, compared with Lot 96 which received the standard 2 h degas treatment. On the other hand, the hydrogen contents of Lots 335 (2 h degas) and 340 (20 h degas) exhibited an opposite trend, with the Lot 340 material approximately twice as high as Lot 96. The higher hydrogen and oxygen content (Table 2) has been attributed to a small leak in Allied's vacuum system which resulted in continual rehydration of the FVS812 material during the 20 h degassing (15). The increase in hydrogen content, coupled with an increase in oxygen content, indicates that the rehydration reaction involved the formation of additional aluminum hydrate on the powder surface. Although the hydrogen content in both lots of material that received an extended degassing treatment are substantially different, longer degassing times appeared to be beneficial to mechanical properties and welding behavior. Those results will be presented in the following sections.

In FVS812 alloys, hydrogen may be present in many forms, including hydrates, hydroxides and absorbed water vapor on the surface and monoatomic hydrogen dissolved in the bulk. Degassing can reduce hydrogen by boiling off water vapor, decomposing hydrates, and at high enough temperatures, reducing bulk hydrogen by diffusion. Since surface hydroxides will not decompose under normal degassing temperatures, all ribbon and powder is stored under a protective dry atmosphere. Water vapor comes off at about 100°C (212°F). The hydrates usually decompose from a triple hydrate to a mono-hydrate and eventually to alumina, as indicated: $Al_2O_3{\cdot}3H_2O \longrightarrow Al_2O_3{\cdot}2H_2O \longrightarrow Al_2O_3{\cdot}H_2O \longrightarrow$

a) LONGITUDINAL

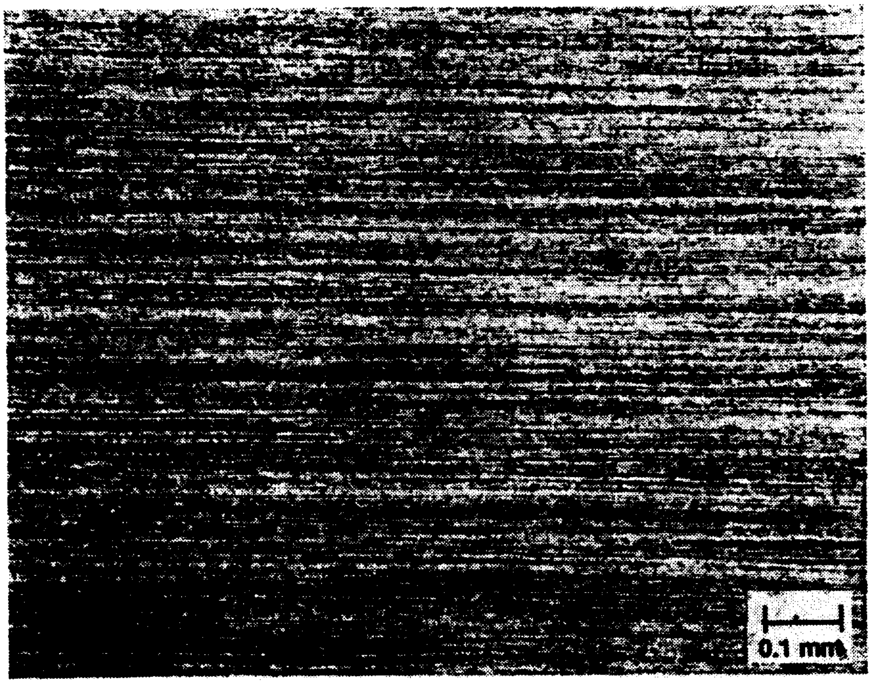

b) TRANSVERSE

**Fig. 5 As-Received Microstructure of FVS812 Alloy (Lot 96, 2 h Degas)**

$Al_2O_3$. Break-down of the mono-hydrate only occurs at temperatures above approximately 500°C. Reaction of water vapor with the aluminum produces hydrogen gas and oxygen, which is scavenged to form alumina ( $Al_2O_3$). Therefore, oxygen content during the decomposition of the hydrates will remain essentially constant even though the hydrogen level is reduced (15).

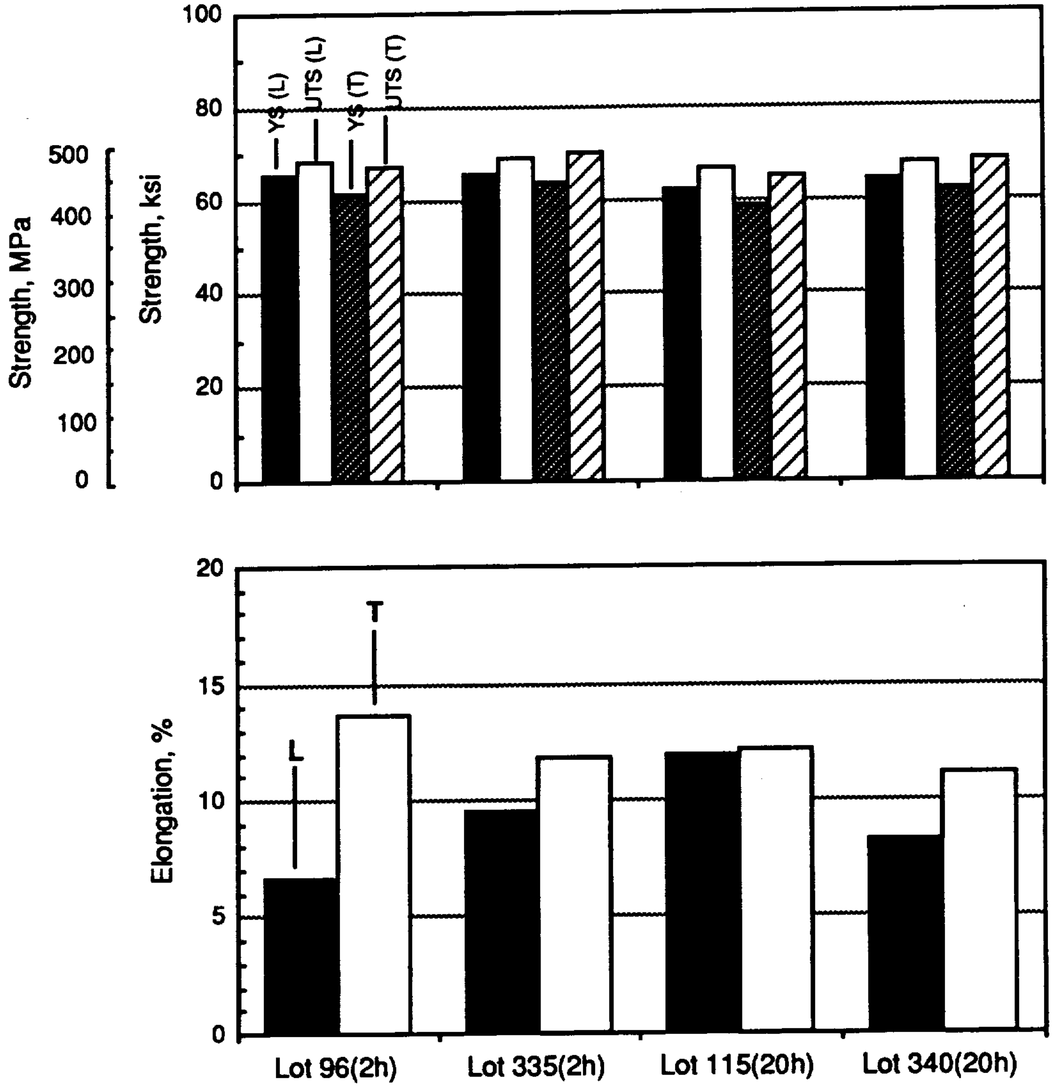

**Fig. 6** Comparison of Room Temperature Tensile Properties of FVS812 Alloys

## 5.2 MECHANICAL TESTING

***Tensile.***

***Effect of thermal exposure on room temperature properties.*** The effect of thermal exposure on the room temperature tensile properties of FVS812 (i.e., Lot 96-2 h degas and Lot 115-20h degas) are shown in Fig. 7-9. In general, there is no significant effect on the yield or ultimate strength of either alloy in the L or T-orientation after exposures up to 315°C (600°F) for 1000 h. In each case, the percent elongation is generally lowered after exposure. In Lot 96, elongation in the T-orientation in the as-received condition is about twice that of the L-orientation (Fig. 7). Higher elongation in the T-orientation has also been observed in standard-degassed , 2.2 mm (0.085 in. ) thick FVS812 alloy sheet (1). This behavior may be due, in part, to the prior alignment of primary silicide rods and oxide fragments in the billet form, i.e., the less ductile orientation in the billet, the T-orientation, becomes the L-orientation in sheet form because of a cross-rolling procedure (20).

After thermal exposure, the elongation for all conditions are more nearly the same but some scatter is observed. In Lot 115, the elongations for both test directions are comparable in the as-received condition and generally reduced after exposure (Fig. 8). The ultimate strength and elongation of both alloys in the L-orientation are compared in Fig. 9. The strength for both are equivalent but average ductility is approximately 40 to 70 % greater in the Lot 115 (20 h degassed) alloy after the various exposures. Thus, it appears that extended degassing may have a beneficial effect on ductility. Also, the elongation data in Fig. 9 (also Fig. 7, 8) indicate that the ductility for both alloys after 315°C exposure is slightly higher than after 200°C exposure. After thermal exposure, there appear to be no clear trends on elongation due to prior billet orientation. A tensile fracture surface characterized by fissuring associated with prior ribbon boundaries is shown in Fig. 10; this was typical for both conditions. Similar tests on the Lot 335 (2 h degassed) and Lot 340 (20 h degassed) alloys might have clarified this data but such tests were not conducted because of the late arrival of those materials.

There appear to be two effects, i.e., improved ductility in the extended degassed material and the relatively lower ductility after thermal exposure at 200°C (392°F), which may be related to the presence of hydrogen. A tensile elongation dependency on hydrogen concentration has been observed in Al-Fe-Ce alloys (21) which could account for differences due to billet degassing in this work. Lowered ductilities after thermal exposure may be related to evaporation and decomposition reactions at relatively low temperatures involving adsorbed $H_2O/O_2$ mixtures and hydrated aluminum oxides (21). For example, up to 200°C (392°F), evaporation of $H_2O/O_2$ is expected; between 150-350°C (300-660°F), decomposition of the hydrated oxide could produce water vapor; and between 300-500°C (570-930°F), hydrogen gas is expected. Hydrogen in the microstructure may be the most detrimental at low temperatures because of limited mobility (22). The effect of shorter exposure times on tensile properties was not evaluated for these materials.

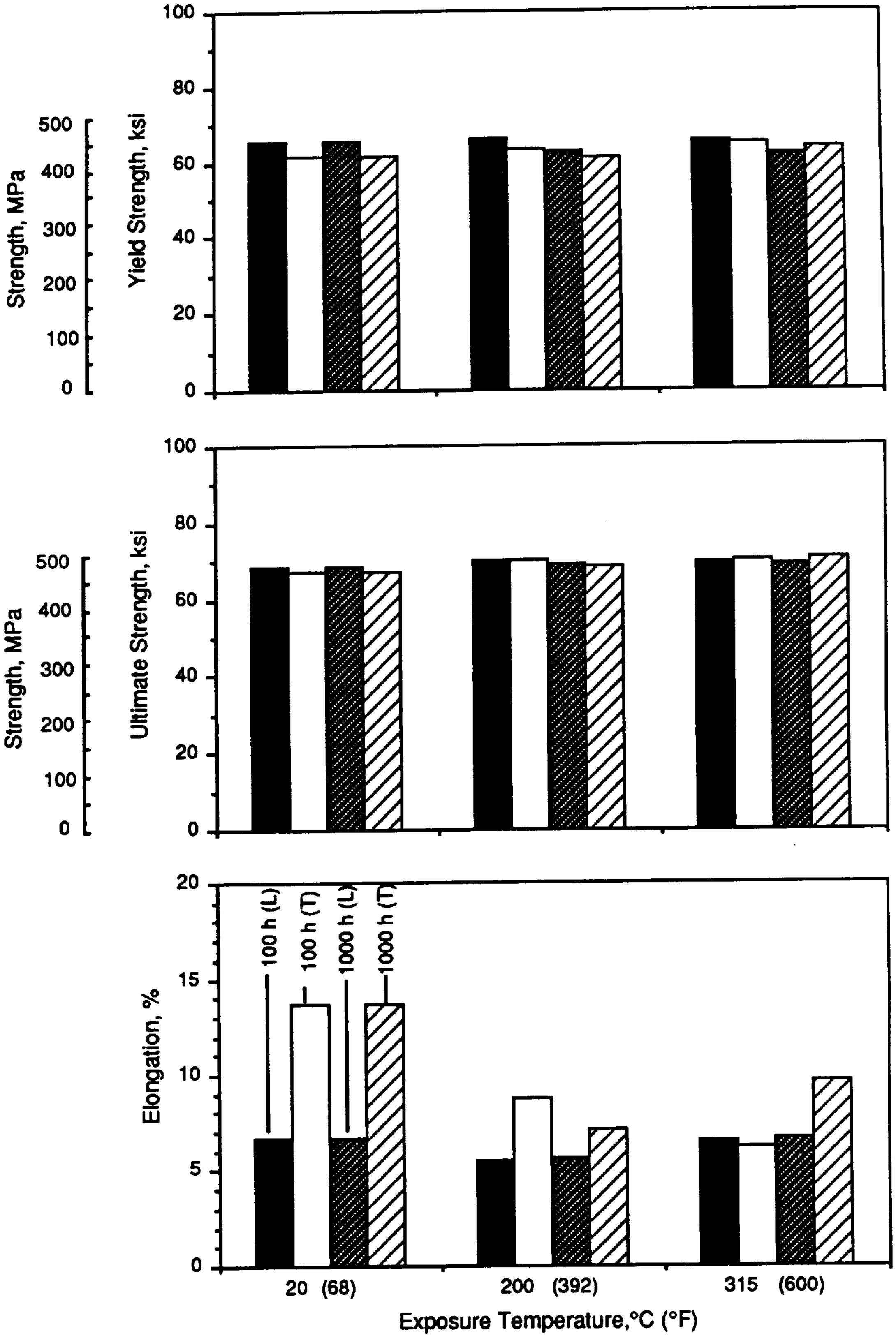

Fig. 7 **Effect of Thermal Exposure (100 h and 1000 h) on Room Temperature Tensile Properties of FVS812 (Lot 96, 2 h Degas)**

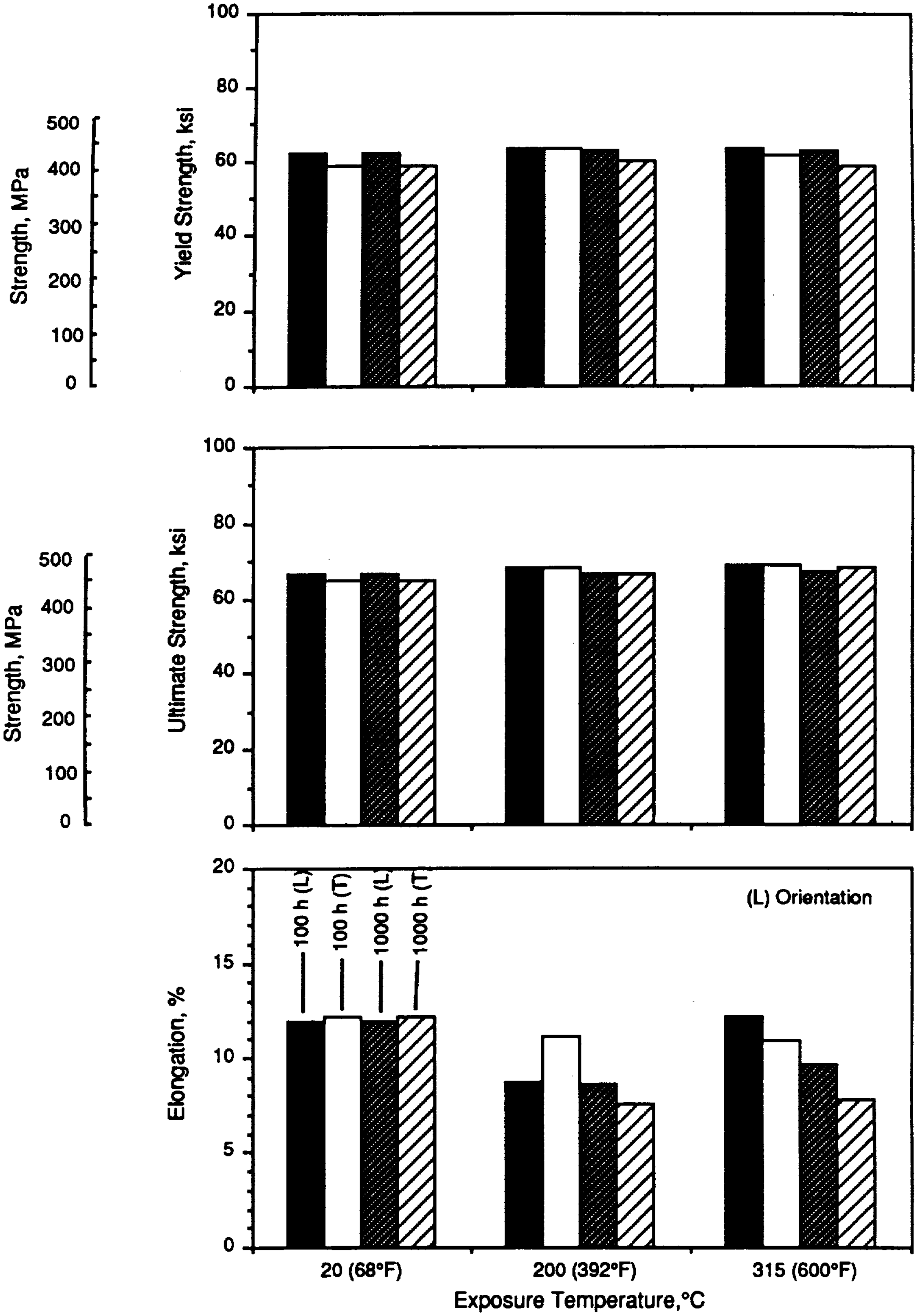

**Fig. 8** Effect of Thermal Exposure (100 h and 1000 h) on Room Temperature Tensile Properties of FVS812 (Lot 115, 20 h Degas)

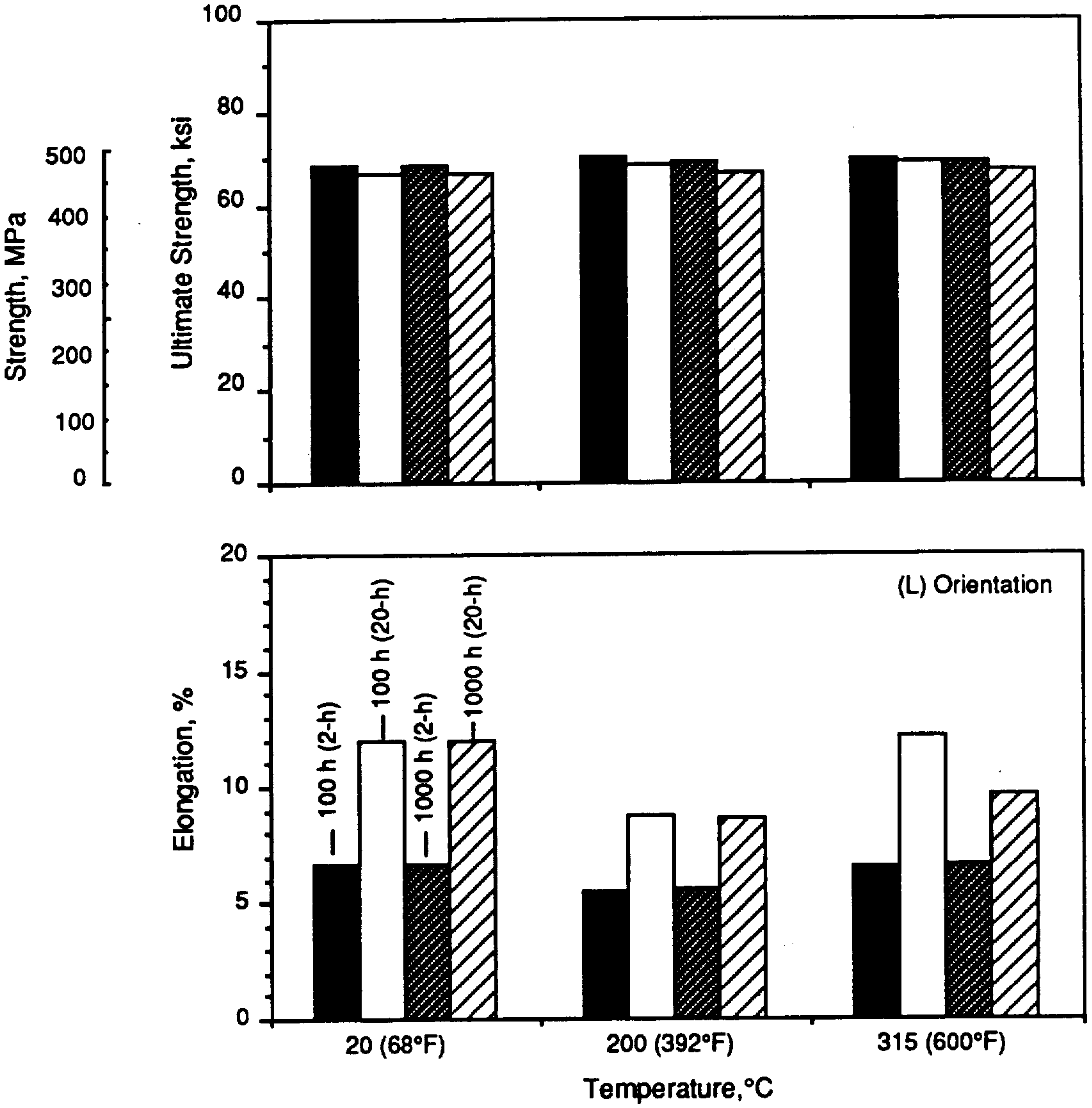

Fig. 9 Effect of Thermal Exposure (100 h and 1000 h) on Room Temperature Tensile Properties of 2 h (Lot 96) and 20 h (Lot 115) Degassed FVS812 Alloy

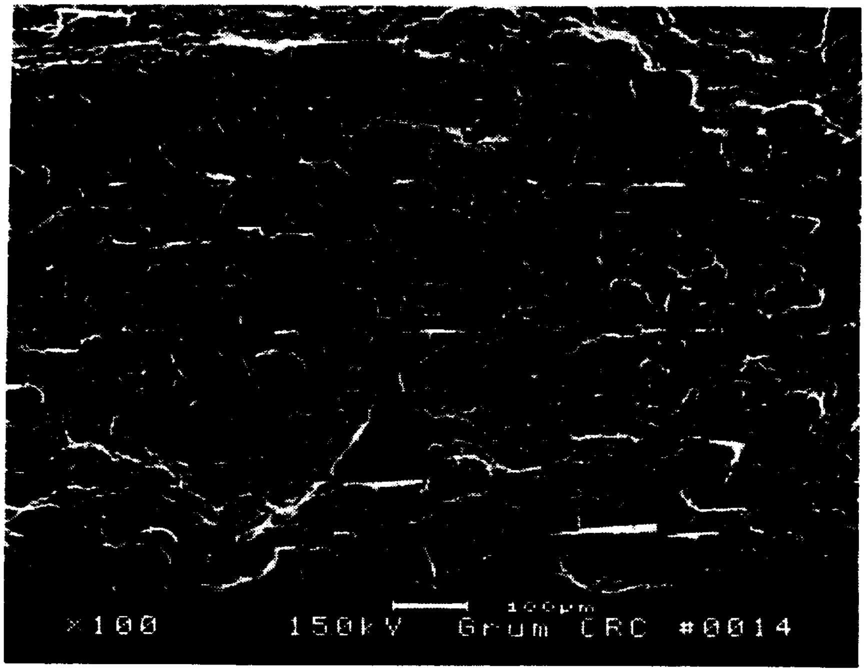

**Fig. 10** **Tensile Fracture Surface of FVS812 Alloy (Lot 96, 2 h Degas), As-Received**

***Effect of thermal exposure on elevated temperature properties.*** The effect of thermal exposure on elevated temperature properties of Lot 115 (20 h degas) is shown in Fig. 11 and 12. Although strength is unaffected by thermal exposure up to 315°C (600°F) for 1000 h when tested at room temperature or 315°C(600°F), there was an effect on ductility. When tested at room temperature after exposure, elongation is approximately the same for all conditions. But when tested at 315°C (600°F) after exposure, elongation is significantly increased. This effect is not explained at the present time.

***Elevated temperature properties of Lot 115 (20 h degas).*** The elevated temperature properties of Lot 115 (20 h degas) are shown in Fig. 13 (The data are presented in Table A-4). Yield strength decreases with temperature but tensile ductility is significantly reduced at intermediate temperatures, (80°C (175°F) to 175°C (350°F). The reduction in ductility is attributed to dynamic strain aging (DSA). In these alloys, the phenomenon of DSA occurs at low to intermediate temperatures and is characterized by reduced ductility and increased flow stress and is attributed to the interaction of mobile dislocations and solute atmospheres (23, 24, 25). This effect also manifested itself during hot forming studies of these alloys, where severe cracking occurred during bending in the same temperature range.

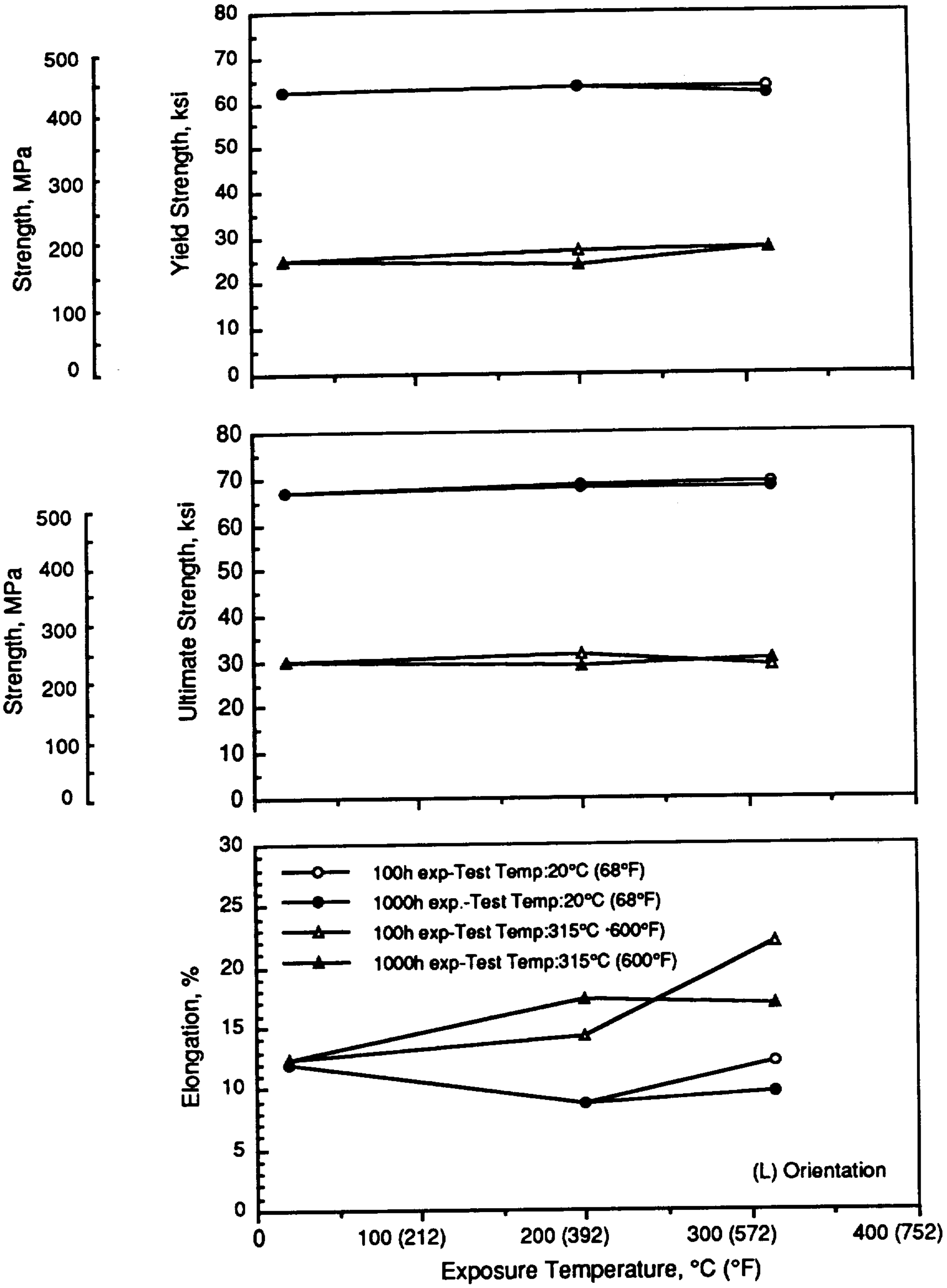

**Fig. 11 Effect of Test Temperature on Tensile Properties of Lot 115 (20 h Degas) After Long Term Exposure**

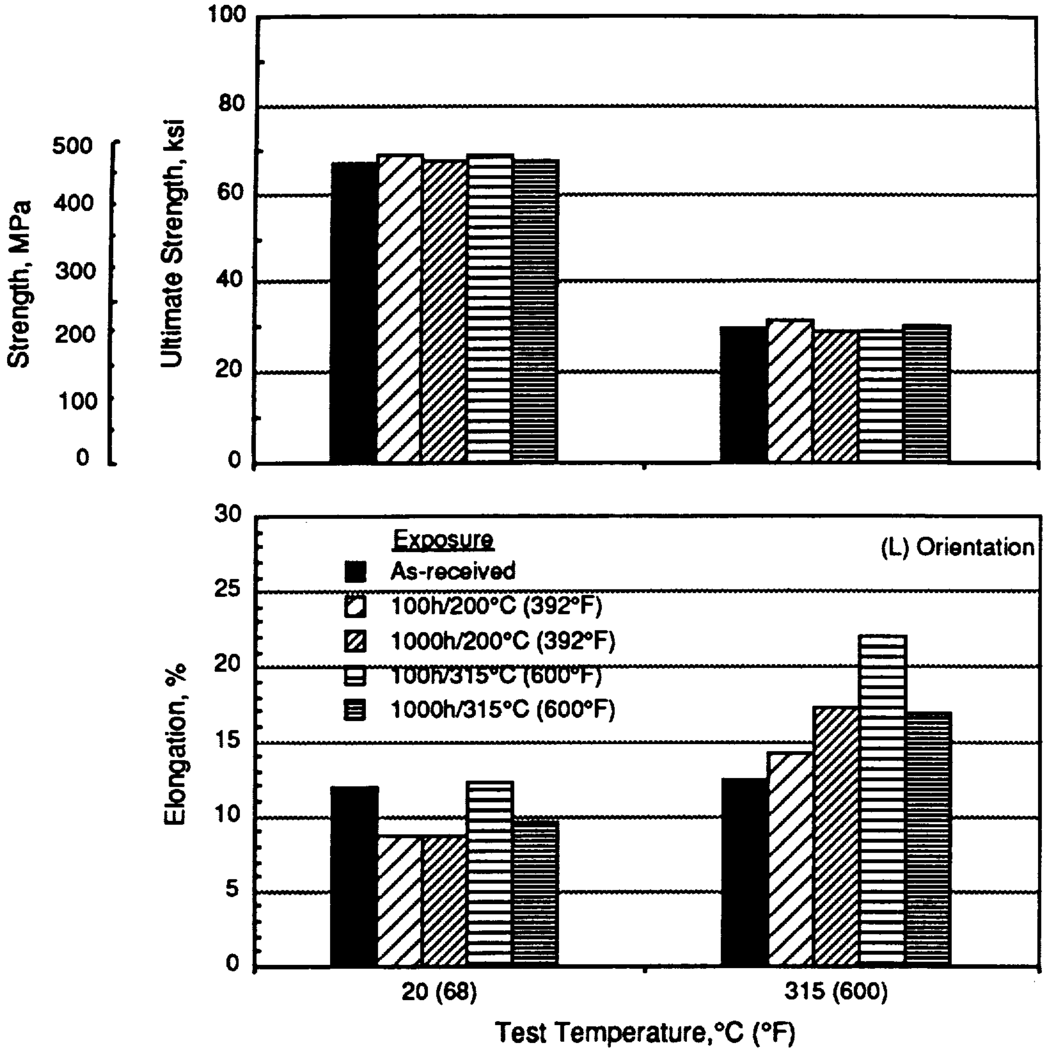

**Fig. 12 Effect of Thermal Exposure on Strength and Ductility in Lot 115 (20 h Degas)**

***Effect of strain rate.*** The effect of strain rate on tensile properties is shown in Fig. 14 and 15 ( The data are presented in Table A-5). Flow stress gradually increased with strain rate at test temperatures up to 482°C (900°F), as expected(26). At room temperature, tensile ductility gradually decreased with strain rate. At 315°C (600°F) there was no significant effect but, at 482°C (900°F), some strain rate sensitivity was observed. At 482°C, (900°F) the elongation increased approximately 75 % from 0.001 to 0.1 $s^{-1}$, and at strain rates > 0.1 $s^{-1}$, it decreased slightly. Ductility appears to significantly improve between 315°C (600°F) and 482°C (900°F). Similarly, during the forming studies, cracking was usually observed during bending, up to 315°C (600°F), while crack-free bends were produced at higher temperatures. The forming studies in this work were conducted at forming rates ≈ 0.1 $s^{-1}$.

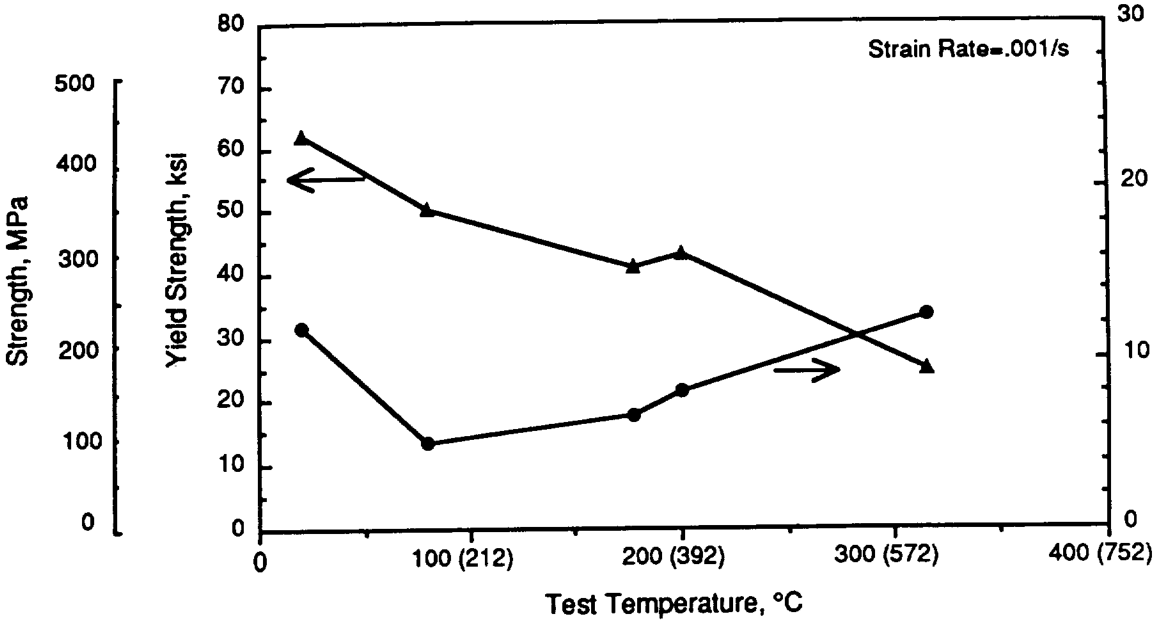

**Fig. 13** **Elevated Temperature Tensile Properties of FVS812 (Lot 115, 20 h Degassed)**

The Al-Fe-V-Si alloys showed very little strain hardening at room temperature, 200°C (392°F), and 300°C (572°F) but did exhibit a small strain rate sensitivity increase at strain rates near 0.01 and 0.10 s-1 at higher temperatures approaching 600°C (1112°F)(6). At the lower temperatures, where the typical load vs time data indicated a very rapid increase to the maximum load followed by gradual load decrease prior to localized neck formation and failure, the load reduction was attributed to diffuse necking. The evidence indicated that strain hardening at low strain rates occurred very rapidly in the very early stages of deformation. However, at higher temperatures, the strain level at which load reduction occurred, increased with strain rate. In this work, possible enhanced plastic stability, which apparently increased elongation, was observed during deformation at 480°C. The improved plastic stability suggests that another deformation mechanism was operative, namely thermally induced dislocation climb through vacancy diffusion (14). At high temperatures where there is climb, the dispersoid particles are no longer effective at limiting slip through residual dislocation interaction (i.e., Orowan bowing). As dislocation climb is diffusion rate driven, there is an associated rate effect and a "strain rate sensitivity" might be encountered under climb conditions. The observed increase in strain rate sensitivity in this work might be the result of such a rate dependence and could have been observed in the "strain" hardening behavior observed under high strain rates.

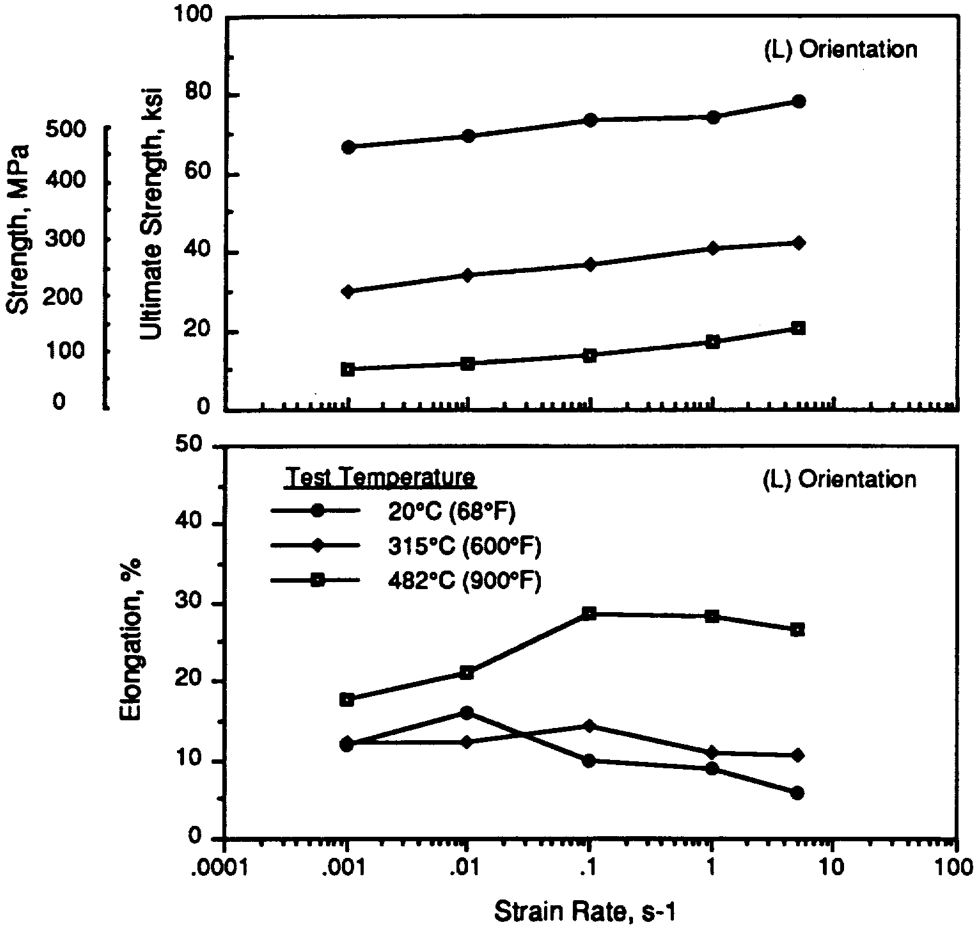

**Fig. 14** **Effect of Strain Rate on Tensile Properties of Lot 115 (20 h Degas)**

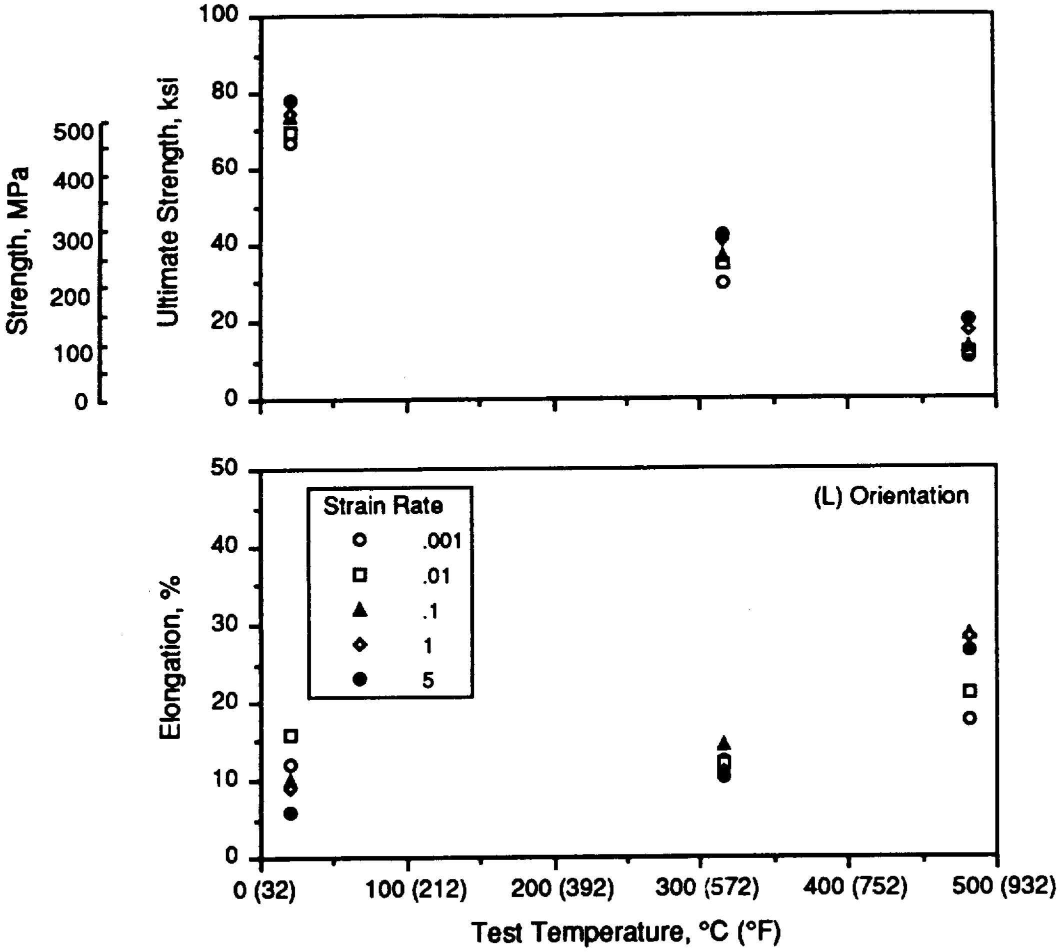

**Fig. 15 Effect of Temperature on Tensile Properties of FVS812 (Lot 115, 20 h Degas)**

**Compression.** Compression yield strength in the as-received condition for each of the two material degas conditions ( 2 h and 20 h) was determined for the design of the zee-stiffened compression test panels. The test results are presented in Fig. 16 ( The data are presented in Table A-6). In each case, the compressive yield strength was 15-20 % higher in the transverse direction (approximately 55 ksi). Since higher strength in the transverse direction was unexpected, additional compression yield tests were conducted to determine the effect of annealing at 300, 400 and 500°F (570, 750 and 930°F) on compressive yield strength in the as-received condition for each of the two material degas conditions ( 2 h and 20 h). The overall results indicate that annealing had an aging effect and that compressive yield strength in the L and T orientations increased with temperature but that strength in the longitudinal direction of both alloys was still relatively low (Fig. 16). This strength differential may be attributed to a microstructural texturing effect resulting from hot rolling.

In view of the unexpected behavior under compressive loading, tensile tests were conducted on the same FVS812 alloys and degas conditions, exposed to the same exposure conditions as their compression counterparts, to determine the effect of thermal exposure. Thermal exposure slightly decreased tensile yield strength in the L-orientation of both degas conditions but did not significantly affect the yield in the T-orientation (Fig. 17 and Table A-7). Tensile ductility, on the other hand, decreased in the T-orientation of both alloy conditions and behaved somewhat erratically in the L-orientation (Fig. 18). From these observations, it was concluded that strength anisotropy was pronounced under compressive loading but not in tension, and that tensile elongation appears to be sensitive to the effects of thermal exposure, all of which are not yet completely understood.

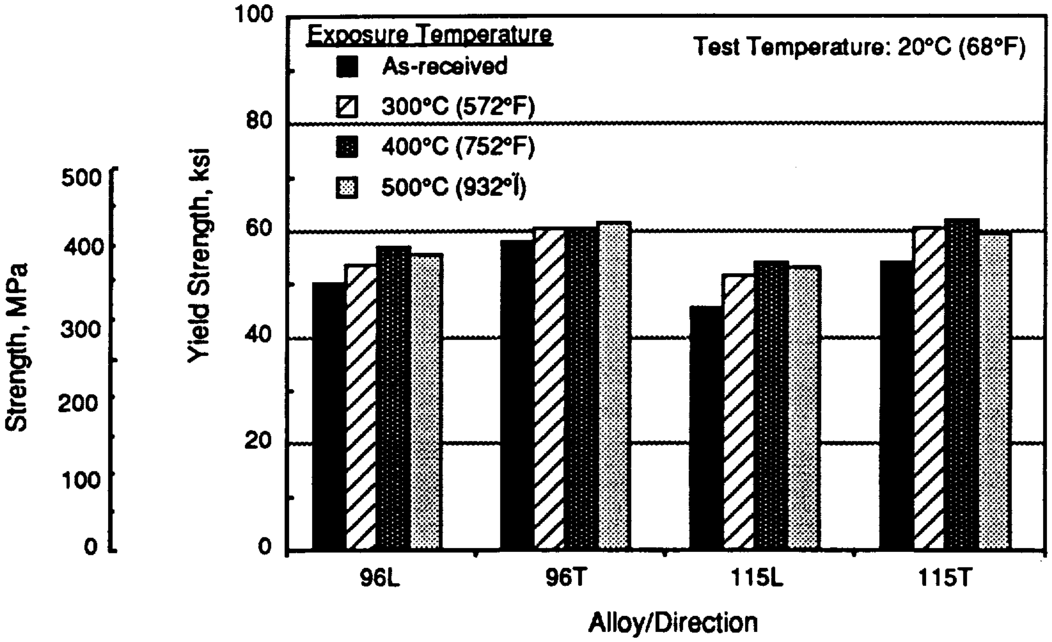

**Fig. 16 Effect of 20 h Thermal Exposure on Compressive Yield Strength of FVS812 Alloys**

Metallographic examination of the sheet indicated that the compression yield strength differential appears to be attributed to a microstructural texturing effect resulting from hot rolling, as shown in Fig. 5. The alignment of prior ribbon boundaries during billet fabrication may create a mechanical column effect, which is subject to earlier instability compared with compression loading in the T-orientation. However, in other work, this behavior was considered to be due to the development of residual bending in the mill-supplied sheet (1). In the present work, the effect seems to be the result of prior ribbon boundary alignment, since it persisted after annealing. After thermal exposure at the temperatures and times indicated, the overall increase in compressive yield strength for all conditions is probably due to the presence of equilibrium $Al_{13}Fe_4$ or $Al_3Fe$ phase, which forms by the transformation of the coarse silicide dispersoids (27).

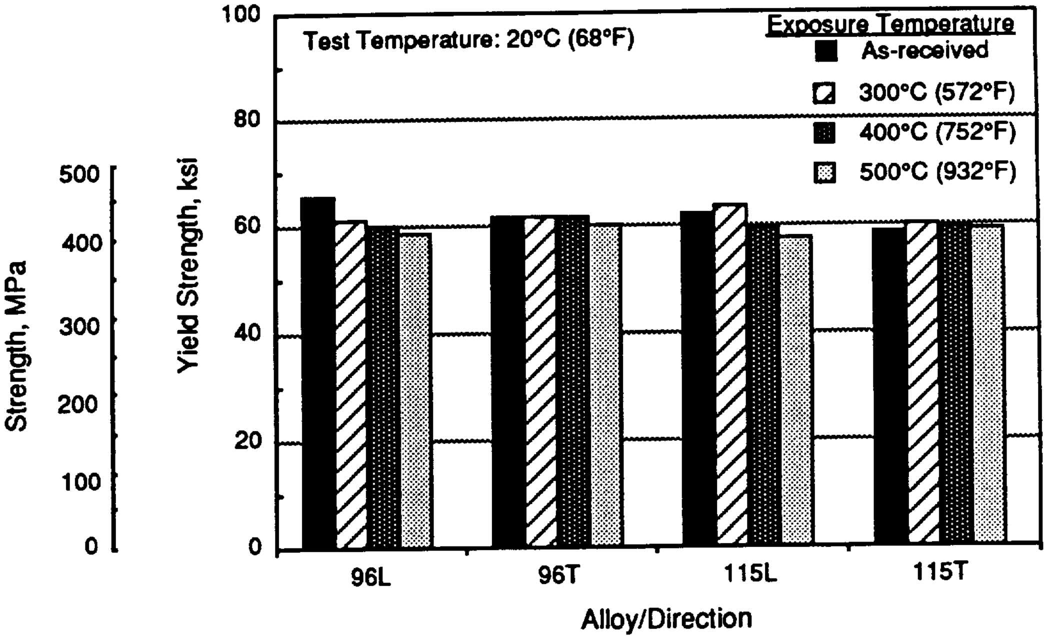

Fig. 17 Effect of 20 h Thermal Exposure on Tensile Yield Strength of FVS812 Alloys

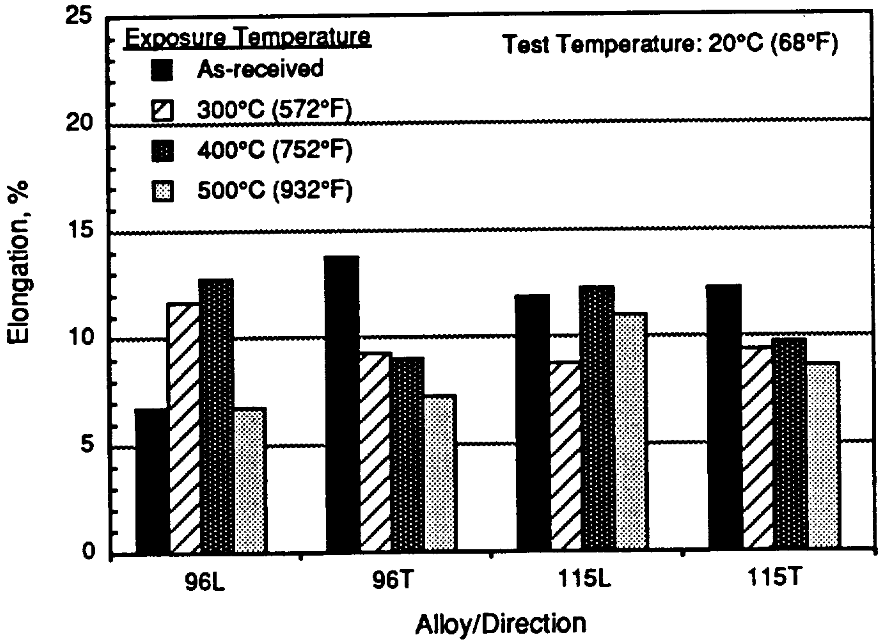

Fig. 18 Effect of 20 h Thermal Exposure on Ductility of FVS812 Alloys

***Toughness (Kahn Tear Test).*** The Kahn Tear test provides a measure of notch toughness by comparing the ratio of tear strength to yield strength (TS/YS)(16, 17, 18). Tear strength is the combined direct stress and bending stress developed by the specimen and is computed from the maximum load, as follows:

Tear strength, (MPa) = $P/A+Mc/I = P/bt+3P/bt = 4P/bt$ ((17, 18)).
where:

$P$ = maximum load, N (lb)
$A$ = net area, $mm^2 (in^2)$
$M$= moment, J, mm-lb (in-lb)
$c$ = distance from centroid to extreme fibers, mm ( in.)
$I$ = moment of inertia, $mm^4$ ($in^4$)
$b$ = width at root of notch, mm ( in.)
$t$ = thickness, mm ( in.)

The primary criterion of an aluminum alloy's tear resistance derived from this test is considered to be the unit propagation energy (UPE). The UPE ($J/mm^2$) is equal to the energy required to propagate a crack divided by the initial net area of the specimen and is a measure of stable crack resistance.

***Tear strength-to-yield strength (TS/YS) ratio.*** The effect of thermal exposure on the TS/YS ratio for both lots ( i.e., Lot 96-2 h degas and Lot 115-20 h degas) of FVS812 is shown in Fig. 19 ( The data are presented in Tables A-8, A-9 and A-10). In general, the TS/YS ratios are relatively high for aluminum alloys, ranging from 1.29 to 1.45 for all conditions . The values for the L-T orientation in each lot are slightly more consistent than those of the T-L orientation. At room temperature, the TS/YS ratio for the T-L orientation of both lots is about 5% greater than that of the L-T orientation. After thermal exposure under various conditions, there is no systematic orientation effect observed and the ratios vary within a few percent. There appears to be no significant effect of degas time on TS/YS ratio.

Compared with room temperature TS/YS ratios, the effect of thermal exposure on L-T values was less than that on T-L values, in general. In Lot 115, L-T values were reduced by 3% after 100 and 1000 h at 200°C (392°F); after 100 and 1000 h at 315°C (600°F) values were reduced 1%. In the T-L orientation of Lot 115, values were reduced 11 and 8 % after exposure for 100h at 200 and 300°C (392 and 600°F), respectively; after 1000h, there was no reduction for 200°C (392°F) exposure and 1% for 315°C (600°F). In Lot 96, L-T values were slightly reduced after 100h exposure at both temperatures, but were slightly increased after 1000h at the same temperatures. In the T-L orientation of Lot 96, values were reduced about 4 and 3% after 200°C (392°F) for 100h and 1000h and were reduced 9 and 11% for the same times at 315°C (600°F).

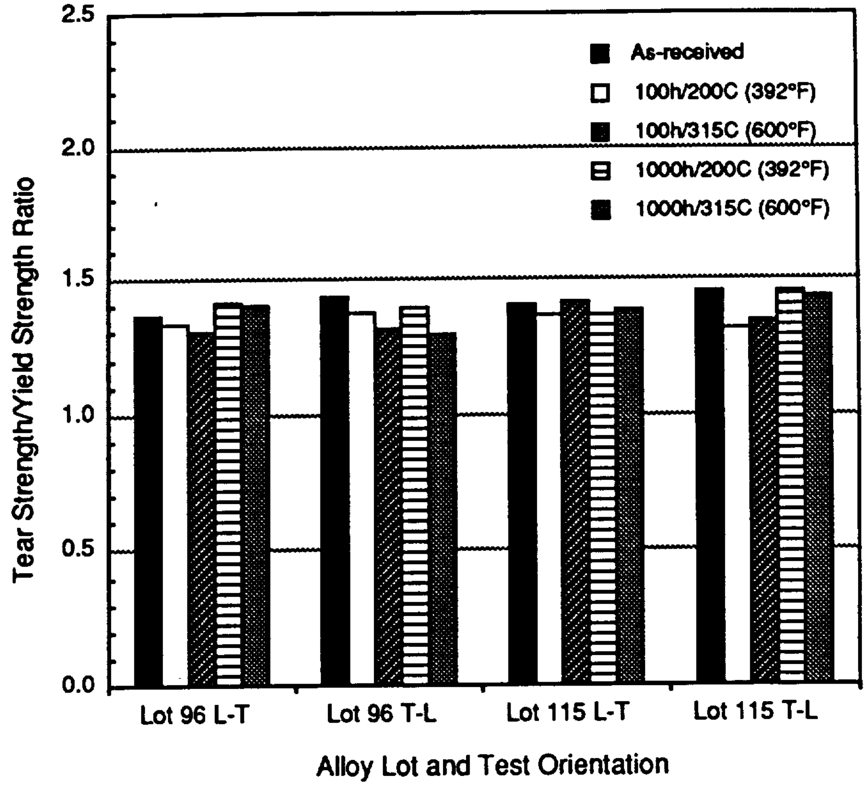

**Fig. 19 Effect of Thermal Exposure on Tear Strength/Yield Strength Ratio of FVS812 Alloy**

***Unit propagation energy (UPE).*** The effect of temperature on UPE for both lots is shown in Fig. 20 and 21 and both alloys are compared in Fig. 22. The UPE for the L-T orientation is significantly higher in both lots of material. In Lot 115, UPE values range 31 to 47% greater than T-L for the various conditions reported. In Lot 96, L-T values range 19 to 45% greater than T-L values for the various exposure conditions. Lower fracture toughness in the T-L orientation has been observed for these alloys and appears to be related related to crack propagation predominantly along weak prior particle interfaces, where oxide fragments form a preferential fracture path (12, 22). Low magnification SEM fractography of FVS812 showed secondary cracking or delamination, perpendicular to the crack front, in both the L-T and T-L orientations, as shown typically in Fig. 23. In other work, where delaminations were not observed in the T-L orientation of compact tension specimens, the mechanical effect of delamination was considered to increase the apparent resistance to crack growth (22).

In Lot 115, UPE for the L-T orientation is systematically lowered by 3 and 10% after thermal exposure for 100h at 200 and 315°C (392 and 600°F), compared with room temperature values, as shown in Fig. 20. After 1000h exposure at 200°C (392°F), UPE is reduced 9% but after 1000h/315°C (600°F) exposure is reduced only 2%. In the T-L orientation, UPE is reduced with temperature but the reductions are less after 1000h exposure at both temperatures.

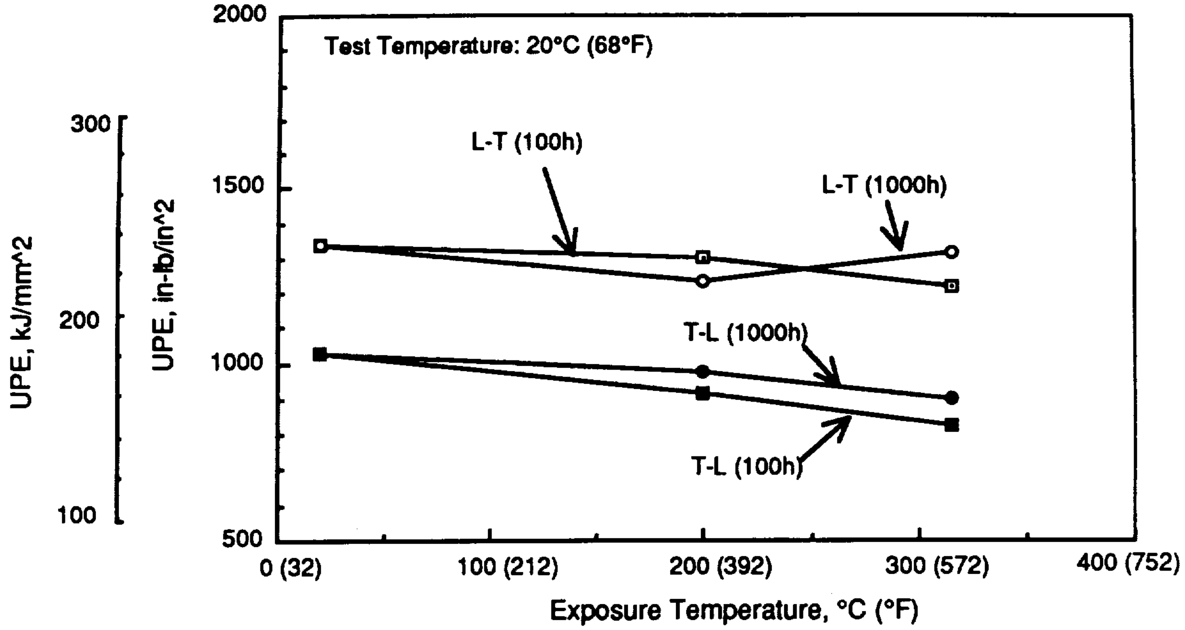

Fig. 20 Effect of Temperature on Unit Propagation Energy (UPE) of FVS812 Alloy (Lot 115, 20 h Degas)

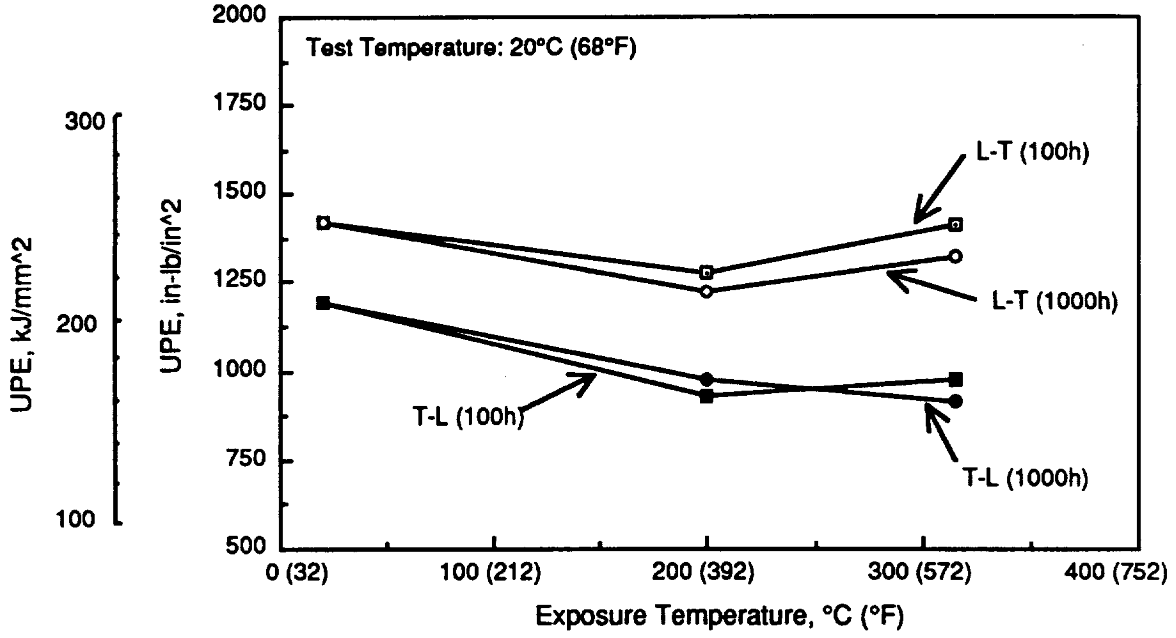

Fig. 21 Effect Of Temperature on Unit Propagation Energy (UPE) of FVS812 Alloy (Lot 96, 2 h Degas)

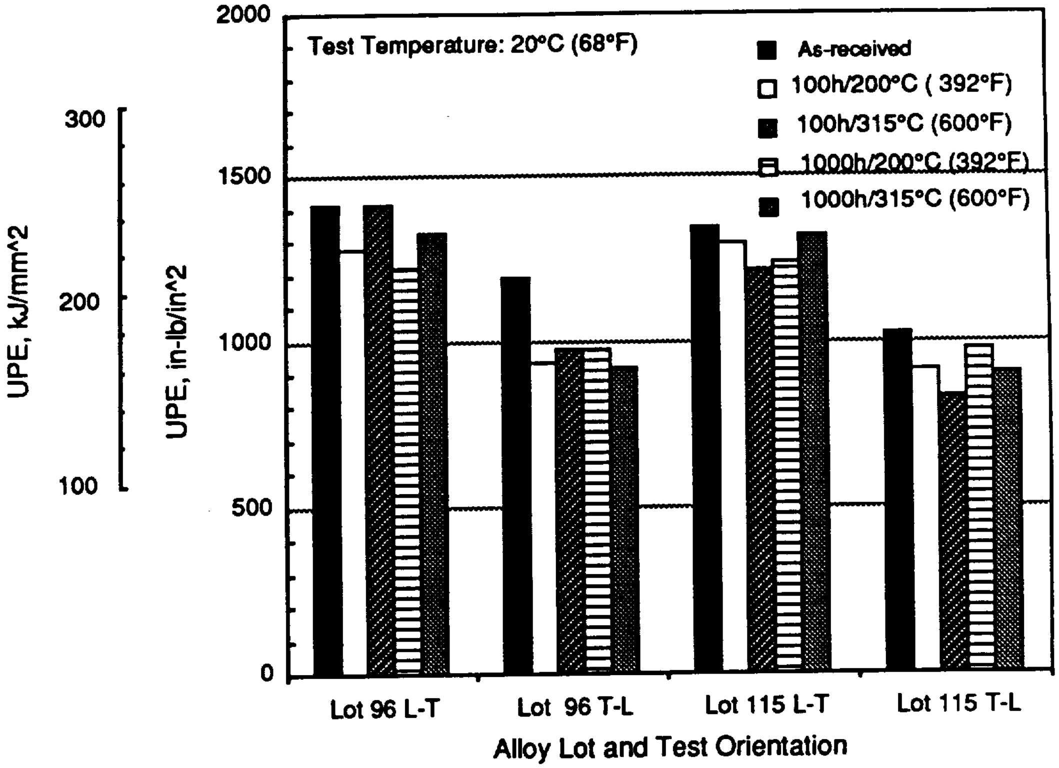

**Fig. 22 Effect of Thermal Exposure on Unit Propagation Energy (UPE) of FVS812 Alloy**

In Lot 96, UPE for the L-T orientation is lowered by 11 and 16% after thermal exposure for 100 and 1000h at 200°C (392°F), compared with room temperature values, as shown in Fig. 21. At 315°C (600°F), there was no reduction in UPE after 100h and 7% after 1000h. The lower UPE values in the L-T orientation at 200°C (392°F) may be related to the evolution of water vapor and hydrogen from reactions involving adsorbed $H_2O/O_2$ mixtures and hydrated aluminum oxides, as noted above for the effect of thermal exposure on tensile elongation. In the T-L orientation, reductions in UPE with temperature ranged from 22 to 30%.

There appears to be no overall clear systematic effects of degas time on UPE, as shown in Fig. 22. At room temperature, UPE values for Lot 96 are 6 and 16% greater than that of Lot 115 for the L-T and T-L orientations, respectively. The effects of various thermal exposures on UPE are mixed and are not well understood at this time. In general, the UPE values of the Lot 115 alloy appear slightly more uniform which may be related to extended degassing. The variation in UPE values ( and tensile yield strength) is greater in Lot 96 than in Lot 115. In Lot 96, L-T and T-L values ranged from 16 to 30% ( yield strength ranged from 6 to 8%). In Lot 115, L-T and T-L ranged from 10 to 24% ( yield strength ranged from 4 to 11%).

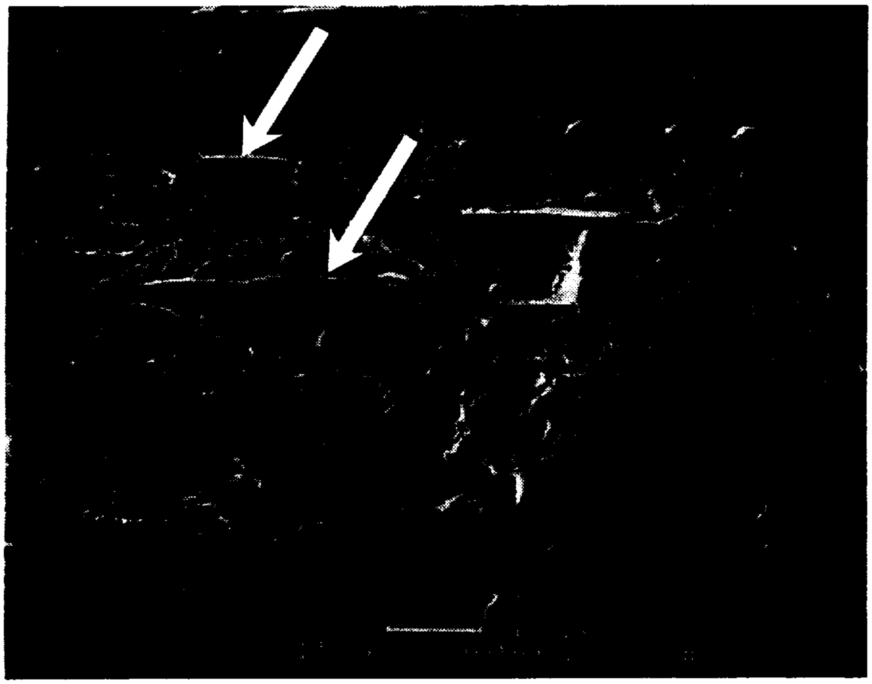

**Fig. 23** **Fracture Surface of Kahn Tear Test Specimen: FVS812 (Lot 115, 20 h Degas), T-L (Arrows Point to Typical Secondary Cracking)**

Overall, the FVS812 alloys appear to provide a superior level of tear resistance relative to other aluminum alloys, as shown by a comparison of UPE as a function of yield stress in Fig. 24. There is a tendency for the UPE of both lots of the FVS812 alloys in the T-L orientation to decrease with yield stress, which is similar to the other alloys shown. However, the results are mixed for the L-T orientation of the FVS812 alloys: the UPE of Lot 115 decreases with yield strength but that of Lot 96 increases which can't be explained at this time. Obviously, a wider range of data is required to verify such trends. The FVS812 alloys have relatively good notch toughness compared with conventional ingot metallurgy aluminum alloys based on a comparison of tear strength to yield strength (TS/YS) ratios. The TS/YS ratio for the L-T orientation of both lots of FVS812 tend to be less sensitive to thermal exposure than the T-L orientation. The TS/YS ratio of the Lot 115 (20 h degas) alloy was slightly more consistent than that of the Lot 96 (2 h degas) alloy over the range of conditions evaluated. In comparison, 2024-T81 and 2219-T62 are far more sensitive to thermal exposure, as expected (Fig. 25 and 26). Their TS/YS ratios and UPE values increase with thermal exposure, which reflect decreasing yield strength.

The tear resistance of the FVS812 alloys, based on unit propagation energy (UPE) measured by the Kahn Tear test, is very high compared with other aluminum alloys. UPE values of the L-T orientation for both lots of FVS812 are significantly greater than those of the T-L orientation. The lower T-L values are most likely associated with the low fracture resistance of prior ribbon particle boundaries. A minimum in UPE at 200°C was observed in both lots of FVS812 after thermal exposure and may be related to hydrogen effects but needs to be substantiated.

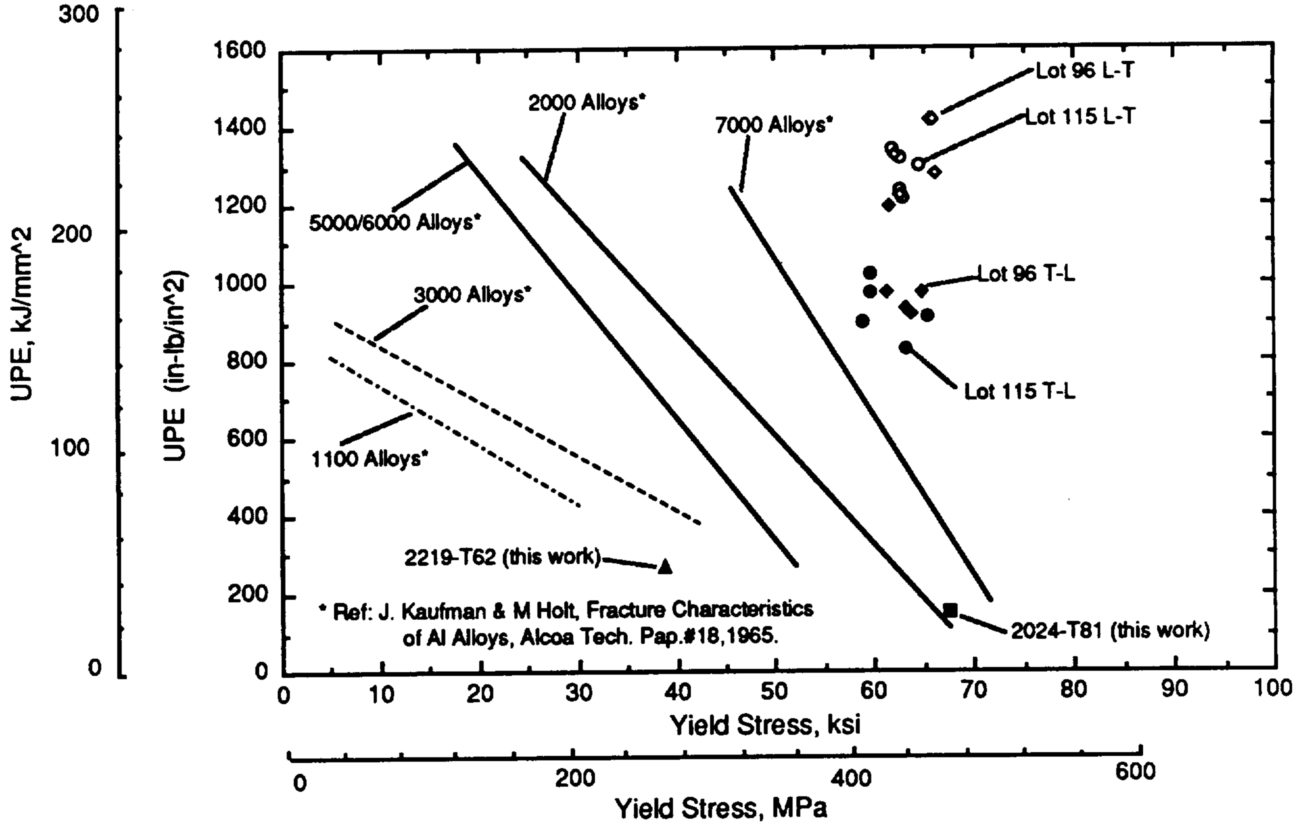

**Fig. 24** Comparison of Unit Propagation Energy (UPE) vs Yield Stress for FVS812 and Various Classes of Aluminum Alloys

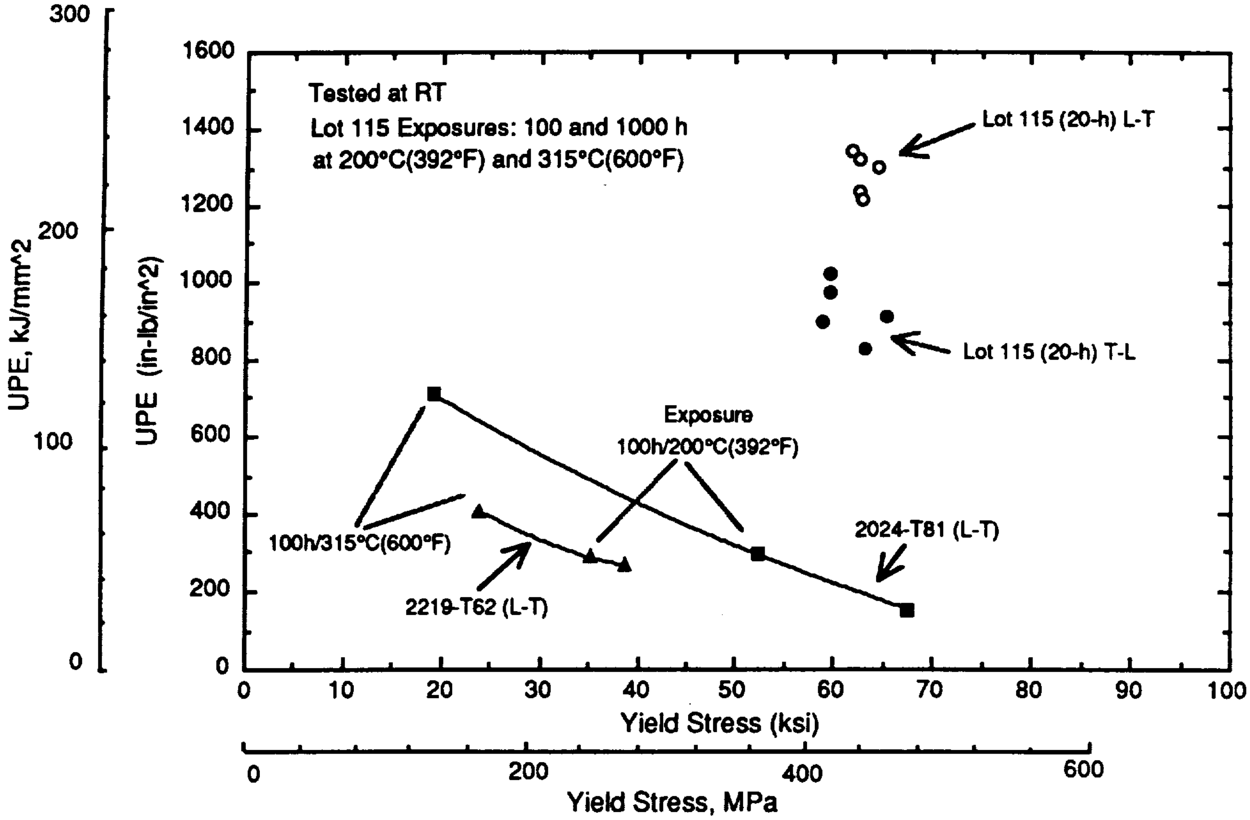

**Fig. 25 Effect of Thermal Exposure on Unit Propagation Energy (UPE) on FVS812, 2024 and 2219 Al Alloys**

***Fatigue.*** In general, the S-N fatigue behavior of FVS812 was acceptable under the conditions tested. There was virtually no anisotropy exhibited and the stability of the strengthening dispersoids appeared to be excellent for all conditions. Fatigue behavior for the extended 20 h degassed alloy, Lot 115 and the standard degassed alloy, Lot 96, before and after thermal exposure at 315°C (600°C) for 100h for the L and LT orientations is shown in Fig. 27-29 and in Fig. 30-32, respectively ( The data are presented in Tables A-11, A-12 and A-13). The S-N curves for each condition are plotted as a minimum line, with all data points lying on or above the lines shown. For the Lot 115 material, it can be seen that very little difference exists between these conditions, especially from the mid-life range of 100,000 cycles to the high cycle range where the S-N curves are nearly superimposed .

For Lot 96, no difference appeared to exist between the fatigue life of the longitudinal and transverse conditions (Fig. 30 and 31). However, after exposure at 100h/315°C, fatigue strength increased approximately 20% for both the L and T conditions (Fig. 32). This effect may be related to the results observed in this work for the tensile elongation and Kahn UPE toughness after thermal exposure and may involve hydrogen evolution and migration. In this case, it appears that fatigue crack initiation life was enhanced in the Lot 96 (2 h degassed) material after thermal exposure. This effect was not observed in the Lot 115 (20 h degassed) alloy. No data are available relating to the fatigue crack initiation or

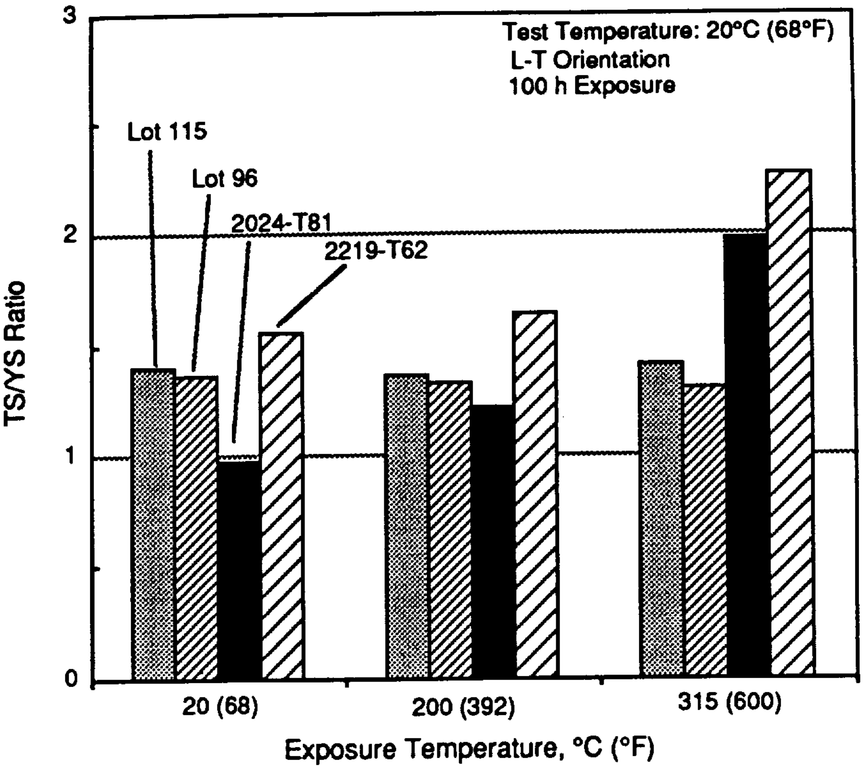

**Fig. 26** **Comparison of Tear Strength/Yield Strength (TS/YS) Ratio for FVS812, 2024-T81 and 2219-T62**

fatigue crack growth behavior at room and intermediate temperatures for the FVS812 alloy.

The fatigue life of each alloy after thermal exposure at 315°C for 100 h is comparable to that of 2024-T81 from the mid-life to high cycle range, as shown in Fig. 33. The 2024-T81 alloy was tested in the as-received condition only, since thermal exposure at 315°C reduced tensile strength by approximately 50%. The effect of test temperature on fatigue life is shown in Fig. 34-36. In general, fatigue behavior of both FVS812 alloy degas conditions was essentially identical at elevated temperature and there was no significant effect of sheet orientation. At 100,000 cycles, fatigue strength at 200°C (392°F) is reduced approximately 20% from the room temperature condition and, at 315°C (600°F), by approximately 38%. However, a comparison between the two degassed conditions at room temperature shows improved fatigue life for the 20 h degassed material. For example, maximum stress for the 20 h material is 20% higher at $10^7$ cycles (Fig. 36). This improvement in fatigue strength may be related to extended billet degassing.

There was no apparent effect due to dynamic strain aging (DSA) during testing at 200°C (392$^o$F) . An effect of DSA resulting in reduced plasticity might be more apparent during low cycle fatigue testing under strain controlled conditions or at points of stress concentration in structures subjected to cyclic service loadings, such as fastener holes in conventional built-up panels. In fact, knowledge of fatigue crack initiation and growth is critical to the development of accurate life predictions for uncracked structure. Based on

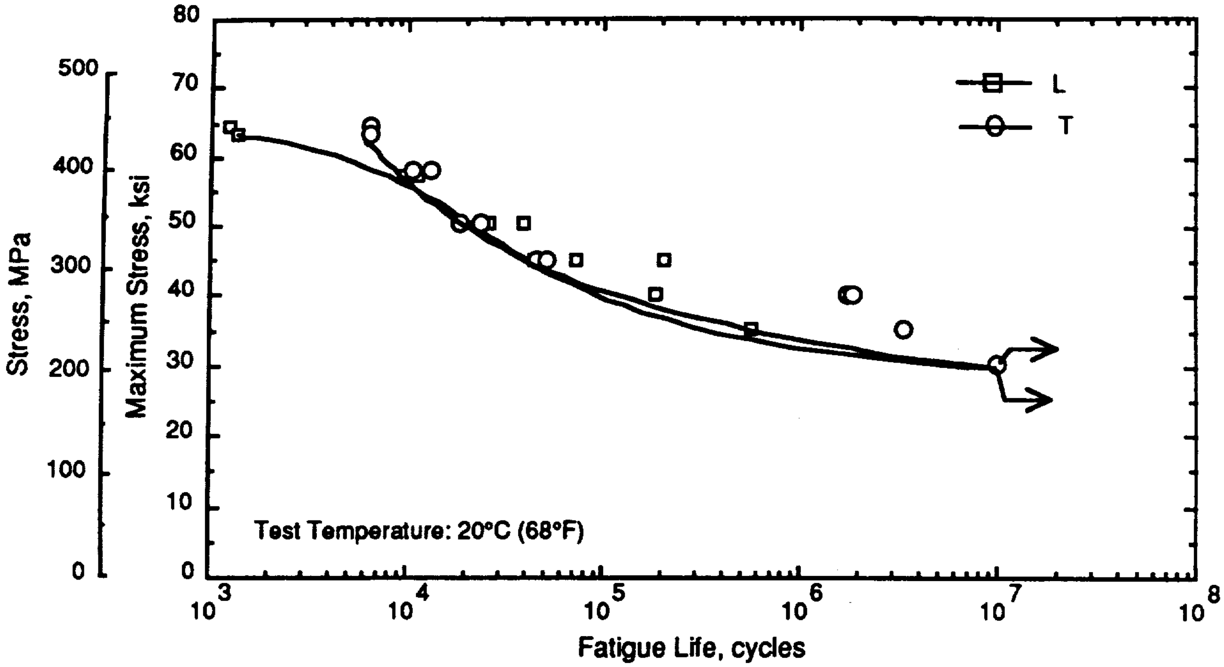

Fig. 27 Stress-Life (S/N) Fatigue Behavior in As-Received FVS812 (Lot 115, 20 h Degas) for L and T Direction

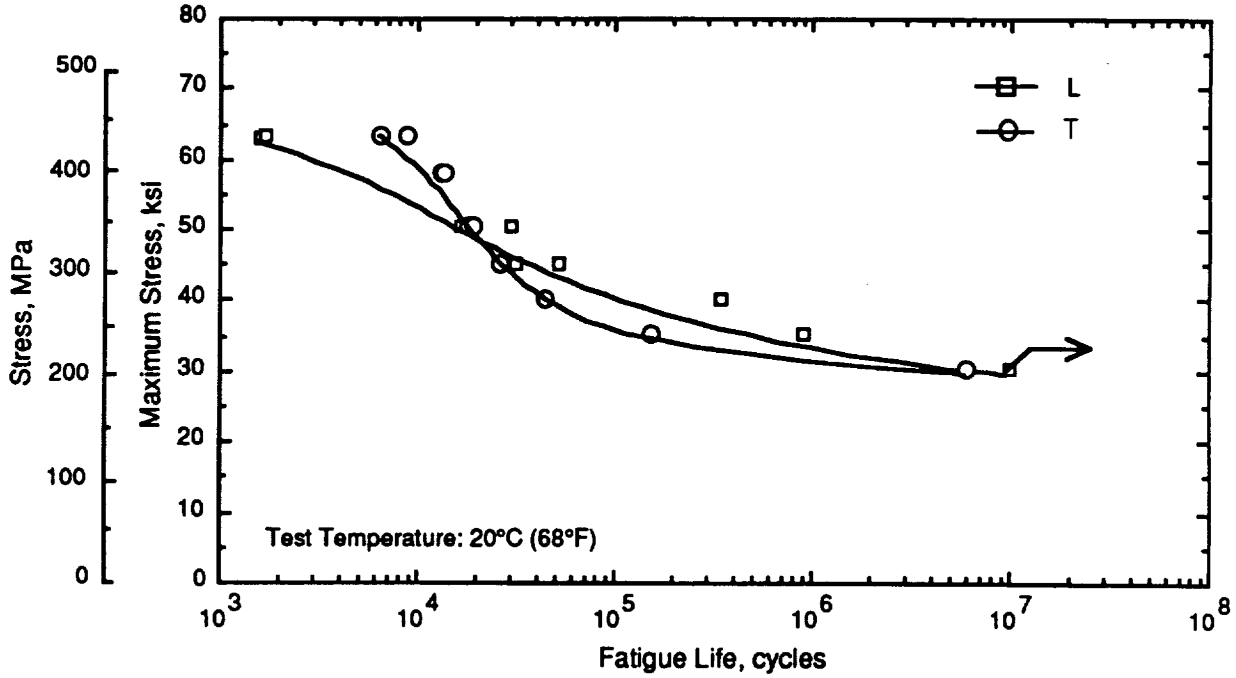

Fig. 28 Stress-Life (S/N) Fatigue Behavior in FVS812 (Lot 115, 20 h Degas) After Thermal Exposure for 100 h at 315°C for L and T Direction

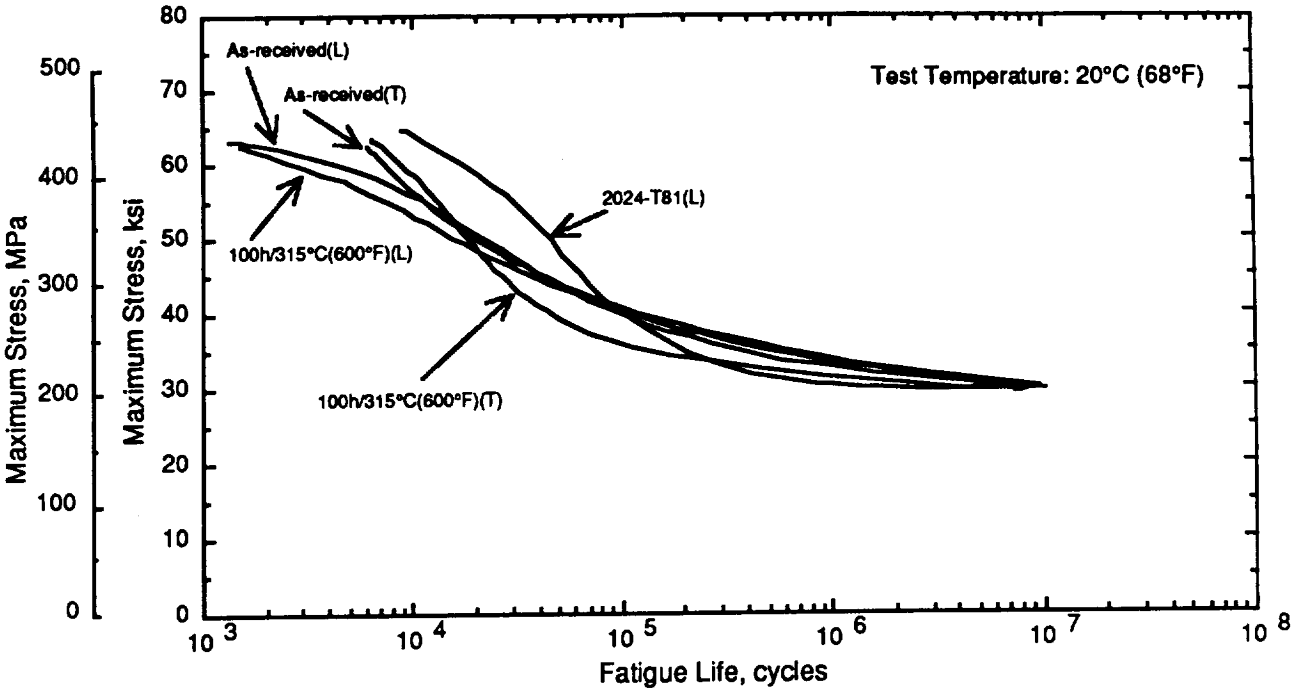

Fig. 29 Effect of Thermal Exposure on Fatigue Life in FVS812 (Lot 115, 20 h Degas)

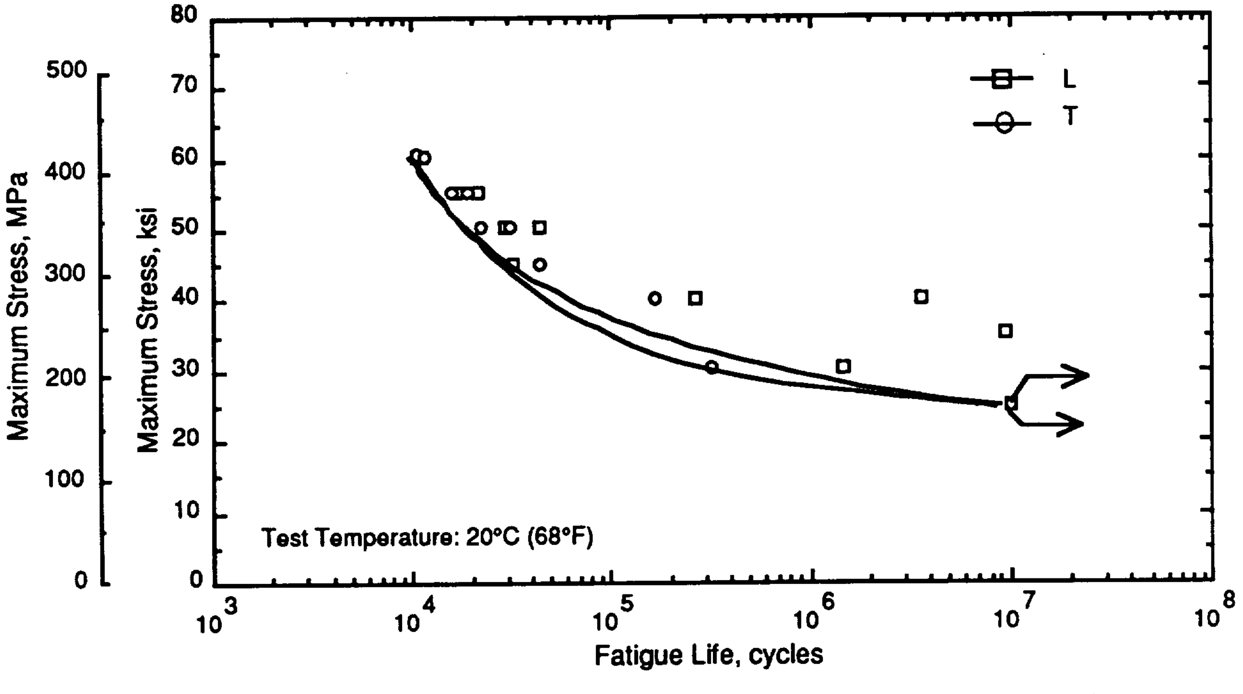

Fig. 30 Stress-Life (S/N) Fatigue Behavior in As-Received FVS812 (Lot 96, 2 h Degas) for L and T Direction

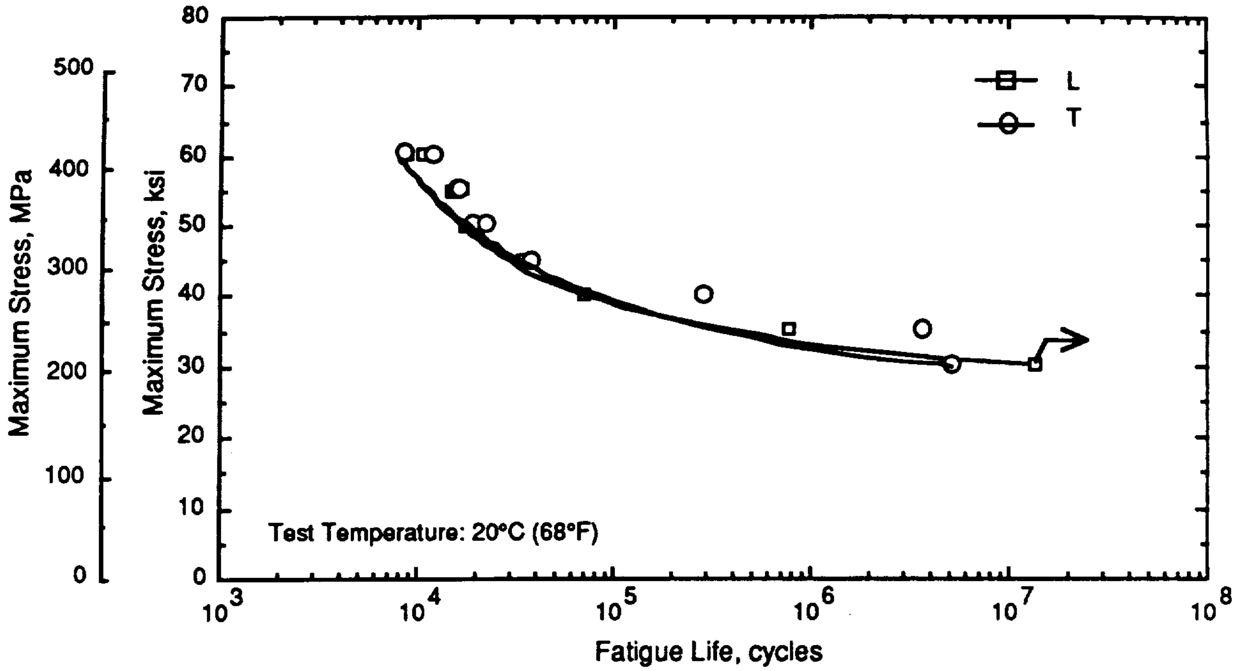

**Fig. 31 Stress-Life (S/N) Behavior in FVS812 (Lot 96, 2 h Degas) after Thermal Exposure for 100 h at 315°C for L and T Direction**

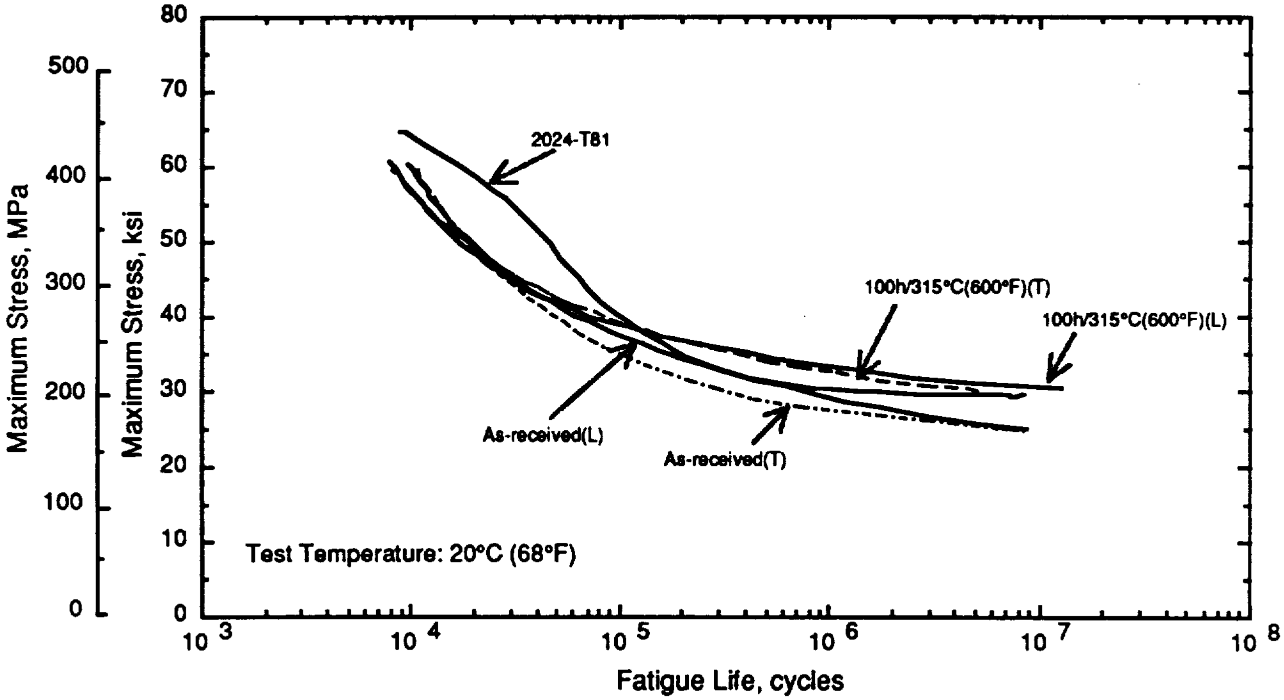

**Fig. 32 Effect of Thermal Exposure on Fatigue Life in FVS812 (Lot 96, 2 h Degas)**

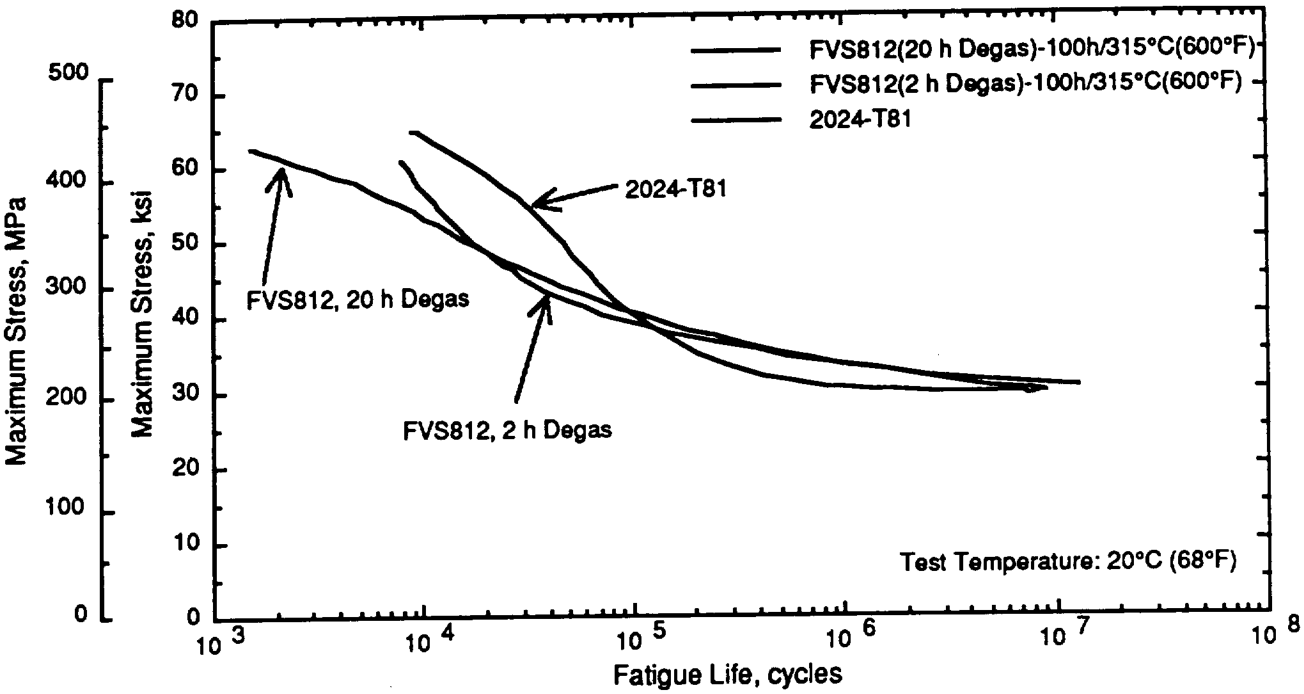

Fig. 33 Comparison of Fatigue Life Between 2 h and 20 h Degassed Material After Thermal Exposure of 100 h/315°C (L Orientation)

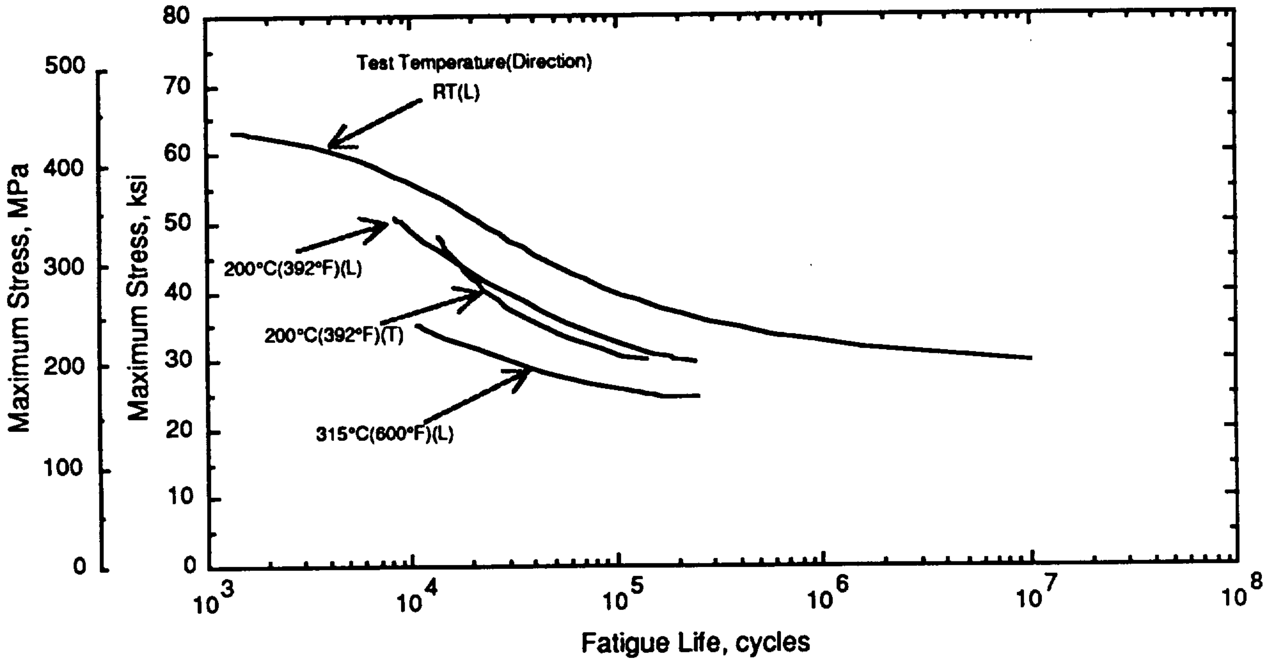

Fig. 34 Effect of Test Temperature on Fatigue Life in FVS812 (Lot 115, 20 h Degas)

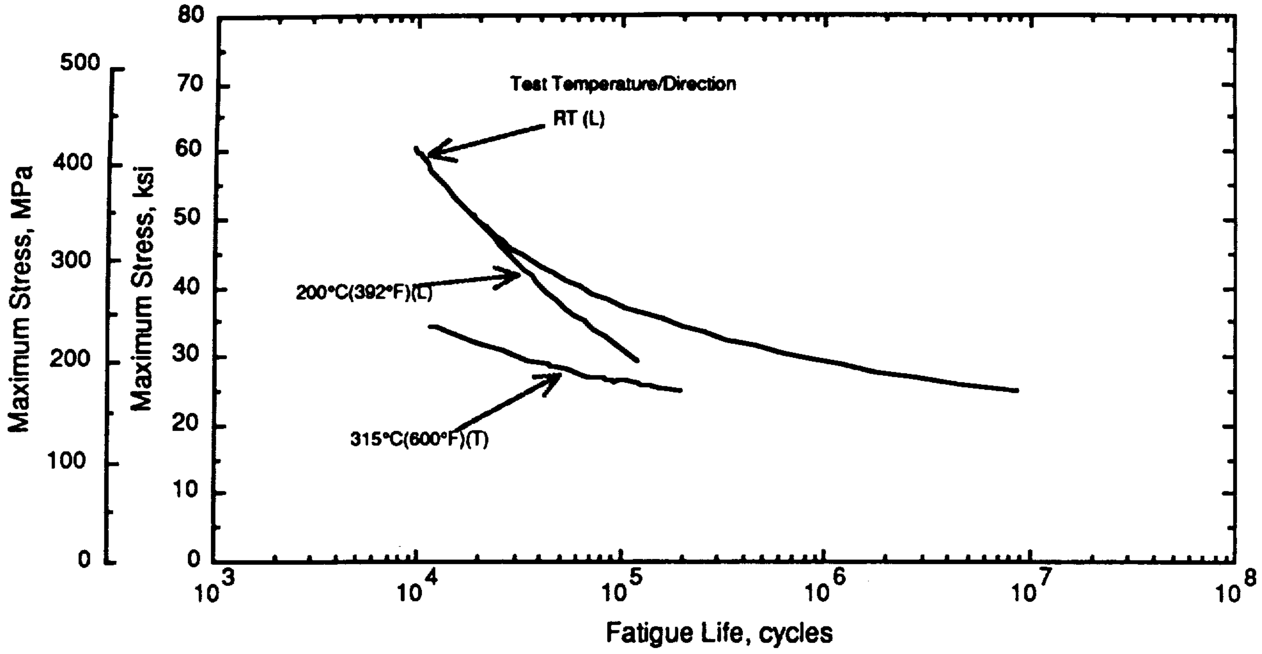

**Fig. 35 Effect of Test Temperature on Fatigue Life in FVS812 (Lot 96, 2 h Degas)**

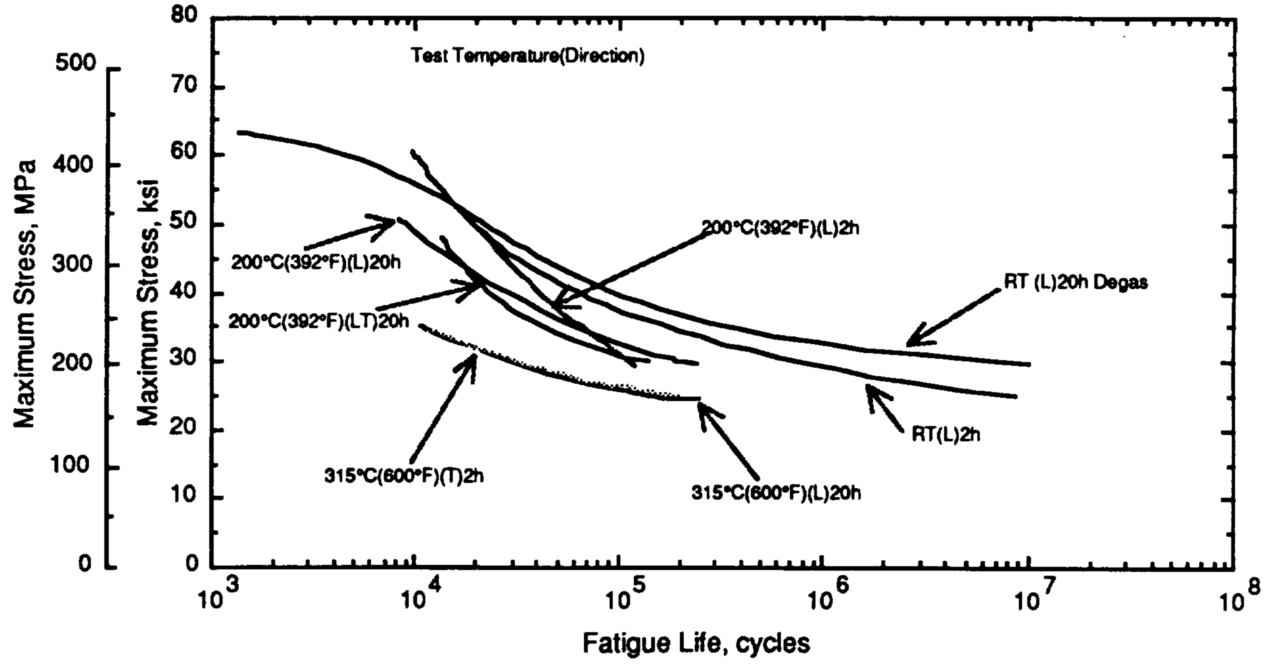

**Fig. 36 Comparison of Fatigue Life in 2 h and 20 h Degassed Material as a Function of Test Temperature**

the general improvement in elevated temperature strength of the Al-Fe-V-Si alloys compared with conventional aluminum alloys, the expected improvement in fatigue life should be significant, especially after long term thermal exposure of structural components. The fatigue crack propagation of other RS alloys, Al-8Fe-4Ce and Al-4.7Fe-4.7Ni-0.2Cr, were not found to be superior to that of 2219-T87 when tested at 25 and 300°C (600°F) but, apparently, there was no long term exposure before testing (28).

Fractographs for Lot 115 after high cycle fatigue at room temperature show the typical fissuring along prior ribbon boundaries which seems to be characteristic for these materials (Fig. 37). Fatigue striations were not observed in any of the samples examined, which is attributed to the extremely fine grain size of the material. Fatigue crack initiation usually occurred at the surface of each specimen. However, two unusual failures occurred with internal initiation sites, both due to contaminants. The first was observed in the Lot 115 material and involved premature failure at a relatively low maximum stress at which run-out was expected (Fig 38). Since SEM/EDAX analysis indicated that the particle basically had the same composition as the surrounding material, it was concluded that the initiation site was agglomerated silicide formed during processing. The fracture surface of the particle had striation-like markings. The other case occurred in Lot 96 material after $5.2 \times 10^6$ cycles and involved initiation at a particle rich in iron and chromium. This was attributed to a piece of stainless steel screen that had broken off during the powder separation process (Fig. 39). Striation-like markings also were observed on the fracture surface of the particle, indicating stable fatigue crack growth in that region.

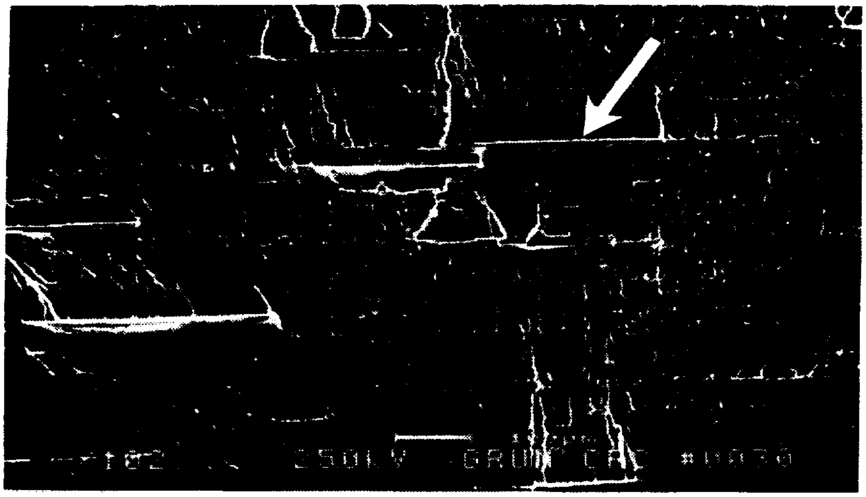

a) TYPICAL FISSURING (ARROW)

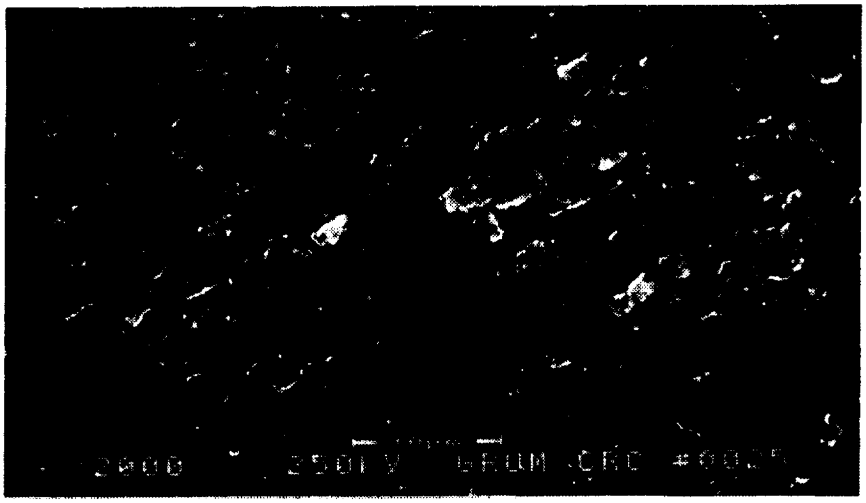

b) INITIATION REGION

c) FAST FRACTURE REGION

**Fig. 37 Fracture Surface in FVS812 Alloy (Lot 115, 20 h Degas) After High-Cycle Fatigue (3.4 x $10^6$~) at Room Temperature**

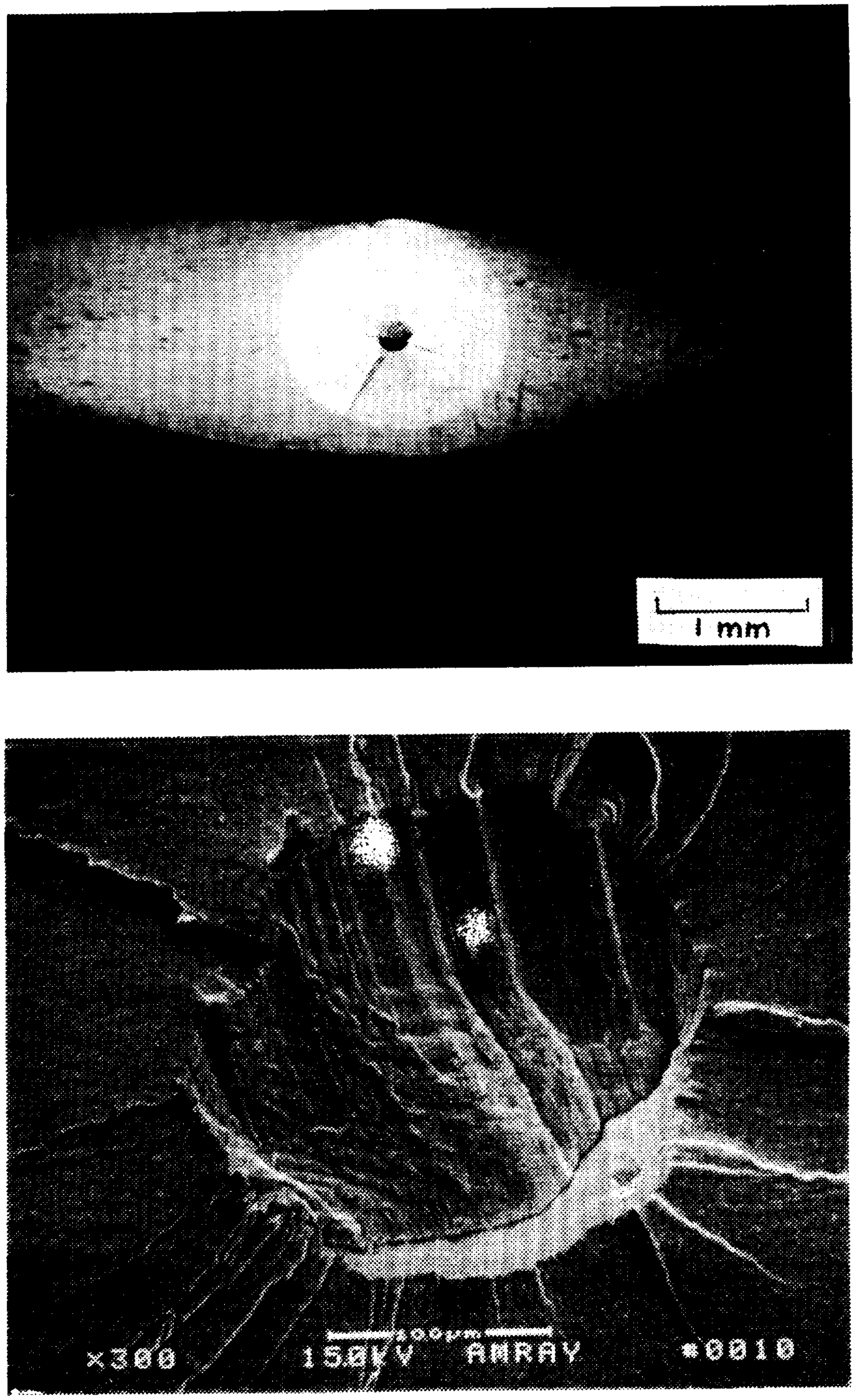

**Fig. 38** Fatigue Fracture in FVS812 Alloy (Lot 115, 20 h Degas) at Internal Initiation Site (321,000 ~)

ORIGINAL PAGE
BLACK AND WHITE PHOTOGRAPH

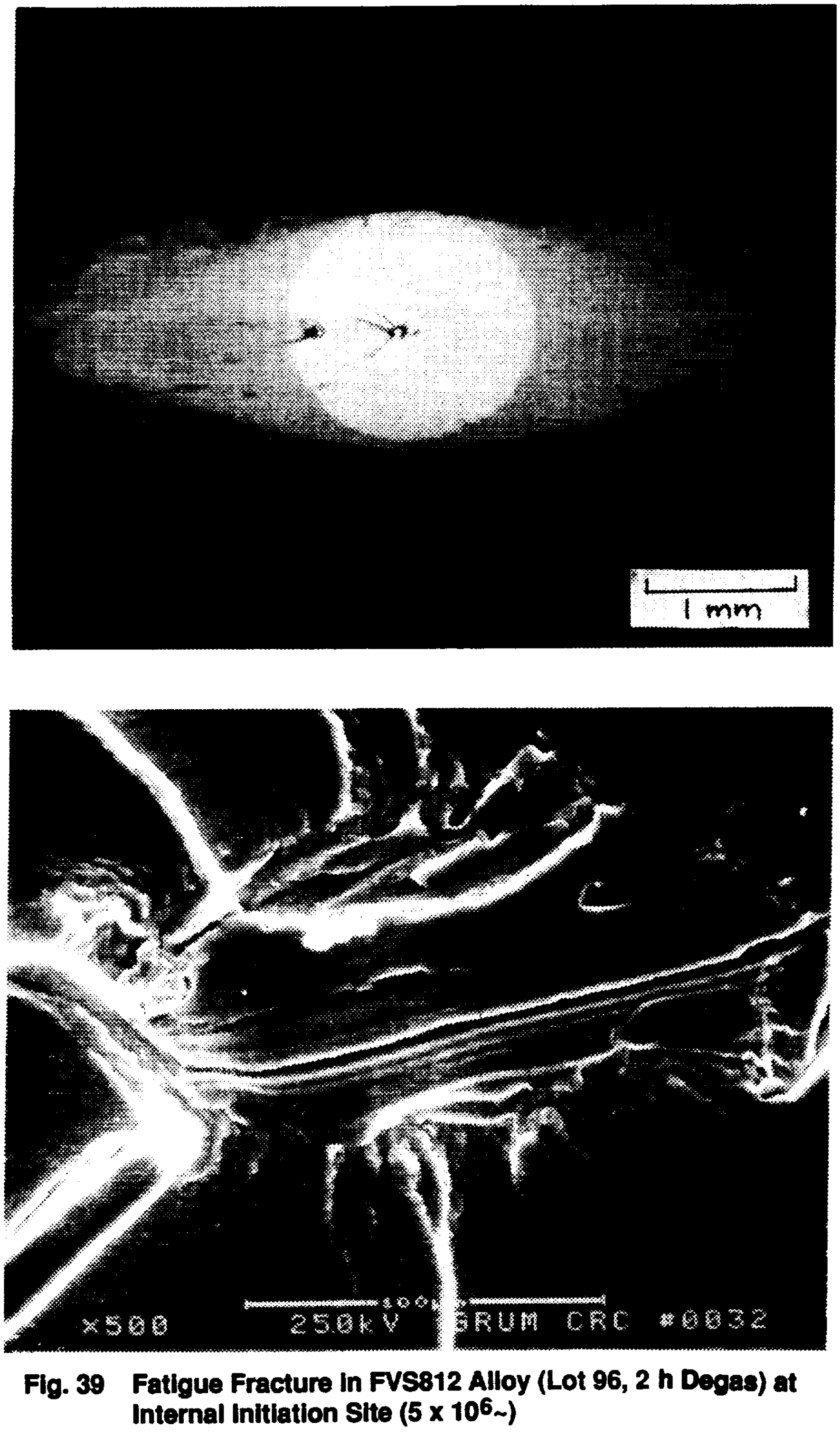

Fig. 39 Fatigue Fracture in FVS812 Alloy (Lot 96, 2 h Degas) at Internal Initiation Site (5 x $10^6$~)

### 5.3 FORMING TESTS

***Hot Forming - 90° Bends.*** The results of hot bending tests at room temperature to 500°C (930°F), with a 90° fixed bend angle and radii ranging from 0.79 mm (0.031 in.) to 4.76 mm (0.188 in.) are presented in Table 5. Minimum bend radii, without cracking, are indicated for each condition tested. Slight cracking, as noted, refers to cracks that were no more than approximately 1.5 mm long and intermittently spaced along the outside bend radius. At room temperature and up to 275°C (530°F), bends made with the bend-line perpendicular to the sheet rolling direction had lower minimum bend radii and tended to crack less than bends made parallel to the rolling direction. The more recent FVS812 material, Lot 335 (2 h degas) and Lot 340 (20 h degas), had lower bend radii at room temperature than the earlier material. But all lots of material exhibited poor bending at room temperature, when the bend-line was parallel to the rolling direction.

The data indicate that unidirectional formed parts, such as zees or channels, may be formable at room temperature when the bend-line is perpendicular to the sheet rolling direction. Stiffeners formed in such a manner may be desirable because the FVS812 alloys have higher compressive yield strength in the transverse direction. In this work the zee-stiffeners used for the compression test panel were oriented for loading in the transverse direction. When forming was conducted at approximately 370°C (700°F) or higher, very low bend radii were possible in both sheet directions, with radii as low as 0.8mm (1/32"). Spring back was negligible at these temperatures. Spring back at 80°C (175°F) was more pronounced than at the higher temperatures. Also, radii at this temperature were not as defined as at the other temperatures.

The worst temperature range for forming was between 80 to 275°C (175-530°F), where minimum bend radii were higher and cracking was more severe. In some cases, as noted, excessive cracking occurred along the entire length of the outside bend radius, virtually separating the flanges. This minimum in ductility also was observed during tensile testing (Fig. 13) and is attributed to dynamic strain aging.(23, 24, 25). The hardness of the formed samples increased when the forming temperatures were $\geq$275°C (530°F), as shown in Fig. 40. This is consistent with the systematic increases observed in compressive yield strength in the L and T orientations after annealing at 300, 400, and 500°C (570, 750 and 930°F) (Fig. 16).

The effect of hot forming on dispersoid stability and strength was evaluated by measuring hardness of formed samples at the maximum bend point, from the inner to the outer radius of the bend, where the reductions in area were approximately 5%. Typical data, shown in Fig. 41, indicate that there was no change in hardness in the material compared with unformed material. Therefore, it appears that slight reductions in area during forming did not cause significant strain induced coarsening and softening. This correlated well with hardness measurements along the test gage of tensile specimens, in the uniform deformation region (5% reduction of area). Hardness did not change signifi-

## Table 5 Minimum 90° Bend Radii of FVS812 Alloys

| Alloy (3) | Bend Orientation to Sheet R.D. | RT | Bend Temperature | | | | | | | |
|---|---|---|---|---|---|---|---|---|---|---|
| | | | 80°C(176°F) | 175°C (347°F) | 275°C (527°F) | 315°C (600°F) | 390°C (734°F) | 445°C (833°F) | 500°C (930°F) |
| Lot 96 (2 h Degas) | parallel | >3T(4) | >3 T (1) | >3 T (2) | 3 T | 2.2 T | 0.5 T | 0.5 T | 0.5 T |
| | perpendicular | 1.5 T | 3 T | >3 T (1) | >3 T (1) | 2.2 T | 0.5 T | 0.5 T | 0.5 T |
| | 45° | >3T(4) | | | | | 0.5 T | 0.5 T | 0.5 T |
| Lot 115 (20 h Degas) | parallel | >3T(4) | >3 T (1) | >3 T (2) | 3 T | 1.5 T | 0.5 T | 0.5 T | 0.5 T |
| | perpendicular | 1.5 T | >3 T (1) | 2.2 T | 0.75 T | 1.5 T | 0.5 T | 0.5 T | 0.5 T |
| Lot 335 (2 h Degas) | parallel | >3T(4) | | | | | | | |
| | perpendicular | 0.5 T | | | | | | | |
| Lot 340 (20 h Degas) | parallel | >3T(4) | | | | | | | |
| | perpendicular | 0.5 T | | | | | 0.5 T | 0.5 T | 0.5 T |

(1) Slight cracking: ≤1.5 mm (0.06 in.) long cracks, intermittently spaced on outside bend radius

(2) Excessive cracking along entire length of outside bend radius

(3) Sheet thickness, T,= 1.6 mm (0.063 in.)

(4) Minimum bend radius >3T but actual minimum not determined

cantly in that region as a result of tensile deformation. However, hardness in the highly deformed necked region (~ 35 % reduction in area) dropped about 5 %, which may be attributed to strain coarsening (Fig. 42). This is consistent with previous work that showed relatively little strain-enhanced and non-strain-enhanced silicide coarsening at temperatures below 500°C (932°F) (6). In that work, grain size in the deformed samples was very similar to the as-received grain size after deformation at 600°C (1112°F) and tensile properties were not degraded after short exposures at 500°C (932°F) up to 4 h.

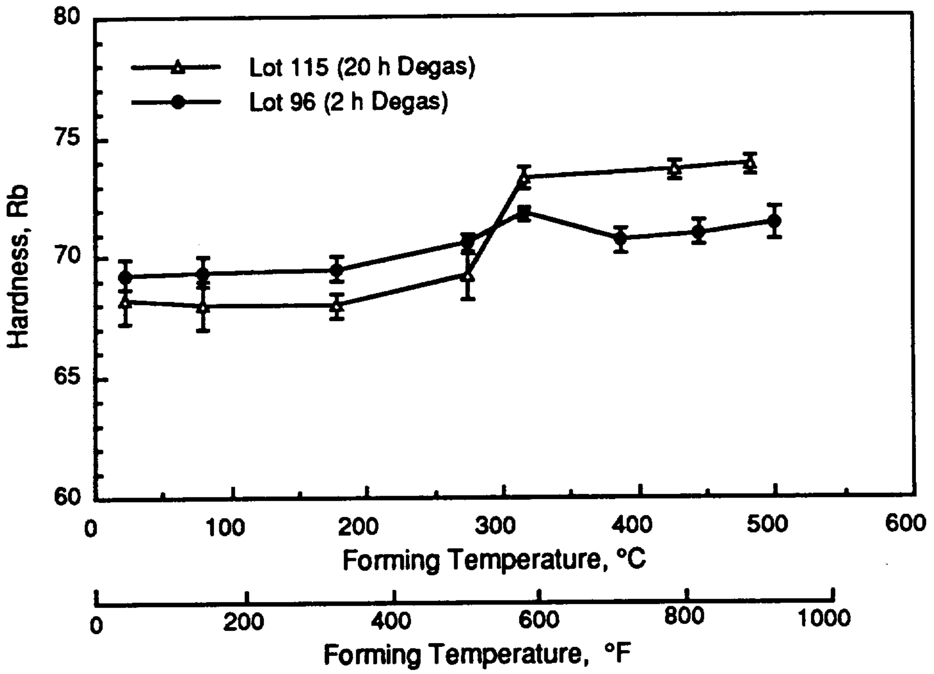

Fig. 40 Effect of Forming Temperature on Hardness of FVS812 Alloys

***Hot Formed Part with Contoured Flange.*** A series of small parts with joggled stretch flanges were fabricated with FVS812 alloy-Lot 110 (2 h degas), 1.6 mm (0.063 in.) thick sheet, by hot wipe-forming from 315°C (600°F) to 480°C (900°F) after various heating times ranging from 2-7 min. The jog was 2.3 mm (0.090 in.) and the bend radius was 3.4 mm avg. (0.135 in.) Acceptable parts, free of cracks at the flanges or radii, were formed at temperatures ≥ 370°C (700°F), as shown in Fig. 43. Some galling or smearing was observed on the outer surfaces of the flanges, where the punch wiped over the material during forming. It is believed that this effect can be eliminated or minimized with proper tool conditioning. Cracking occurred in the flanges during forming at 315°C (600°F), as shown in Fig. 44.

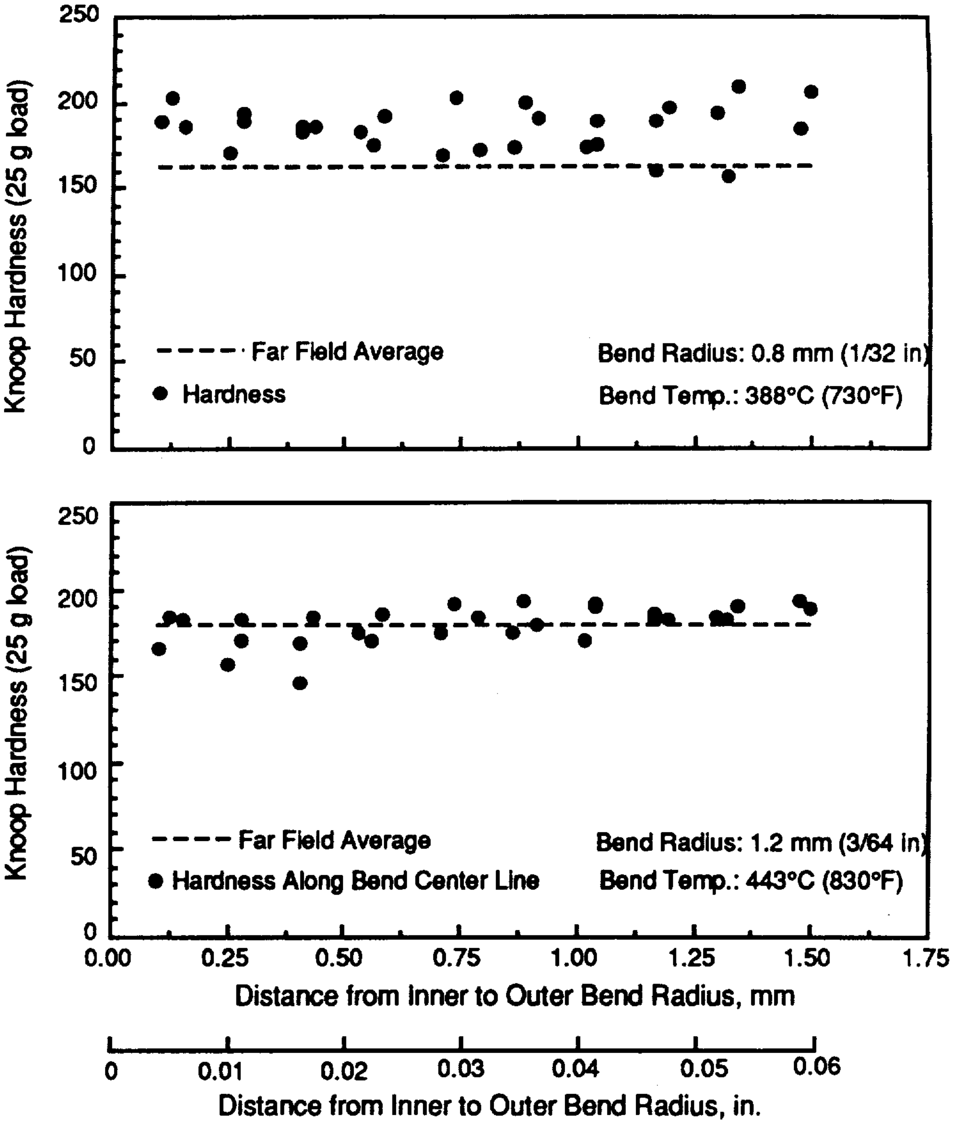

Fig. 41 Effect of Bending on Hardness of FVS812 Alloy (Lot 96, 2 h Degas)

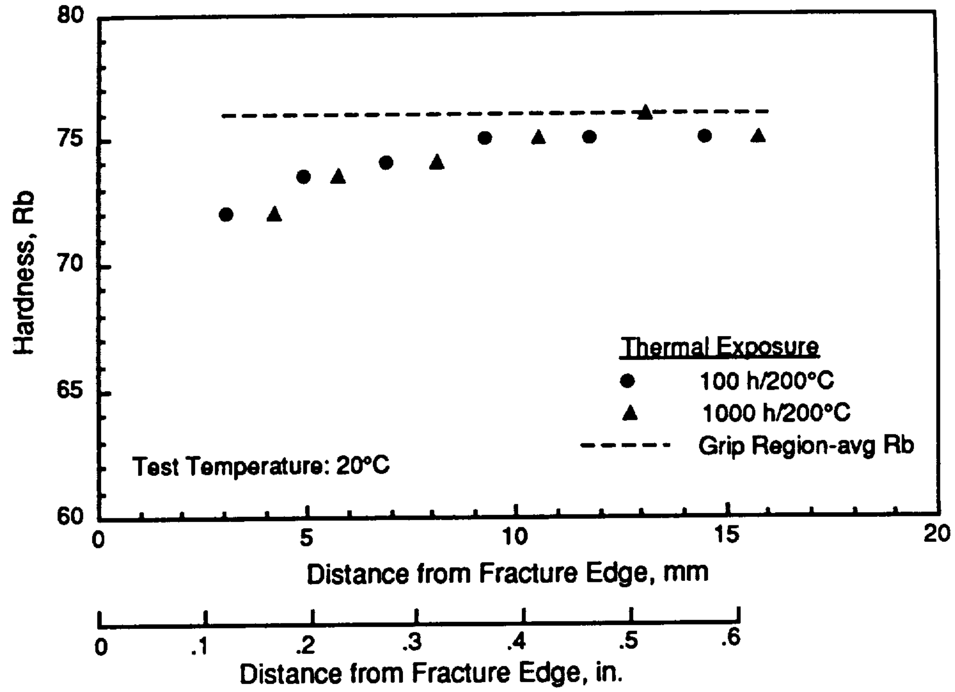

**Fig. 42 Effect of Tensile Loading on Hardness of FVS812 Alloy (Lot 96, 2 h Degas)**

***Hot Formed Part: Pressure-Pad Draw Forming.*** A limited evaluation of hot draw forming the FVS812 alloy was conducted at 455-480°C (850-900°F ). Since an existing die was employed, which normally is used for forming 1.3 mm (0.050 in.) thick titanium alloy, Ti-6Al-4V, it was necessary to chemically mill the FVS812 alloy. Conventional hot and cold chemical milling solutions were evaluated, and, in each case, exceptionally smooth sheet surfaces were achieved after milling from 1.6 to 1.3 mm (0.063 in. to 0.050 in.) thick. Forming resulted in complete tearing at the bottom of the cup, at both ends, as shown in Fig. 45. Two attempts were made to form the part, each with different soak times (0.5 and 1-h) at temperature. The failure sites were characterized by localized necking and tearing, which is consistent with the typically low strain rate sensitivity index, m, observed in this material(6, 29). Since these alloys do not exhibit significant strain hardening, it is possible that extensive deep drawing may not be feasible. It was beyond the scope of this work to evaluate the effect of the significant deep-drawing variables, such as blank shape, clearance, punch and die corner radii, pad pressure, friction and lubrication, and punch speed. The design of drawing dies for irregular shaped parts is complex and analytical studies for work are limited(26, 30). Further work in this area is recommended.

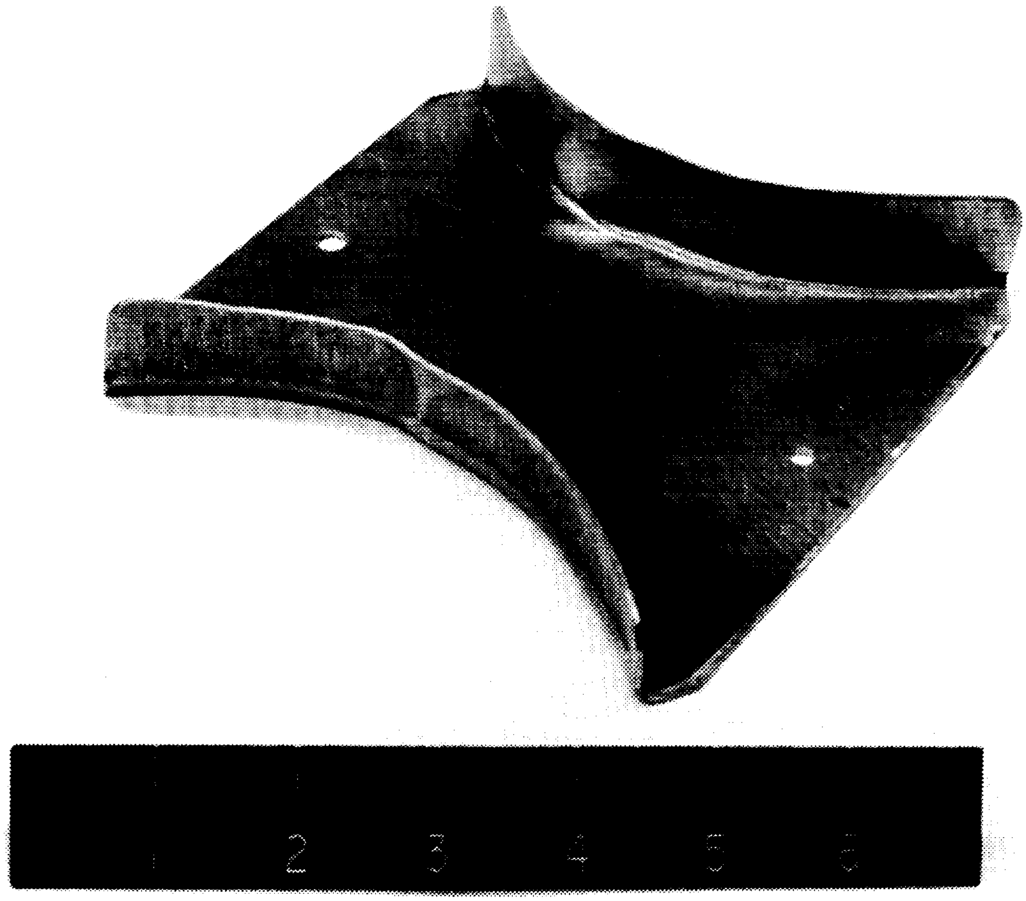

Fig. 43 Hot-Formed Part with Contoured Flange

ORIGINAL PAGE
BLACK AND WHITE PHOTOGRAPH

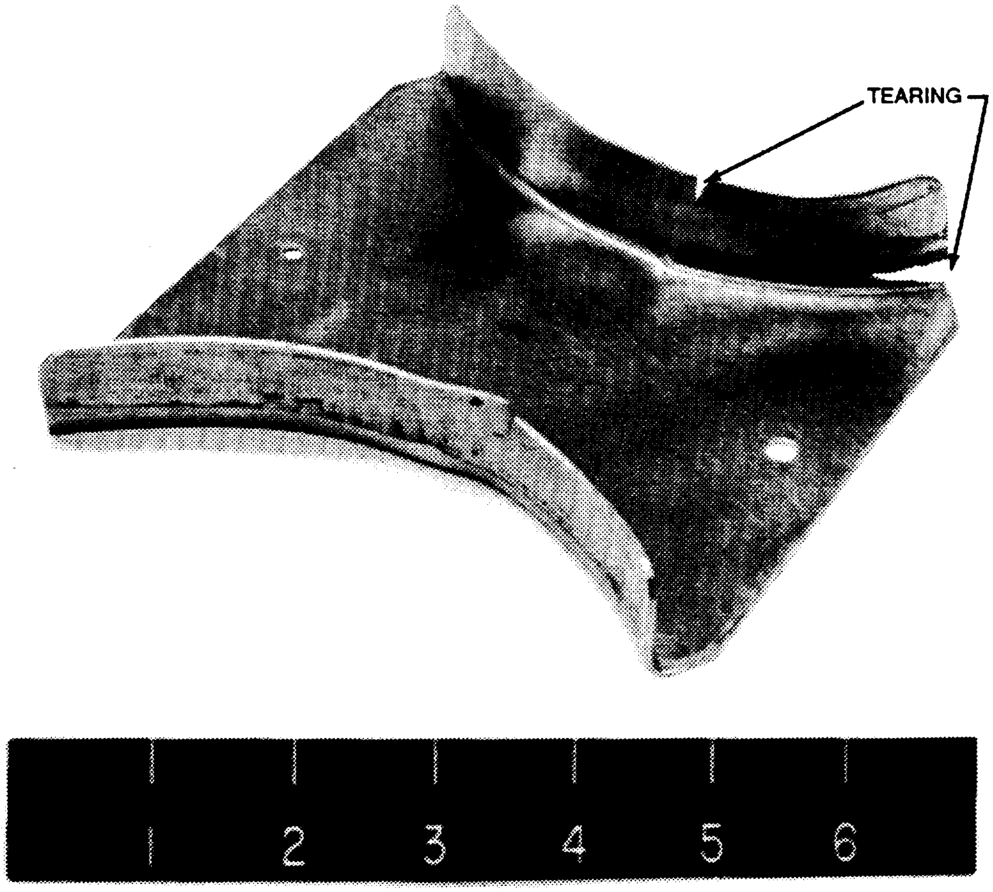

Fig. 44 Formed Part at 315° C (600°F) Showing Tearing

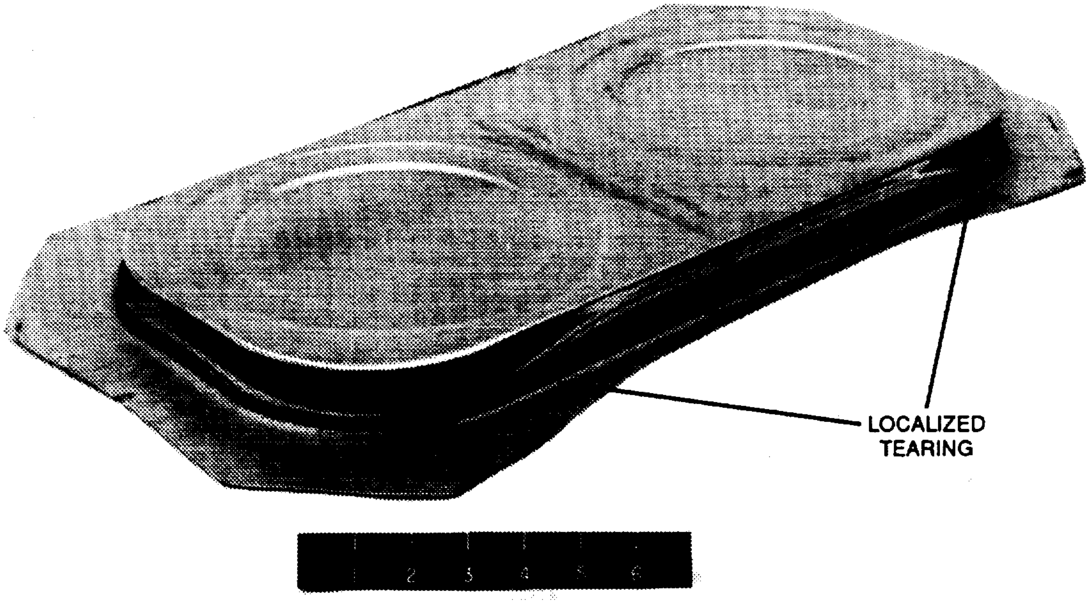

Fig. 45 Hot-Draw-Formed Part

## 5.4 WELDING

***Fusion***.

***Electron beam (EB) welding.*** Electron Beam welds were made in the flat, horizontal and vertical positions for both FVS812 alloy degas conditions, Lots 96 (2 h) and Lot 115 (20 h). The energy input required to produce autogenous welds was approximately 25% less than that required for a typical wrought aluminum alloy such as 5052 (Table 6). All EB welds on the FVS812 alloy exhibited violent, incendiary-like outgassing during welding, which was promoted by the vacuum condition inherent with the EB process. Welding position or alloy degas condition did not diminish the violent outgassing. Radiographs of the weldments and visual inspection revealed massive void formation, as shown in Fig. 46 for an EB butt weld in the horizontal position. Beam oscillation during welding, both longitudinal and transverse, was employed in the attempt to improve weld quality but proved to be ineffectual. Excessive silicide coarsening and formation of primary intermetallic phase due to thermal exposure and melting were observed (Fig. 47). In the weld metal, the long needles tend to be $Al_{13}Fe_4$(Si) and the blocky particles are $Al_7$(Fe,V) or $Al_{13}(Fe,V)_4$ (20).

**Table 6 Electron Beam Welding Parameters**

| Alloy | Voltage kv | Current mA | Travel Speed mm/s (ipm) | Energy Input kJ/mm (kJ/in.) |
|---|---|---|---|---|
| Al 5052 | 25 | 50 | 50 (50) 59.1 | (1.50) * |
| FVS812 | 25 | 40 | 55 (55) 42.9 | (1.09) * |

*Typical acceptable weld parameters

Extended degassing did not have any significant effect on reducing porosity and massive void formation during EBW, even though such an effect was evident during gas-tungsten arc welding. Due to the extreme severity of the outgassing problem no further work was performed using the EB welding process. Therefore, it was not possible to determine if optimization of EBW parameters would lead to minimization of silicide coarsening and acceptable weld joint efficiencies. Other work on electron beam welding of degassed FVS812, with hydrogen levels at approximately 4 wppm, indicated that relatively fine microstructures were retained but weld porosity was not eliminated (31). Defect-free, high integrity EB welds were produced in RS-PM Al-8Fe-2Mo, 0.65 mm thick sheet, with hydrogen below 1 wppm (32). Minimization of weld energy input resulted in an extremely fine microstructure and weld joint efficiencies over 85% but with significantly lower ductility. Based on these results, further research on the effect of improved degassing treatments, lowered hydrogen contents and sheet thickness on EBW is recommended.

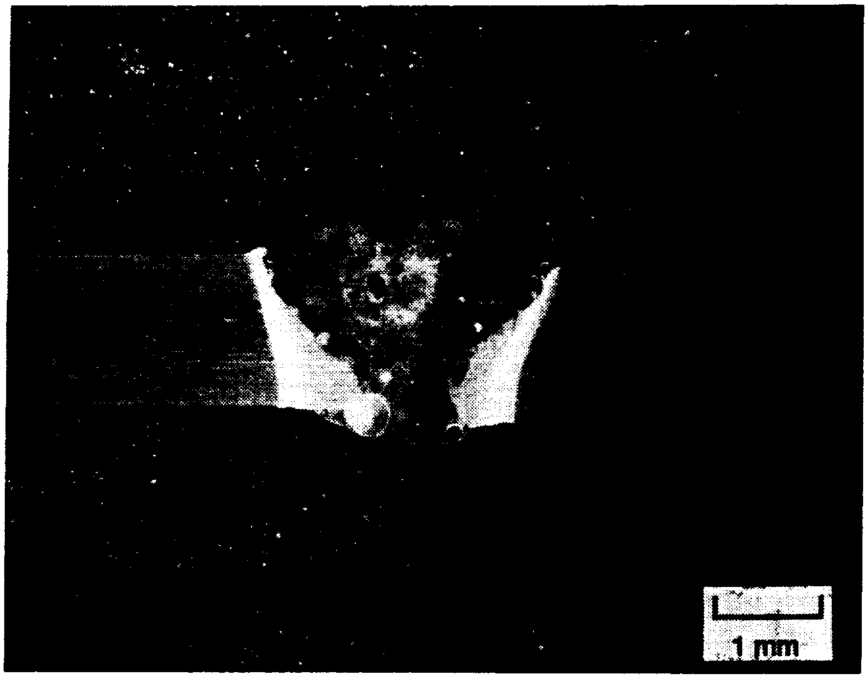

a) WELD CROSS SECTION

b) POROSITY IN WELD METAL

Fig. 46 Electron Beam Weld In FVS812 Alloy (Lot 115, 20 h Degas)

a) WELD METAL: CENTER

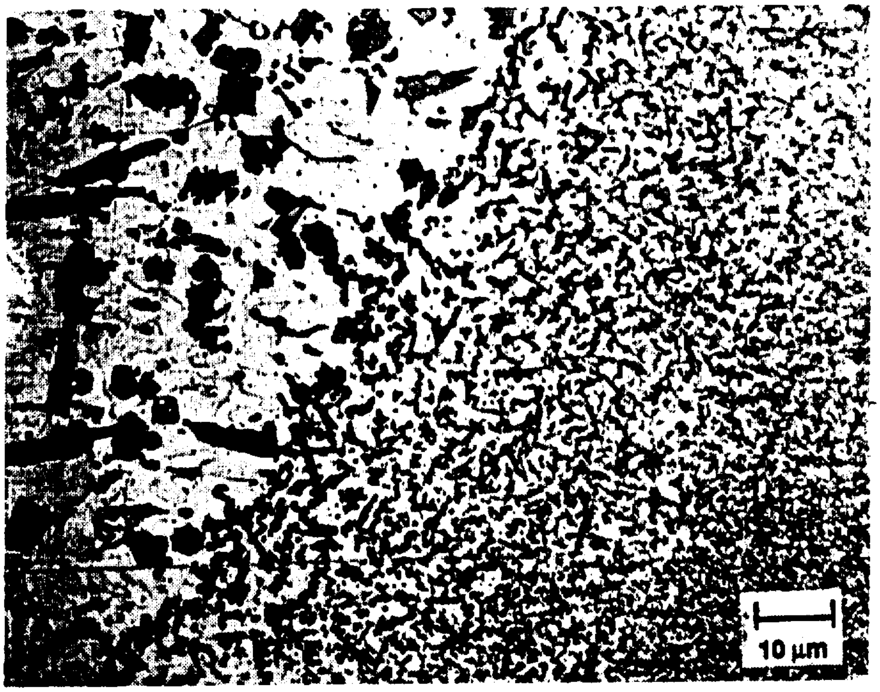

b) WELD METAL: EDGE

**Fig. 47 Microstructure of Electron Beam Weld in FVS812 Alloy (Lot 115, 20 h Degas)**

***Gas-tungsten-arc welding.*** Smooth, continuous autogenous welds were produced in both alloy degas conditions (Lot 96 and Lot 115) with no visual indications of cracks or porosity. Welds were made with various energy inputs in the 20 h degassed material by systematically varying travel speed. The welding parameters are presented in Table 7. The baseline energy input was 228 kJ/m (5.78 kJ/in.), however, energy inputs as low as 127 kJ/mm (3.22 kJ/in.) and as high as 650 kJ/m (6.50 kJ/in.) were achieved. Even the highest energy welds retained acceptable visual characteristics without significant undercut or excessive drop through.

**Table 7 Gas-Tungsten-Arc Welding Parameters**

| Voltage V | Current A | Travel Speed mm/s | (ipm) | Energy Input kJ/mm | (kJ/in) |
|---|---|---|---|---|---|
| 19.5 | 55 | 8.5 | (20.0) | 126.8 | (3.2) |
| 19.0 | 55 | 7.2 | (17.0) | 144.9 | (3.7) |
| 18.5 | 55 | 5.9 | (14.0) | 171.7 | (4.4) |
| 18.0 | 55 | 5.1 | (12.0) | 194.9 | (5.0) |
| 17.5 | 55 | 4.2 | (10.0) | 224.4 | (5.7) * |
| 17.5 | 55 | 3.4 | (8.0) | 284.3 | (7.2) |
| 17.5 | 55 | 2.5 | (6.0) | 379.1 | (9.6) |
| 17.5 | 55 | 1.5 | (3.5) | 653.1 | (16.6) |

*Typical acceptable weld parameters.

Radiographs of welds on the standard 2 h degassed alloy using the baseline energy input 228 kJ/m (5.78 kJ/in.), showed extensive, fine, linear porosity at all edges of the weld. Cross sections of these welds indicated that the porosity was stacked to all depths at the weld edges. Careful examination of the porosity revealed that it was migrating from the fusion interface with the base metal towards the center of the weld. Radiographs and cross sections of welds made on the 20 h degassed material using the baseline energy input showed much less porosity (Fig 48). However, the continuous linearity of the porosity at the edge of the welds made them unacceptable to the requirements of NASA MSFC-SPEC-504B for a Class I weld. Radiographs of the welds made at the fastest speed (lowest energy input) showed the porosity to be scattered throughout the weld in addition to being stacked at the edge (Figs. 49 and 50). As welding speed decreased and energy input increased, the scattered porosity near the center of the weld pool had additional time to escape the weld and was finally eliminated at the slowest speeds, leaving only the edge porosity. However, porosity was never completely eliminated by controlling energy. It must be concluded that although porosity was greatly reduced in the 20 h extended degassed material, it was never totally eliminated. Qualitatively, based on the appearance of weld cross-sections, porosity in the extended degassed material was reduced approximately by an order of magnitude. This dramatic reduction doesn't appear to correlate well with the

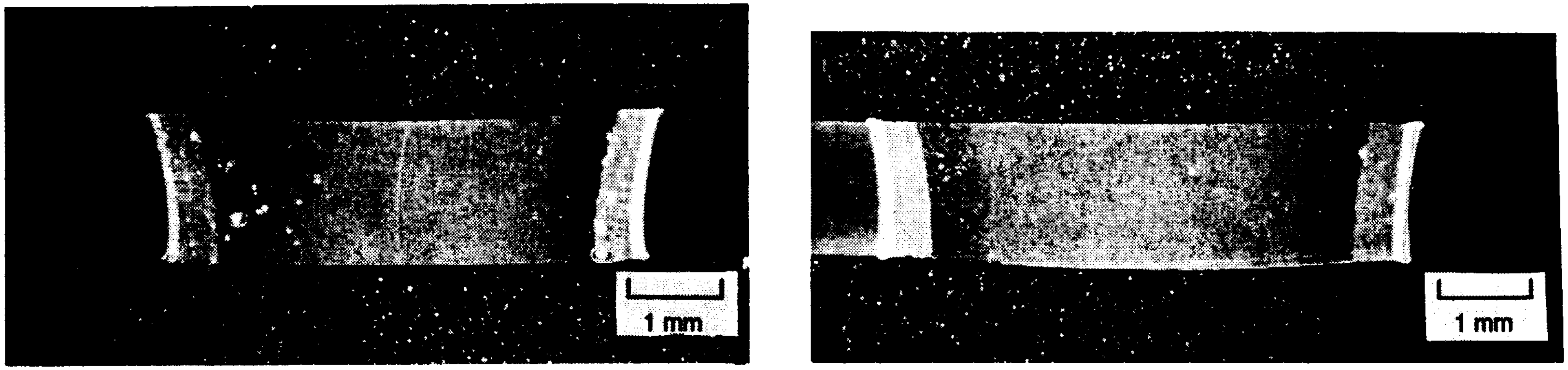

a) LOT 96, 2 h DEGAS

c) LOT 115, 20 h DEGAS

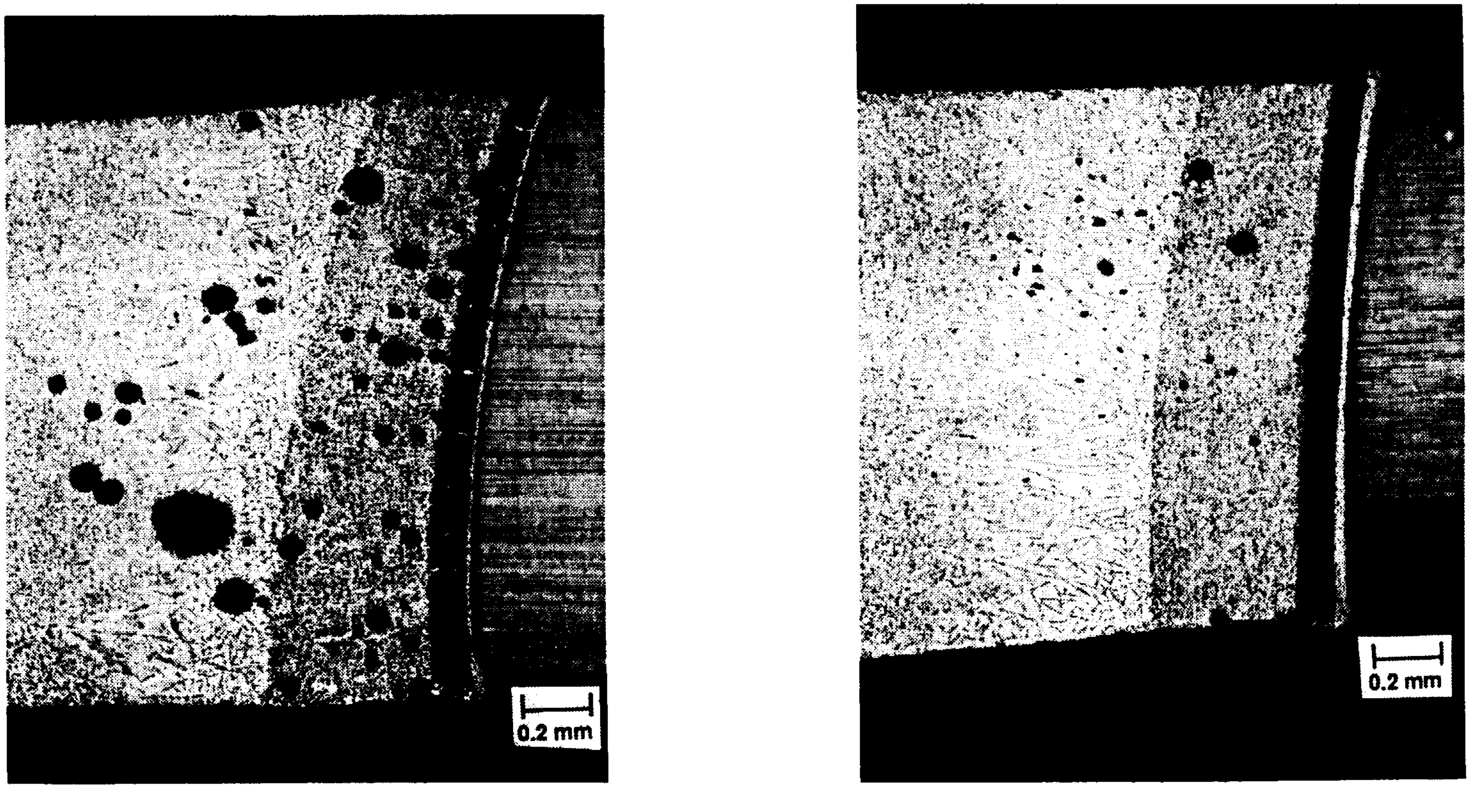

b) LOT 96, 2 h DEGAS

d) LOT 115, 20 h DEGAS

Fig. 48 Porosity in Gas-Tungsten Arc-Welded FVS812 Alloy

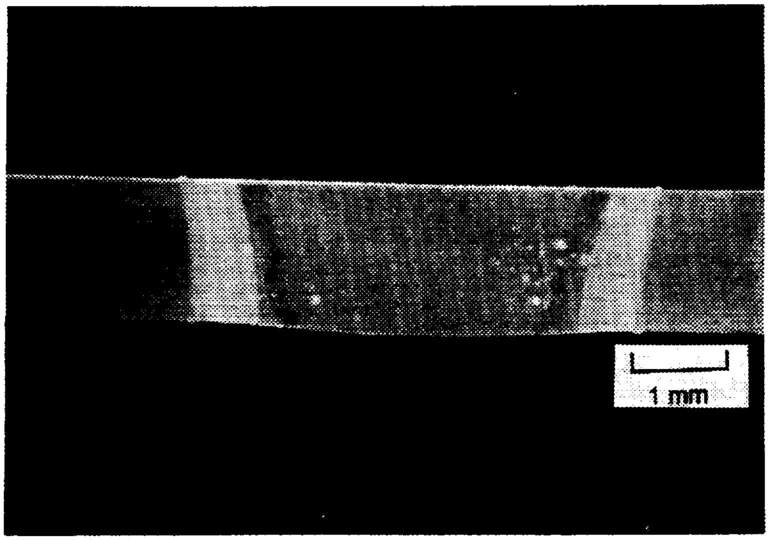

a) 127 KJ/m (3.22KJ/in.)

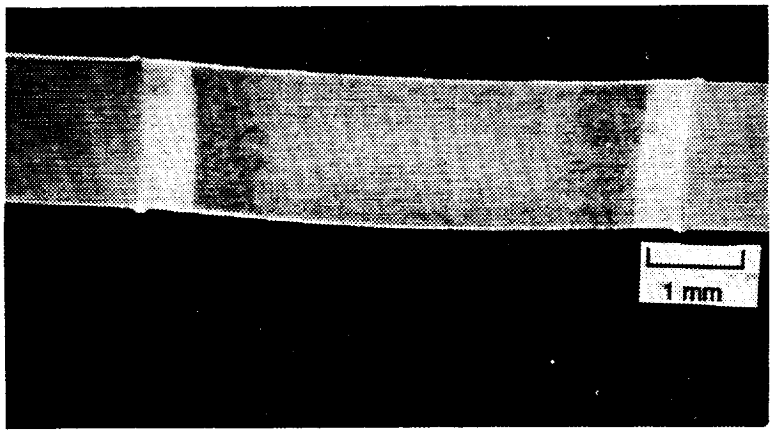

b) 228 KJ/m (5.78 KJ/in.)

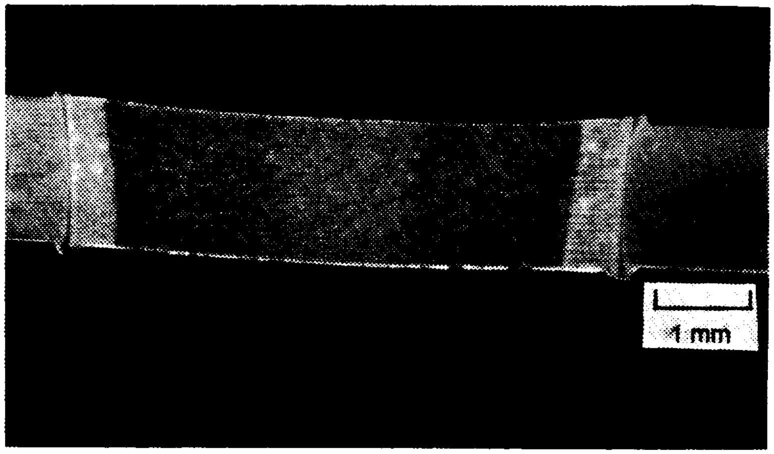

c) 650 KJ/m (16.50KJ/in.)

**Fig. 49 Effect of Weld-Energy Input on Cross Section of Gas-Tungsten ARC Welds in FVS812 Alloy (Lot 115, 20 h Degas)**

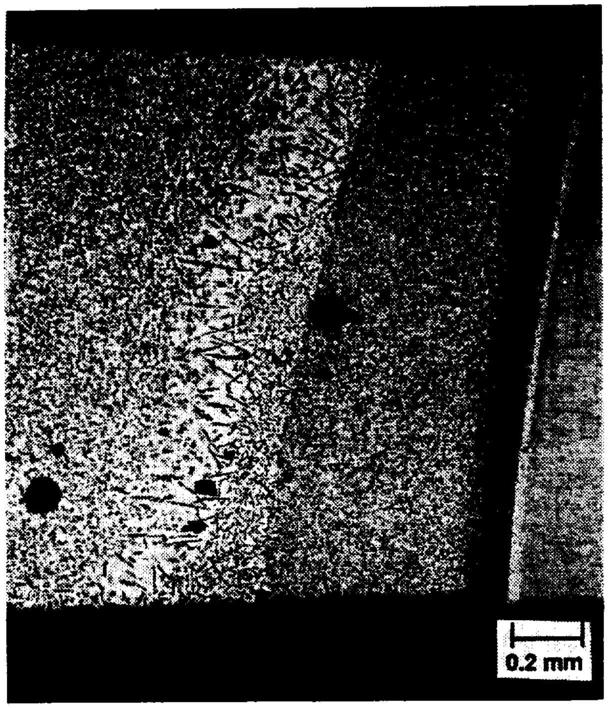

a) 127 KJ/m (3.22 KJ/in.)

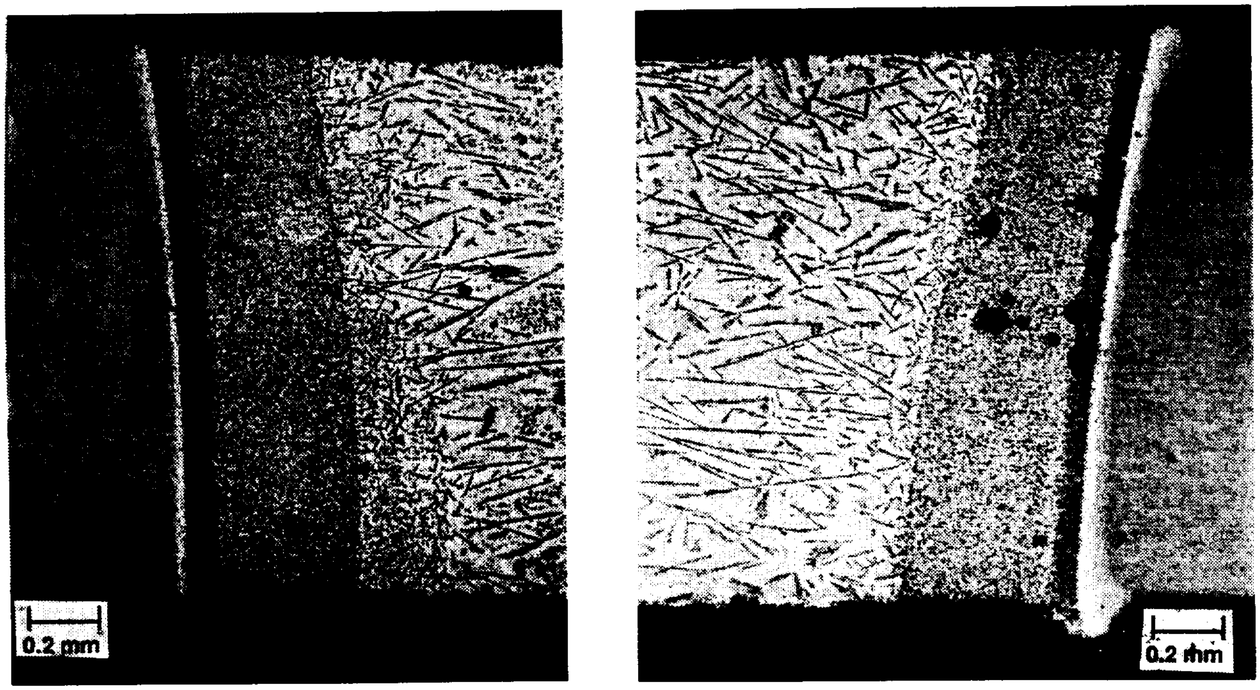

b) 228 KJ/m (5.78 KJ/in.)

c) 650 KJ/m (16.50 KJ/in.)

Fig. 50 Effect of Weld-Energy Input on Porosity in Gas-Tungsten Arc Welds in FVS812 Alloy (Lot 115, 20 h Degas) reduction in hydrogen concentration which was approximately 20 %. A similar effect was observed in GTA welding of Al-10Fe-5Ce but was not explained (33).

As expected, silicide coarsening increased with weld energy input, as shown in Fig. 50. The formation of primary intermetallic phases, similar to EB welds, occurred as a result of GTA welding (Fig. 51). In general, the size of the primary phase particles formed in the weld metal was cooling rate dependent. A relatively fine primary phase spacing in the weld metal occurs near the heat-affected zone (HAZ). A comparison of this region between typical EB and GTA welds shows that the relatively lower heat input of the EB process resulted in less microstructural coarsening (Fig.52). Of interest is the relatively whitish, particle-free zone in the weld metal, which was consistently observed in both types of welds, as shown in Fig. 52 and 53. This zone looks like a typical overaged region found in conventional heat-treatable aluminum alloys. But the FVS812 alloy is not solution heat-treatable in the classic sense, i.e., strengthening precipitates cannot be placed into solution by heating and rapid cooling. Instead, the evidence indicates that this region is largely a rapidly solidified microcellular structure, containing very fine primary silicide dispersoids that are non-etching due to their fineness, i.e., "A-zone" structure (20, 32, 34). This region of the weld metal did not indicate the presence of chemical segregation based on SEM/EDAX analysis and had very high hardness ( Knoop, KHN, 170) compared with KHN 157 of the base metal and KHN 100 at the weld center. It is believed that the effect observed in this case results from complex weld thermomechanical interactions, and that, in part, material expansion during welding produces the upset at the weld edge (Fig. 53).

The tensile properties of GTA butt welds in 20 h degassed FVS812, made without the addition of filler wire, were determined for three conditions: as-welded-tested at RT, welded + exposure at 315 °C/100 h-tested at RT, and welded + exposure at 315 °C (600°F) /100 h-tested at 315 °C (600°F) (Table 8). Based on these results, it is clear that fusion welding significantly degrades base metal strength and ductility for these conditions. Weld strength is reduced more than half that of base metal and RT ductility is reduced to less than one percent.This degradation is attributed to silicide coarsening and embrittlement that occurs during welding,as shown in the fractograph in Fig. 54. Fracture typically occurred through the coarse primary intermetallic region of the weld metal. Since embrittlement was so severe, it was concluded that even perfectly porosity-free welds could not improve strength or ductility. Similar results were determined for GTA welding of Al-Fe-Ce RS-PM alloys (33, 35).

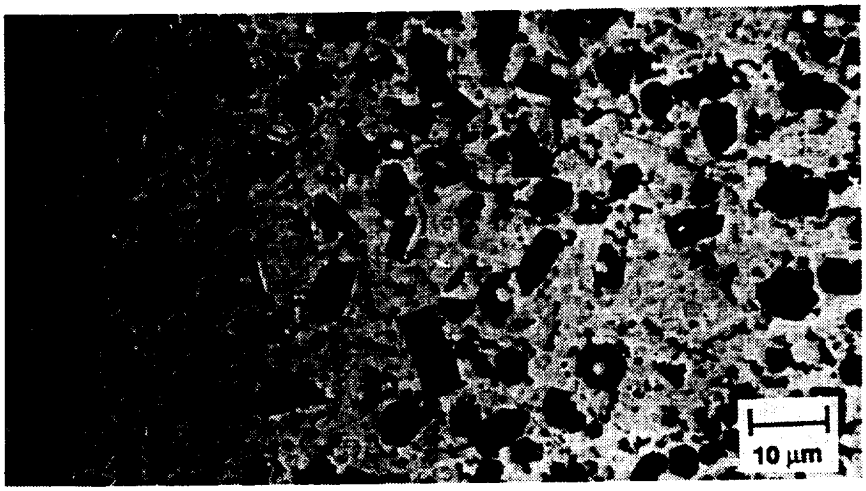

a) WELD METAL: CENTER

b) OFF-CENTER

c) NEAR HAZ

**Fig. 51 Fusion-Zone Microstructures of Gas-Tungsten Arc Welds in FVS812 Alloy, Lot 115, 20 h Degas (228 kJ/m (5.78 kJ/m))**

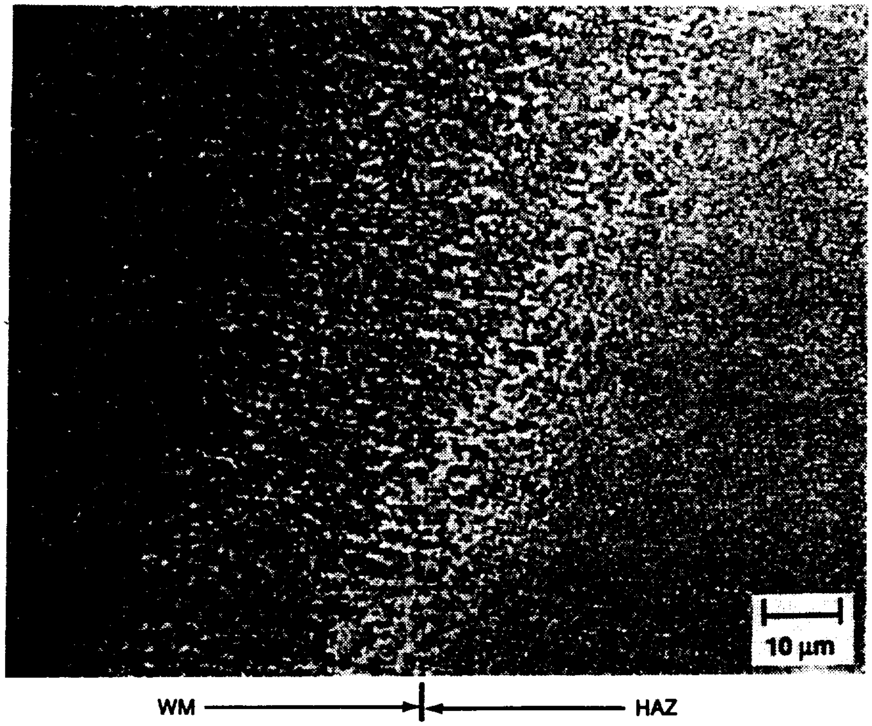

a) EB WELD

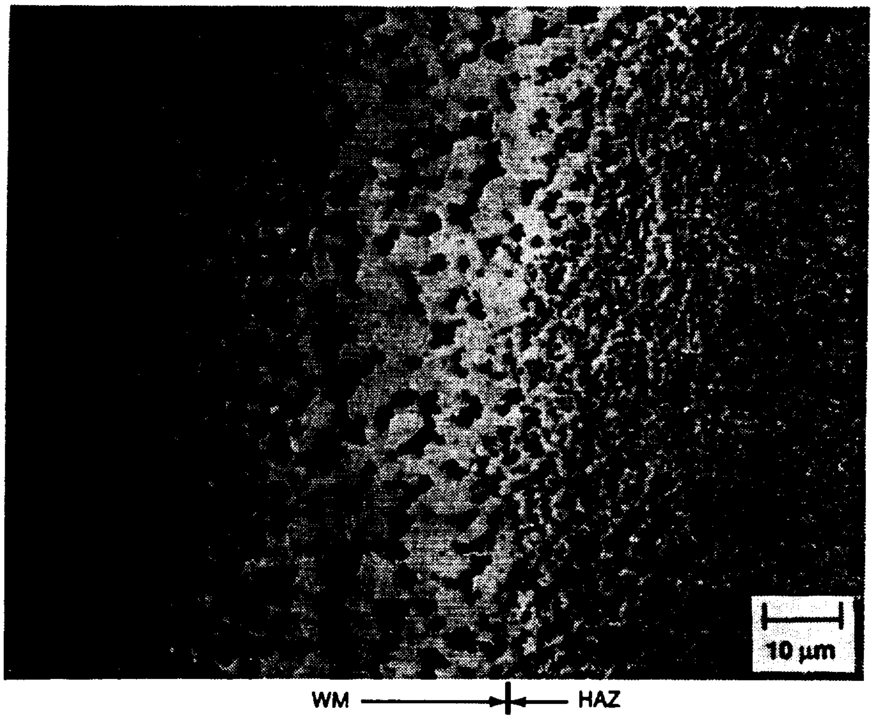

b) GTA WELD

Fig. 52 Comparison of EB and GTA Welds in FVS812 Alloy

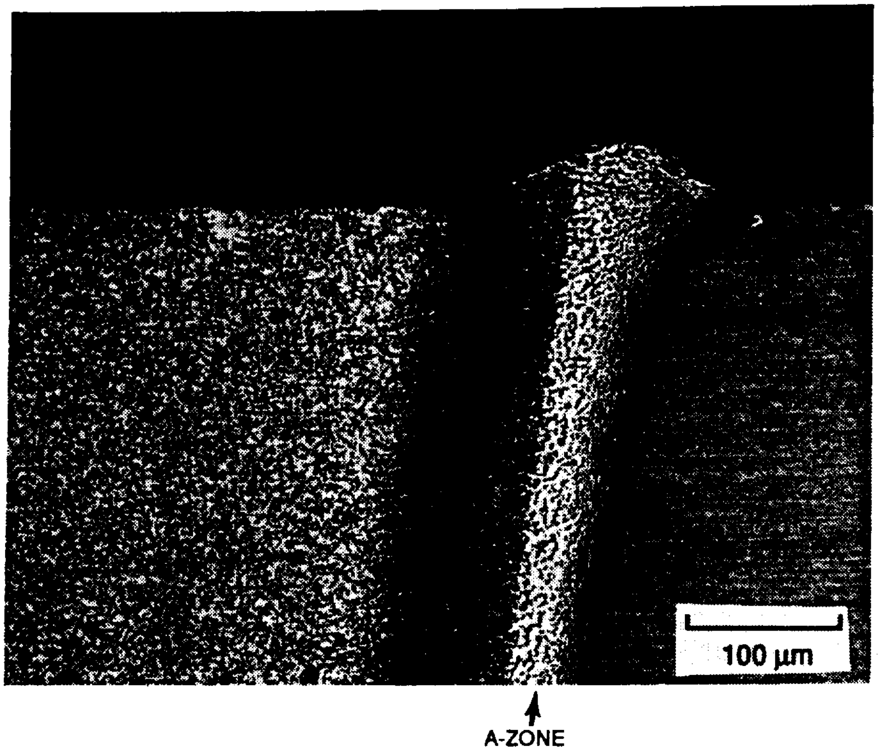

Fig. 53 Cross Section of GTA Weld in FVS812 Alloy

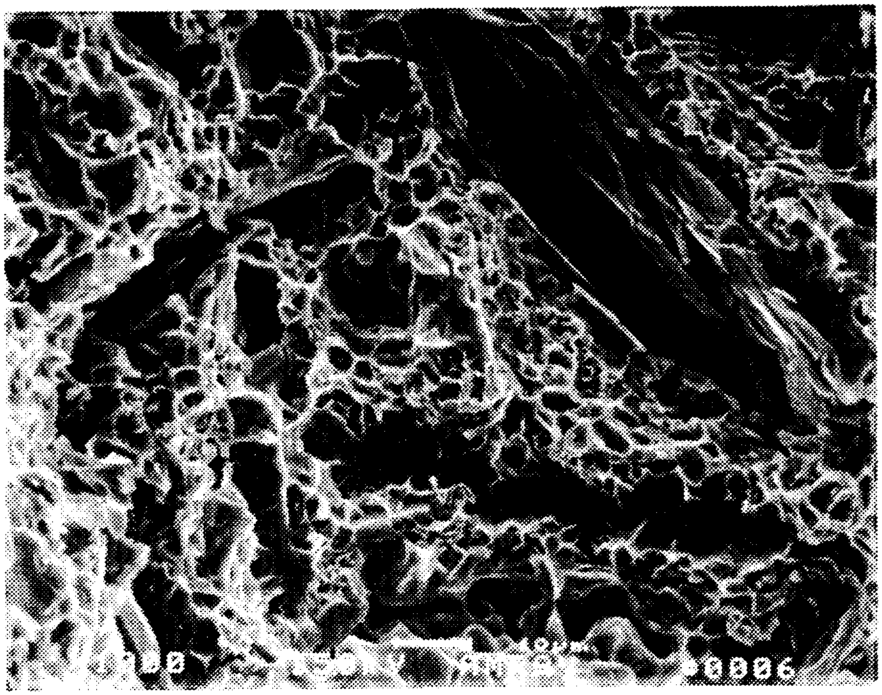

Fig. 54 Tensile Fracture Surface of GTA Weld in FVS812 Alloy, Lot 115, 20 h Degas, As-Welded

## Table 8 Tensile Properties of Fusion Welded FVS812 Alloy

| ID | Alloy | Exposure | Direct. | Strain Rate | Test Temp. °C (°F) | | 0.2 % Yield ksi | Strength (MPa) | Ultimate ksi | Strength (MPa) | Elong. (%) | Modulus 10^6 psi | (GPa) |
|---|---|---|---|---|---|---|---|---|---|---|---|---|---|
| NTW-36a | Lot 115 | As-welded (W) | L | 0.001 | 20 (68) | | 26.2 | (181) | 29.6 | (204.2) | 0.6 | 7.8 | (53.7) |
| NTW-36b | (20 h Degas) | | | | | | 28.5 | (197) | 31.3 | (216.1) | 0.8 | 8.6 | (59.2) |
| NTW-36c | | | | | | | 26.7 | (184) | 30.4 | (209.9) | 0.6 | 9.1 | (62.7) |
| | | | | | | *avg.* | *27.2* | *(187)* | *30.5* | *(210.0)* | *0.7* | *8.5* | *(58.5)* |
| NTW-37a | | W+315°C/100h | L | 0.001 | 20 (68) | | 24.5 | (169) | 27.1 | (186.9) | 0.4 | 6.4 | (44.1) |
| NTW-37b | | | | | | | 24.6 | (169) | 28.0 | (193.0) | 0.6 | 6.8 | (46.8) |
| NTW-37c | | | | | | | 22.8 | (157) | 27.2 | (187.3) | 0.6 | 4.4 | (30.4) |
| | | | | | | *avg.* | *24.0* | *(165)* | *27.4* | *(189.1)* | *0.5* | *5.9* | *(40.5)* |
| NTW-38a | | W+315°C/100h | L | 0.001 | 315 (600) | | 14.2 | (98) | 14.4 | (99.0) | 2.1 | 2.3 | (15.6) |
| NTW-38b | | | | | | | 13.2 | (91) | 14.1 | (97.2) | 3.4 | 4.0 | (27.2) |
| NTW-38c | | | | | | | *** | one specimen broke during set-up | | | *** | *** | |
| | | | | | | *avg.* | *13.7* | *(94)* | *14.2* | *(98.1)* | *2.8* | *3.1* | *(21.4)* |

***Resistance Spot Welding.*** The starting point for parameter development were weld schedules for conventional high strength aluminum alloys, previously certified to Mil-W-6858D, Class A and modified as necessary to produce acceptable weld quality on the FVS812 alloy. Initial tests indicated that the slightly higher weld and forge forces used on 2024-T3 material produced welds with less porosity than the lower forces used in welding 6061-T6. All subsequent welding was performed with the higher weld and forge forces. The certified weld schedule was used for all parameters except that the weld current was reduced by approximately 25% to eliminate expulsion during welding. A summary of the weld parameters is shown in in Table 9.

**Table 9 Initial Spot Weld Parameters**

---

Machine Type and Rating: Sciaky 3 Phase Frequency Converter rated at 100 kVA and 63,000 secondary amps, equipped with a Weld ComputerTM microprocessor controller with weld expansion monitoring capability.

Electrodes: RWMA Class 1, 11.1 mm (7/16 in.) face dia. by 25.4 cm (10 in.) radius

Squeeze Time: 25 cycles

Hold Time: 25 cycles

Weld Heat Time: 3 cycles

Weld Heat Percent: 52% for High Temperature Alloy, 70% for 2024-T3

Current Decay Time: 6 cycles

Current Decay Percent: 25

Weld Force: 5.34 kN (1200 lb)

Forge Force: 13.79 kN (3100 lb)

Forge Initiation Delay: 4 cycles from start of Weld Heat Time

---

During the parameter development tests, it was observed that the rate of expansion for FVS812 was greater during the latter part of the weld cycle than that for 2024-T3 Al. This higher rate of expansion and heating was apparently the cause of the porosity and expulsion that occurred late in the weld cycle. A reduction of approximately 25% in weld current reduced the rate of expansion so that it more closely followed that of the 2024 alloy. This eliminated the expulsion and greatly reduced the porosity found in the weld with an approximate 10% reduction in average shear strength.

Radiographic tests on welds produced with the certified weld schedule were found to be acceptable according to the requirements of Mil-W-6858D Class A. Shear strength of the welds was considerably below that of 2024-T3 and did not meet the minimum requirements of MIL-W6858D. Also, ductility was low in comparison to 2024 Al but acceptable to the minimum requirements of Mil-W-6858. Initially, the consistency of shear strength and the porosity observed in metallurgical cross sections also were not acceptable to Mil-W-6858. Shear strength consistency improved with subsequent testing, to be discussed. Cross tensile-to-shear strength ratios were acceptable to the Mil-specification but considerably below the 0.5 to 0.7 range usually found in other aluminum alloys (Table 10).

**Table 10 Resistance Spot Weld Properties**

| | Initial Weld Schedule | | | Test Panel Schedule | | |
|---|---|---|---|---|---|---|
| | Lot 115 | | Std. Dev | Lot 340 | | Std. Dev. |
| Average Shear, kN (lb) (1) | 2.8 | (634) | (35) | 3.0 | (662) | (33) |
| High Shear, kN (lb) | 3.6 | (800) | | 3.3 | (740) | |
| Low Shear, kN (lb) (2) | 2.3 | (520) | | 2.7 | (600) | |
| Variation In Shear (3) | 0.44 | (0.44) | | 0.21 | (0.21) | |
| Cross-Tensile Strength, kN (lb) | 1.0 | (217) | (45) | 1.0 | (213) | (42) |
| Cross-Tensile: Avg. Shear Ratio 4) | 0.34 | (0.34) | | 0.32 | (0.32) | |
| Weld Diameter, mm (in) | 5.8 | (0.23) | (0.01) | 5.8 | (0.23) | (0.01) |

(1) Mil-W-6858 minimum average for 386 MPa (56 ksi) ultimate strength =3.74 kN (840 lb)
(2) Mil-W-6858 minium reqquired single shear=2.98 MPa (670 lb)
(3) (high-low)/average, Mil-W-6858=0.25
(4) Mil-W-6858 minimum required ratio=0.25

The FVS812 alloy appears to be readily resistance spot welded, including the standard 2 h degassed and the extended 20 h degassed materials. In general, the resistance welding characteristics for both conditions were similar, but there does appear to be an effect of degassing time on strength and weld porosity. In the extended 20 h material, spot -weld shear strength is increased approximately 6 % compared with the 2 h degassed material (Table 11). and porosity at the weld center is significantly reduced, as shown in Fig. 55. These results indicate that extended vacuum degassing is effective in reducing porosity and should be further investigated.

**Table 11 Comparison of FVS 812 Spot Weld Shear Strength**

| Alloy Lot# | Degas Time, h | Average Shear Strength kN | lb | Strength Variation (1) |
|---|---|---|---|---|
| 110 | 2 | 2.71±0.14 | 610±32 | 0.16 |
| 115 | 20 | 2.89±0.27 | 649±60 | 0.25 |
| 335 | 2 | 2.80±0.32 | 630±71 | 0.35 |
| 340 | 20 | 2.94±0.16 | 660±35 | 0.15 |

(1) (high-low)/average, Mil-W-6858 = 0.25 max

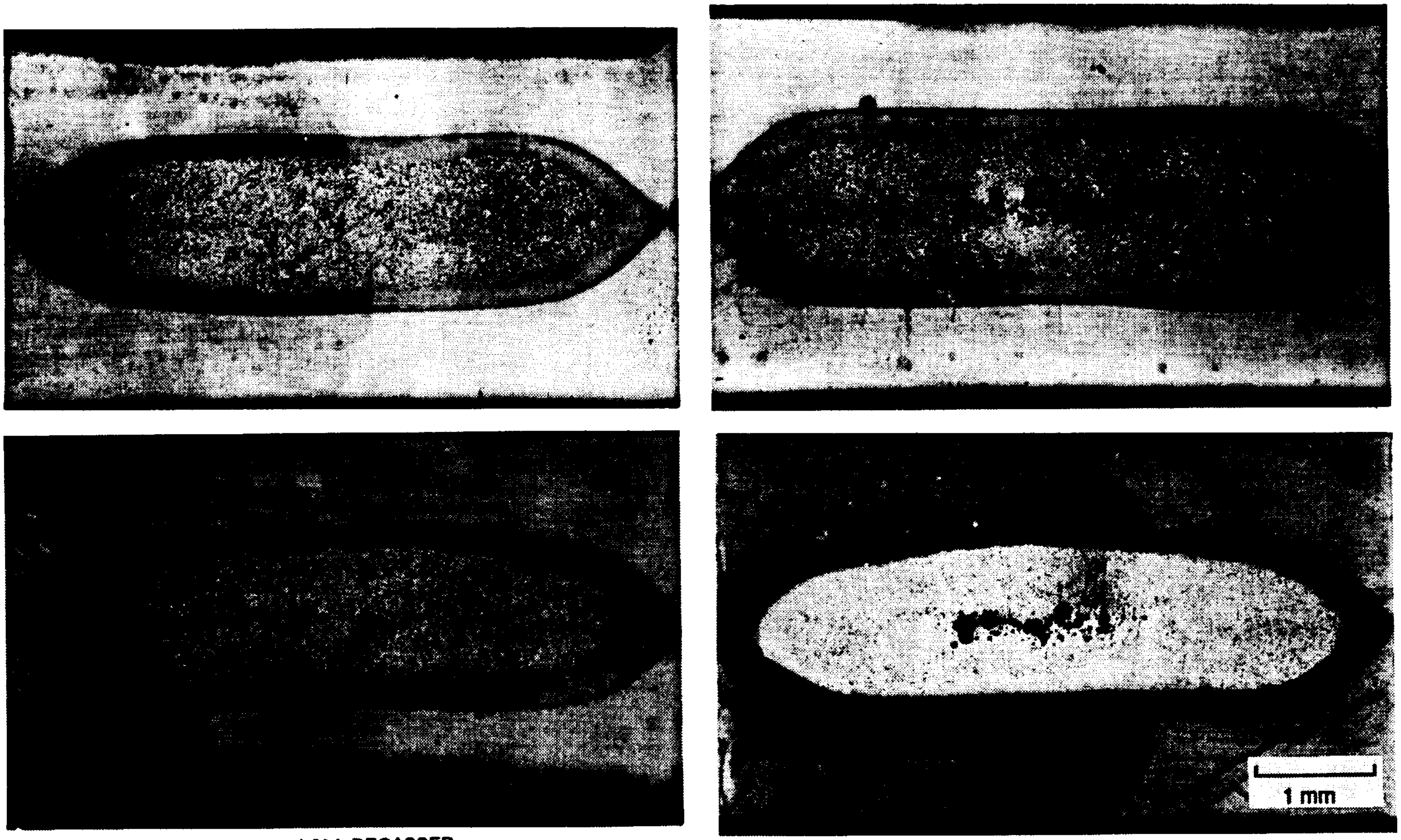

a) 20 h DEGASSED

b) 2 h DEGASSED

Fig. 55 Effect of Billet Degassing on Spot-Weld Porosity in FVS812 Alloy

ORIGINAL PAGE
BLACK AND WHITE PHOTOGRAPH

Coarsening of the strengthening silicides and formation of primary intermetallic phase in the re-cast weld zone occurred during welding and is similar to that observed for fusion welding. The effect of weld thermal exposure on microstructure is shown in Fig. 56 and 57. There was relatively less coarsening than that observed in the fusion welds, and hardness was lower through the weld metal region (Fig. 58).

The static shear strength and S-N behavior of single-spot welds in FVS812 (Lot 340, 20 h degassed) was determined at 20, 200, and 315 °C (68, 392 and 600°F) . At 200 °C (392°F) , the static shear strength is slightly higher than that of room temperature, and at 315 °C (600°F) is decreased to about 80% that of room temperature ( Table 12). A similar effect was observed for fatigue tested FVS812 spot welds (Fig. 59). In comparison, the tensile strength of unwelded base metal tested at 200°C (392°F) drops to about 70 % that of the room temperature value, and at 315°C (600°F) it drops to 45 % (Fig. 13). It appears that spot weld strength was increased as a result of short time exposure at 200° and 315°C,(392 and 600°F), perhaps by improved bonding in the diffusion bond region surrounding the cast zone. The increase in strength at 200°C (392°F) also may be related to dynamic strain aging. The fracture surface of an FVS812 spot weld statically tested at 315°C (600°F) (Fig. 60) shows the characteristic elongated dimple rupture of the outer diffusion bonded corona region after shear failure. The large particle shown on the fracture surface was analyzed to be silicon rich.

**Table 12 FVS 812 Alloy — Spot Weld Shear Strength**

| Test Temperature | | Shear Strength | | Load Fraction, P/Po |
|---|---|---|---|---|
| °C | °F | kN | lb | |
| 20 | 68 | 3.11±0.30 | 699±69 | 1 |
| 200 | 392 | 3.27±0.24 | 735±55 | 1.05 |
| 315 | 600 | 2.65±0.33 | 596±75 | 0.85 |

(20 h Degassed Material, Single Spot)

The effect of test temperature on the strength of spot welds is compared with 2024-T81 (Fig. 61). The load fraction, normalized to spot weld strength at room temperature, reflects the change in strength with temperature. The effect of temperature on 2024-T81 spot welds is more severe. These results indicate that spot welds in FVS812 have excellent high temperature behavior due to the good stability of the strengthening dispersoids. The effect of long- term thermal exposure on weld strength was not determined but, based on tensile behavior, little effect would be expected.

The S-N fatigue behavior of single-spot welds in FVS812 (20 h degassed) was determined at 20, 200, and 315 °C (68, 392 and 600°F) and is compared with 2024-T81 (Fig. 62). The load fraction, normalized to spot weld strength at room temperature, reflects

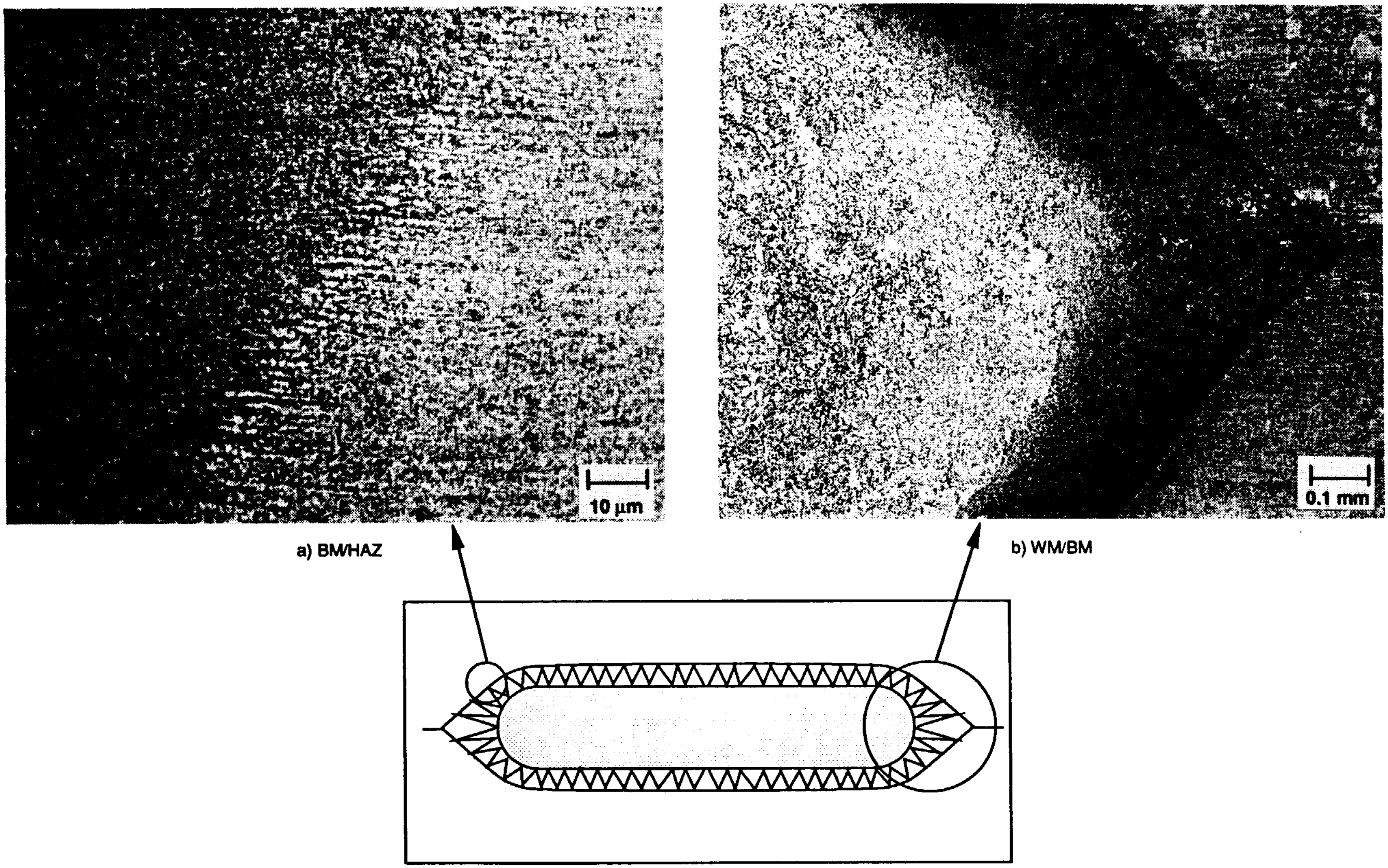

a) BM/HAZ

b) WM/BM

c) WELD SCHEMATIC

Fig. 56 Typical Microstructures in FVS812 Spot Welds (Lot 335, 2 h Degas)

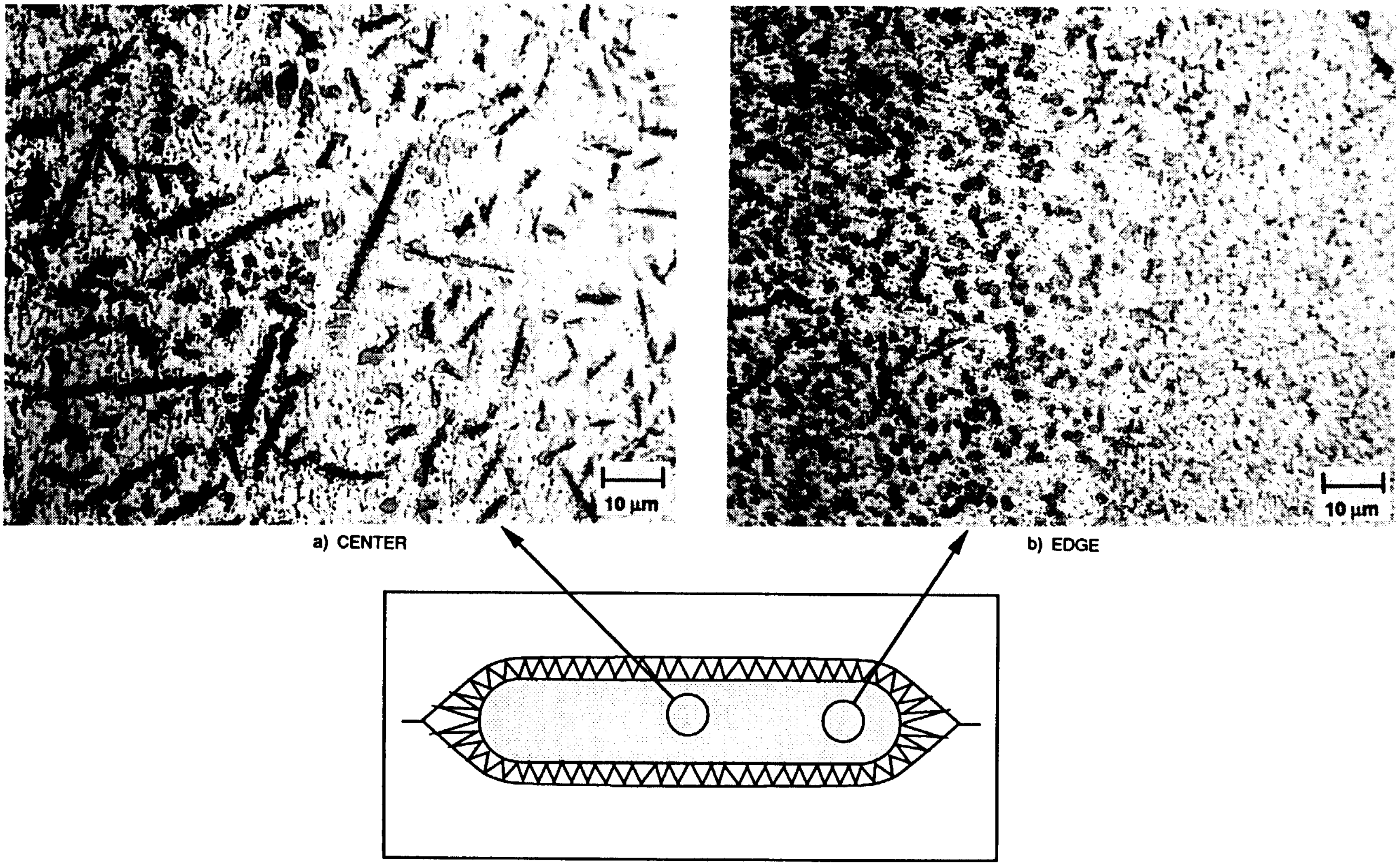

a) CENTER

b) EDGE

c) SCHEMATIC

Fig. 57 Weld Metal Microstructures In FVS812 Spot Welds (LOT 335, 2 h Degas)

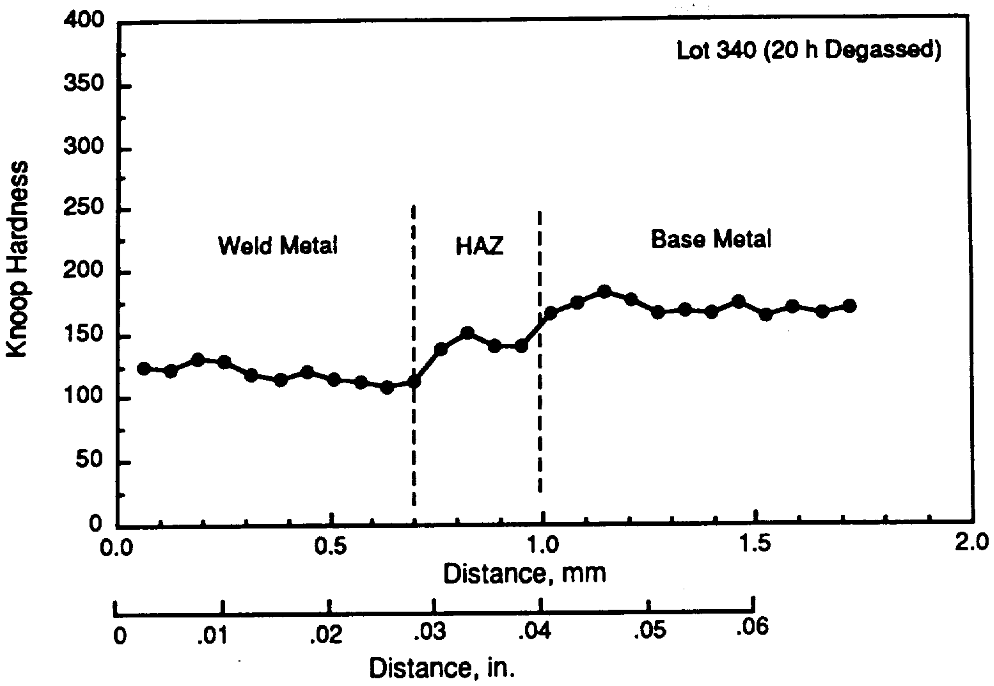

Fig. 58 Hardness Profile in FVS812 Spot Weld

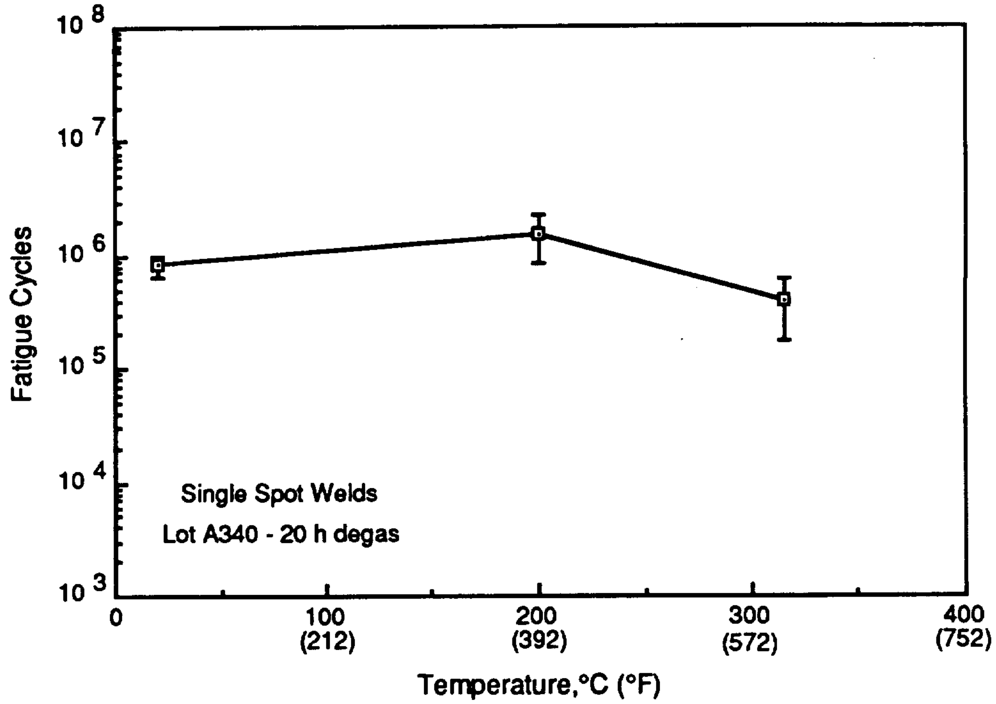

Fig. 59 Effect of Temperature on Fatigue Life of FVS812 Alloy Spot Welds at Load Fraction, P/Po=.25

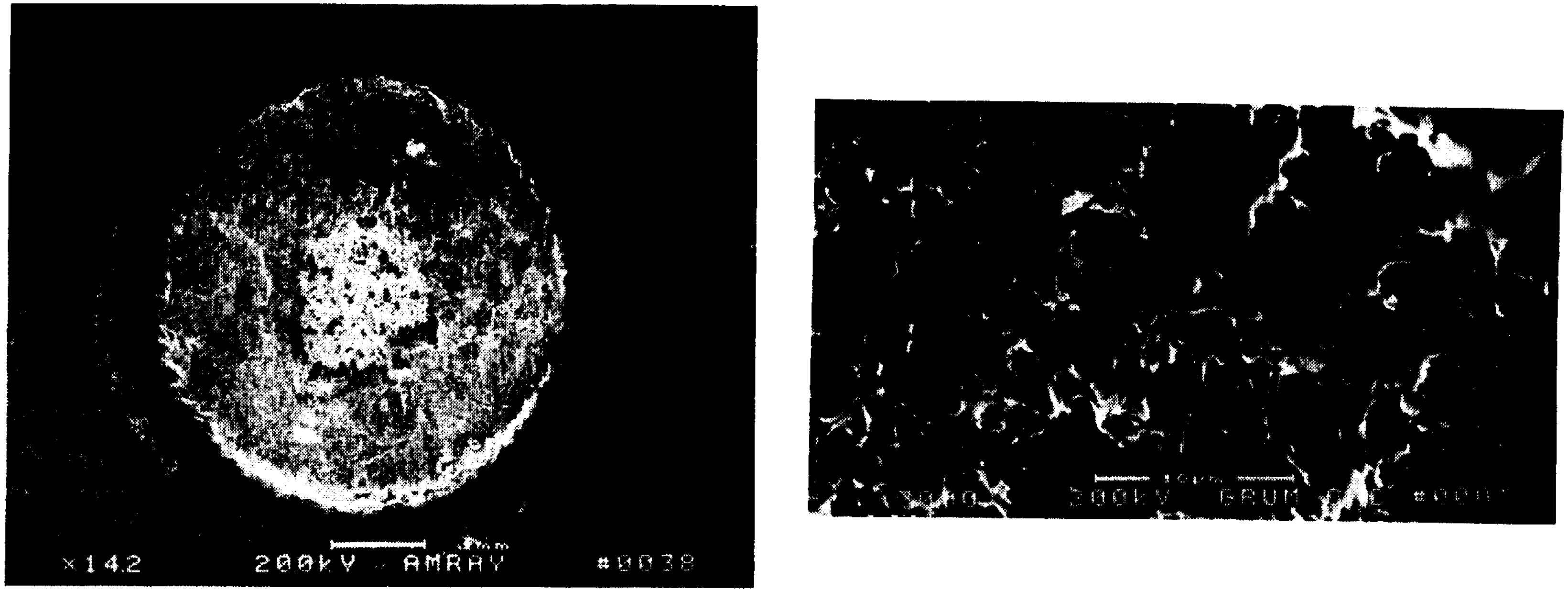

a) OVERALL

b) DIFFUSION-BONDED REGION

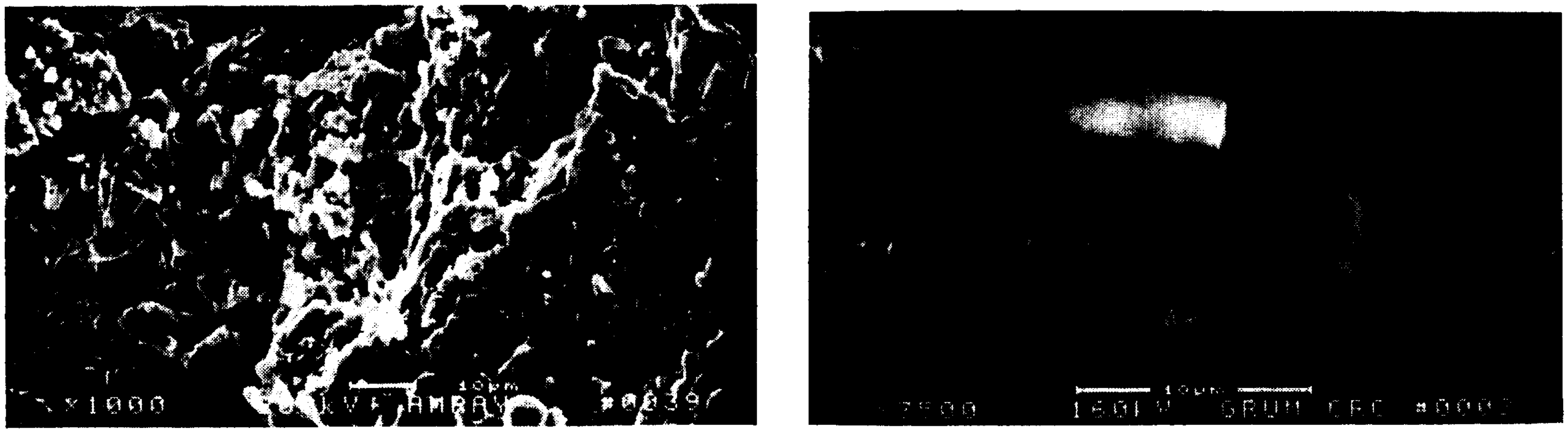

c) CAST ZONE – CENTER

d) SI-RICH PARTICLES

Fig. 60 Fractographs of Tensile-Shear Surface of FVS812 (Lot 340, 20 h Degas) Spot Weld, Test Temperature 315°C (600°F)

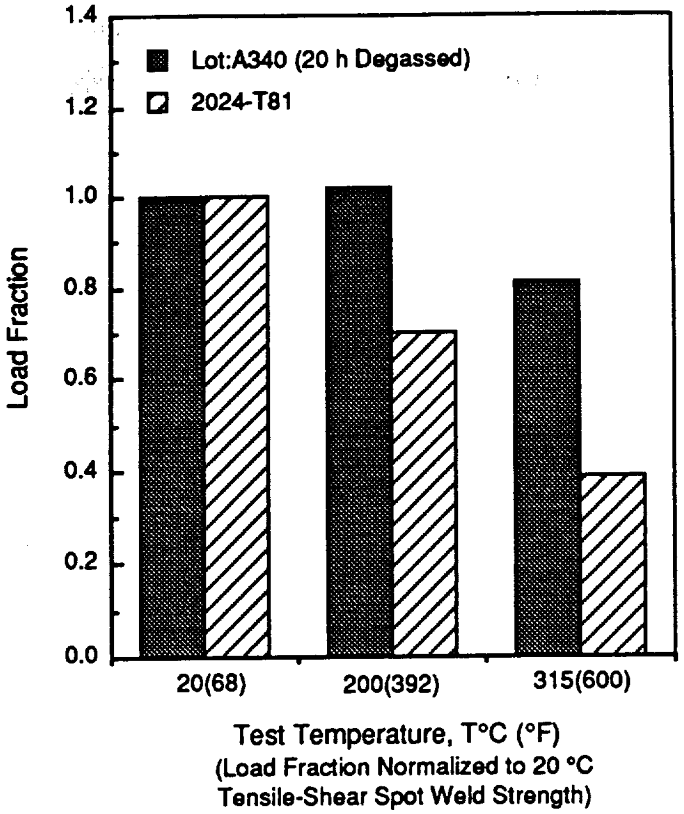

**Fig. 61** Effect of Temperature on Load Ratio of Spot Welds in FVS812 Alloy and 2024-T81

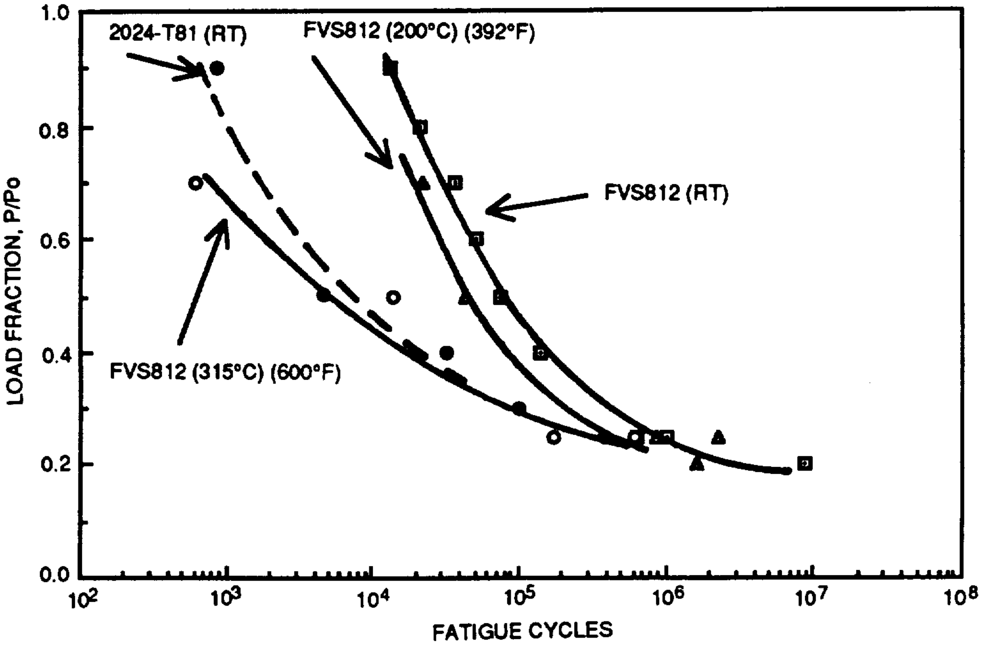

**Fig. 62** Effect of Temperature on Fatigue Life of FVS812 Alloy (20 h Degassed)

**Fig. 63 Typical Fatigue Fracture in FVS812 Alloy**

the change in fatigue behavior with temperature. At 200°C (392°F), the S-N behavior of FVS812 closely parallels the room temperature results. At 315°C (600°F), the S-N behavior of FVS812 is similar to that of 2024-T81 data at room temperature. A typical "normal" fatigue failure at the circumference of an FVS812 spot weld is shown in Fig. 63. These results indicate good fatigue resistance of FVS812 spot welds and demonstrate that they have not been embrittled by the relatively large primary intermetallics observed at the weld center.

Shunting of adjacent welds appeared to be less of a problem than with conventional alloys and thus permitted closer weld spacing. This was attributed to the lower measured electrical conductivity of FVS812 compared with 2024 Al ( i.e., 25.8% IACS versus 31.8% IACS). Also, FVS812 exhibited excellent resistance to deformation adjacent to the electrodes during welding and thus allowed for significantly reduced minimum edge distances. Therefore, it was decided to establish weld parameters for the 1.6 mm (.063 in.) thick material with a flange width of 14.2 mm (0.56 in.) instead of the normally used 19.1 mm (0.75 in.) for conventional aluminum alloys. Welds on 2024-T3 using the lower edge distance showed edge bulging and cracking, while those on the FVS812 alloy were acceptable. A slight reduction in the diameter of the electrode face, from 11.1 mm (7/16 in.) to 9.5 mm (3/8 in.), resulted in a higher pressure per unit inch acting on the weld. As a result of this change it was possible to obtain the same shear and cross tensile values at a 5% reduction in weld current and meet the consistency requirements of Mil-W-6858D (Table 9). The parameters used to fabricate the zee-stiffened test panel are presented in Table 13.

Although FVS812 exhibited generally good resistance weldability, it is believed that weld strength and consistency can be improved by further work to optimize weld parameters, such as electrode face diameter and radius, weld and forge forces and their ratio, and possibly varying the magnitude of the weld current during the cycle to reduce porosity levels. Also, additional work is suggested to optimize joint design criteria, such as minimum edge distance, weld spacing and spacing of multiple rows of welds. The use of high temperature adhesives and resistance welding to fabricate weld-bonded joints is another area of possible development.

**Table 13 - Spot Weld Parameters for Compression Test Panels**

Machine Type and Rating: Sciaky 3 Phase Frequency Converter rated at 100 kVA and 63,000 secondary amps, equipped with a WeldComputerTM microprocessor controller with weld expansion monitoring capability.
Electrodes: RWMA Class 1, 9.5 mm (3/8 in) face dia. by 25.4 cm (10 in) radius
Squeeze Time: 25 cycles
Hold Time: 25 cycles
Weld Heat Time: 3 cycles
Weld Heat Percent: 50
Current Decay Time: 6 cycles
Current Decay Percent: 25
Weld Force: 5.34 kN (1200 lb)
Forge Force: 13.79 kN (3100 lb)
Forge Initiation Delay: 4 cycles from start of Weld Heat Time

## 5.5 ZEE-STIFFENED COMPRESSION TEST PANELS

***Structural Analysis.*** Three small-scale, zee-stiffened compression test panels were designed and fabricated as part of the evaluation of the FVS812 alloy:

- A riveted panel with FVS812 aluminum zees and skins. (Fig. B-1 to B-4)
- A resistance spot-welded panel fabricated with FVS812 aluminum zees and skins. (Drawing TGP-1106, TGP-1106 is identical to TGP 1105 except for stiffener size, which is indicated in Fig. B-5)
- A baseline riveted panel with 2024-T62 aluminum zees and a 2024-T81 aluminum skin (Drawing TGP-1104 is identical to TGP-1105 except for the sheet rolling orientation, which is indicated in Fig. B-6).

The geometrical configuration was obtained by trial-and-error using the Grumman CURVPANL computer program ((36)) and associated room temperature material properties. This program is based upon the analysis procedures described in the Grumman Structures Manual and results in the near optimum design for the constant thickness stiffener and skin shown in Fig. 64. The stiffeners are 216 mm long (8 1/2") and have 25.4 mm (1.00 in.) deep zees, with an attached flange length of 14.3 mm (0.562 in.) and an outstanding flange width of 12.7 mm (0.500 in.). The 1.6 mm (0.062 in.) thick stiffeners have a 2.3 mm (0.090 in.) bend radius and are spaced at 57.2 mm (2.25 in.). The zees are fastened to a 1.6 mm (0.062 in.)-thick sheet with 3.2 mm (1/8 in.)diameter NAS1200M4 Monel countersunk rivets. Details of the panel assembly, end potting details and strain

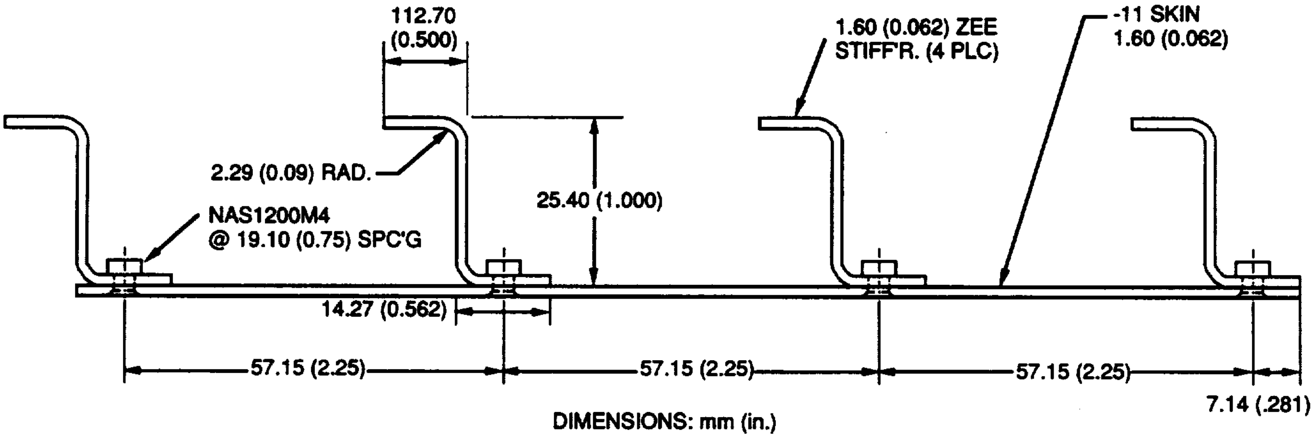

1) RIVETED PANELS: DRAWINGS TGP 1104, 1105
2) LENGTH OF PANEL IS 216 mm (8.50 in.)
3) SPOT-WELDED FVS 812 PANEL IS DETAILED IN DRAWING TGP-1106

**Fig. 64 Geometry of Zee-Stiffened Compression Test Panel**

gage locations are given in Drawings TGP-1104, -1105 and -1106. The strain gages are located along the two faces of the sheet and outstanding flanges to track the onset of sheet and stiffener buckling.

The static tensile stress-strain properties used in the stability compression analyses are listed in Table 14. The properties used for 2024-T81 and 2024-T62 aluminum are respectively based upon MIL-HDBK-5 "B" basis and "S" basis values, while the FVS812 properties are based upon the results of tests from specimens fabricated from the actual 1.6 mm (0.062 in.) sheet used to fabricate the zee-stiffened panel. It is noted that typical room temperature compression yield strengths of 2024-T81 and -T62 are respectively 10% and 20% higher than the statistically based curves. Hence, the compressive failing load of the baseline 2024 panel is expected to be about 15% higher than the load predicted with these stress-strain curves. The compression stress-strain curves for the three alloys used in the panels are plotted in Fig. 65. As shown in the figure, the elastic modulus of the FVS alloy is appreciably higher than that of the 2024 alloys but the plastic stress-strain curve lies between the two 2024 alloys for strains up to 0.85%. Also, it is noted that the density of the new alloy is approximately 5% higher than that of the 2024 alloys. CURVPANL calculations predict stress allowables corresponding to several possible compression failure modes.

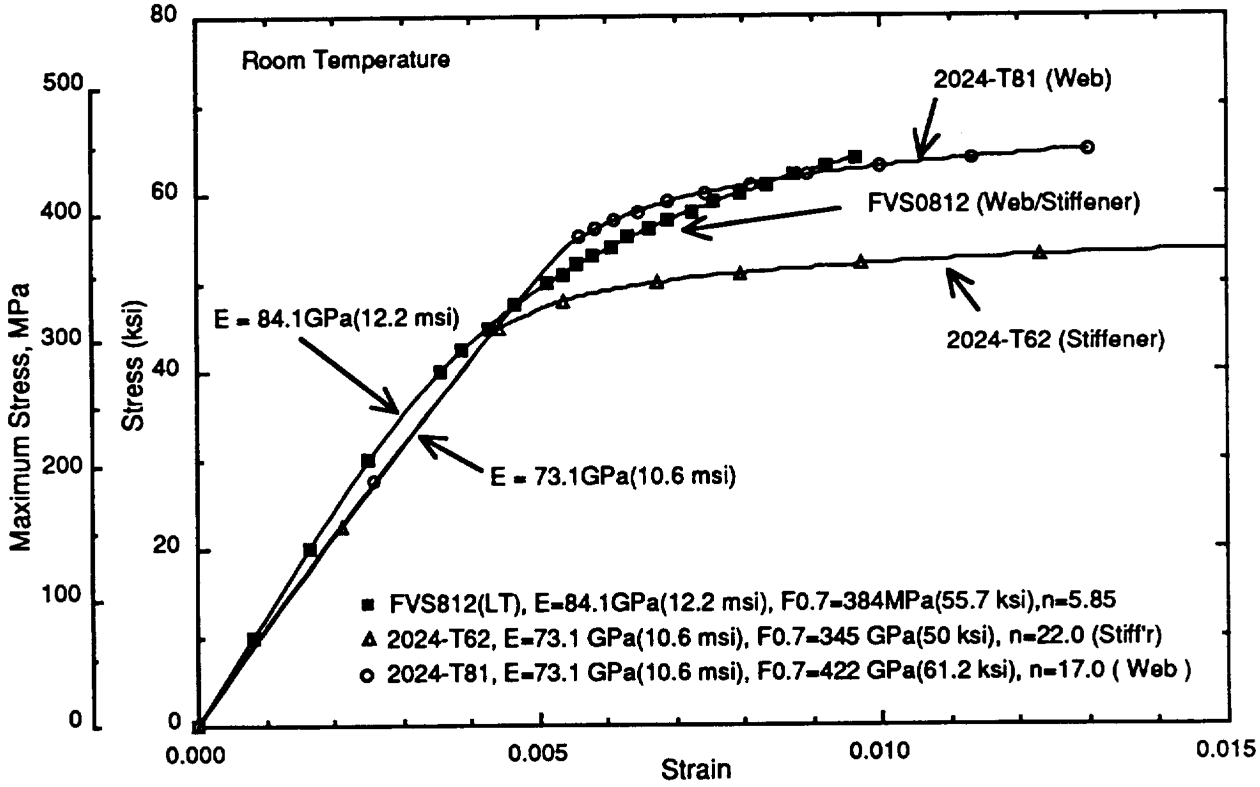

**Fig. 65 Compression Stress-Strain Curves for FVS812, 2024-T81 and 2024-T62 Aluminum**

## Table 14 Room Temperature Mechanical Properties Used for CURVPANL Compression Strength Analysis

| (4)Property | (1)2024-T81 | (2)2024-T62 | (3)FVS0812(LT) | FVS0812(L) |
|---|---|---|---|---|
| E (t), GPa (msi) | 72.4 (10.5) | 72.4 (10.5) | 85.8 (12.4) | 85.5 (12.4) |
| E (c), GPa (msi) | 73.8 (10.7) | 73.8 (10.7) | 84.1 (12.2) | 81.4 (11.8) |
| $E_{avg}$, GPa (msi) | 73.1 (10.6) | 73.1 (10.6) | 84.8 (12.3) | 83.4 (12.1) |
| $F_{tu}$, MPa (ksi) | 468.9 (68.0) | 441.3 (64.0) | 448.9 (65.1) | 455.8 (66.1) |
| $F_{0.7}$ (t), MPa (ksi) | 424.7 (61.6) | 344.8 (50.0) | 406.8 (59.0) | 406.8 (59.0) |
| n (t) | 21.0 | 26.0 | 4.4 | 4.4 |
| $F_{0.7}$ (c), MPa (ksi) | 422 (61.2) | 344.8 (50.0) | 384.1 (55.7) | 316.5 (45.9) |
| n (c) | 17.0 | 22.0 | 5.8 | 4.9 |
| (5)$F_{cy}$, MPa (ksi) | 417.1 (60.5) | 344.8 (50.0) | 385.4 (55.9) | 328.2 (47.6) |
| $F_{0.7}$ (s), MPa (ksi) | 423.3 (61.4) | 344.8 (50.0) | 395.8 (57.4) | 361.3 (52.4) |
| n (s) | 19.0 | 24.0 | 5.1 | 4.7 |

NOTES:

(1) "B" basis properties (t ≤ 6.4 mm (0.25 in)) stored in CURVPANL; note, $F_{cy} \approx$ 462 MPa (67 ksi) (typical).

(2) S" basis properties (t ≤ 12.7 mm (0.50 in)) stored in CURVPANL; note, $F_{cy} \approx$ 413.7 MPa (60 ksi) (typical).

(3) Grumman test data, average of 2 specimens, t = 1.6 mm (0.062 in).

(4) E is elastic modulus( (t)ension, (c)ompression, (s)hear or avg.), $F_{0.7}$ and n are Ramberg-Osgood parameters for tension or compression stress-strain curves and $F_{tu}$ is ultimate tensile strength of the material.

(5) Values of ($F_{cy}$) are calculated from Ramberg-Osgood parameters associated with "B" or "S" basis stress-strain curves.

Note: $F_{cy}$ (typical) ≈ 462 MPa (67 ksi) for 2024-T81 and $F_{cy}$ (typical) ≈ 413.7 MPa(60 ksi) for 2024-T62.

Three fundamental modes of sheet and stiffener deformation are considered in the initial buckling stress calculations: flexural, torsional and local. The flexural mode is characterized by bending of the sheet and is characterized by out-of-plane distortion of a line through the stiffener attachments. This mode is associated with Euler buckling (no distortion of stiffener cross-section) for long buckle lengths, with the wrinkling/forced-crippling behavior for short buckle lengths and with inter-rivet buckling for very short buckle wave lengths. Wrinkling involves local distortion of the stiffener without appreciable bending and inter-rivet buckling involves separation of the sheet between stiffener attachment points, where the stiffener remains straight and undistorted. The torsional mode is characterized by twisting of the stiffener and rotation of the sheet about the stiffener attachment lines. Finally, the local mode is characterized by stiffener distortion and rotation of the sheet about the stiffener attachment lines. Coupling of these modes can result in appreciably lower buckling stresses than in any one of the fundamental modes.

The post-buckling behavior of the panels depends upon the predicted initial stability stresses. Although there is no closed form analysis available that can predict this behavior for flat or curved stiffened panels, the CURVPANL program calculates the post-buckled strength based upon the critical edge stress ($F_{cx}$) of the stiffener or skin and the corresponding average skin buckling stress ($F_{avskn}$). These two stresses are dependent since the sheet properties affect the axis about which the sheet deforms and the average stress in the buckled skin depends upon the initial buckling stress of the stiffener. The compressive failing stress of the panel, $F_c$, is given by:

$$F_c = (F_{cx} A_{stiff} + F_{avskn}\, wt) / (A_{stiff} + wt)\ ,$$

where $A_{stiff}$ is the total area of the stiffeners, w is panel width and t is the skin thickness.

As shown in Table 15, the predicted allowable stresses for skin and stiffener failure modes are shown for each zee-stiffened panel. The compression buckling stress for the 2024 skin (35.2 ksi) is slightly lower than that of the FVS812 skin 256.5 MPa (37.2 ksi). The post-buckling strengths of both test panels are limited by the forced-crippling and flexure-torsion modes, both of which occur nearly simultaneously. It is also noted that the slightly higher predicted average failing skin stress ($F_{avskn}$) for the 2024 panel is balanced by the slightly lower stiffener failing stress ($F_{cx}$), resulting in nearly identical failing loads for the two panels (P = 183 kN (41.1 kips) for the 2024 panel and P = 186.4 kN (41.9 kips) for the FVS panel). However, it should again be pointed out that the 2024 prediction is based on Mil-Hdbk-5 statistical values as compared to the FVS prediction based on measured properties. Hence, the 2024 panel is actually expected to fail at approximately 209 kN (47 kips) if predictions had been based upon typical stress-strain curves. Verification of the compressive stress-strain curves should be performed later, with compression test specimens fabricated from the failed 2024 panel.

**Table 15 Predicted Failure Stresses for Zee-Stiffened Aluminum Compression Panels at Room Temperature**

| (1)Predicted Stress Allowables MPa (psi) | 2024-T81 (skin) 2024-T62 (stiff'r) | | FVS0812 (LT) (skin & stiff'r) | |
|---|---|---|---|---|
| Web: | | | | |
| Comp. Buckling Stress, $F_{ccr}$ | -242.7 | (-35,205) | -256.3 | (-37,178) |
| Wrinkling Stress, $F_{wr}$ | -330.7 | (-47,969) | -359.3 | (-52,106) |
| Edge Stress (strain), $F_{cx}$ | -356.6 | (-53,027) ($\varepsilon = -0.0052$) | -359.4 | (-52,120) ($\varepsilon = -0.0056$) |
| Avg. Skin Stress, $F_{avskn}$ | -296.3 | (-42,976) | -279.2 | (-40,499) |
| Stiffener: | | | | |
| Euler Buckling, $F_{Euler}$ | -342.6 | (-49,691) | -454.8 | (-65,968) |
| Stiffener Crippling, $F_{crip}$ | -356.3 | (-51,674) | -444.1 | (-64,410) |
| Flex./Tors. Buckling, $F_{flxtor}$ | -328.9 | (-47,707) | -373.2 | (-54,123) |
| Forced Crippling, $F_{fc}$ | -335.9 | (-48,714) | -372.5 | (-54,021) |
| Edge Stress (strain), $F_{cx}$ | -330.6 | (-47,947) ($\varepsilon = -0.0052$) | -359.4 | (-52,120) ($\varepsilon = -0.0056$) |
| Panel: | | | | |
| Section Crippling Stress, $S_{ecrip}$ | -343.6 | (-49,831) | -420.6 | (-61,000) |
| (2)Compressive Failing Load, P, MN (lb) | .183 | (41,140) | .186 | (41,900) |
| Compressive Strength, $F_c$, MPa (psi) | 313.4 | (45,460) | 319.2 | (46,300) |
| (3)Specific Compr. Strength, $F_{c/\rho}$ | 113.1 | (450,100) | 109.7 | (440,950) |

NOTES:

(1) Allowable stresses obtained from CURVPANL computer program with section properties obtained from YFUDGE program. See Reference 2.

(2) $P = F_{avskn} \times A_{skin} + F_{cx} \times A_{stiff}$, where $A_{skin} = .186 \times 0.0016 = 2.93 \times 10^{-4} m^3$ ($7.312 \times 0.062 = 0.453$ in$^2$) and $A_{stiff} = 0.1 \times 0.0029 = 2.9 \times 10^{-4} m^3$ ($4 \times 0.1134 = 0.452$ in$^2$) and $F_c = P/(A_{skin} + A_{stiff})$

(3) Density ($\rho$): 2024 = 2.77 g/cc (0.100 lb/m$^3$) and FVS812 = 2.91 g/cc (0.105 lb/in$^3$)

When room temperature testing is completed, it is proposed that additional FVS812 alloy panels be fabricated to demonstrate the high temperature compression strength advantages of this new material. Appreciable weight savings may be achieved using FVS812 in a compression application with prior elevated temperature exposure. For example, the room temperature compression (and tension) yield strengths of 2024-T62/-T81 are both reduced to approximately 2/3 of their room temperature yield strengths after 1,000 hours of thermal exposure at 177°C (350°F) (See Mil-Hdbk-5E) while the yield strength of FVS812 is not degraded. Hence, considering the density and the compression yield of FVS812 compared to 2024 aluminum, a potential weight savings of approximately 25% may be obtained.

***Fabrication.*** The following zee-stiffened compression test panels were fabricated: a baseline riveted panel with 2024-T62 aluminum zees and a 2024-T81 aluminum skin, a riveted panel FVS812 aluminum zees and skins, and a resistance spot-welded panel fabricated with FVS812 aluminum zees and skins (Fig. 66-68).

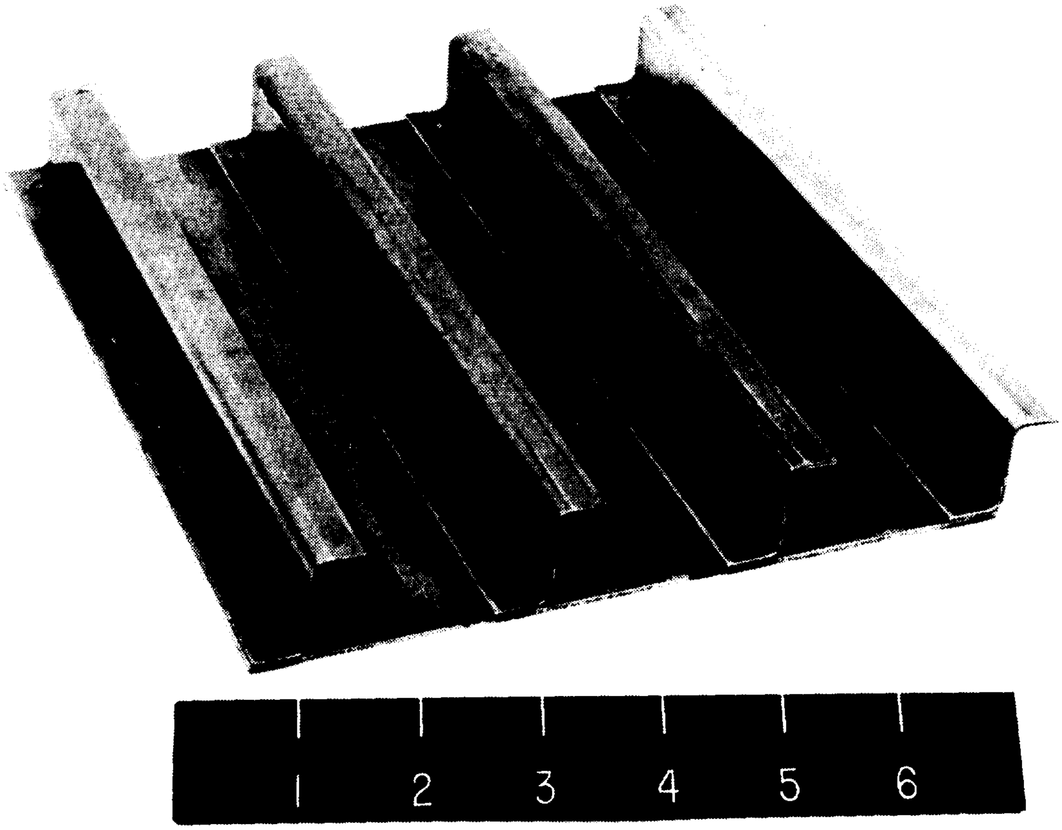

TGP-1104

**Fig. 66 Baseline Riveted Panel: 2024-T62 Zees and 2024-T81 Skin**

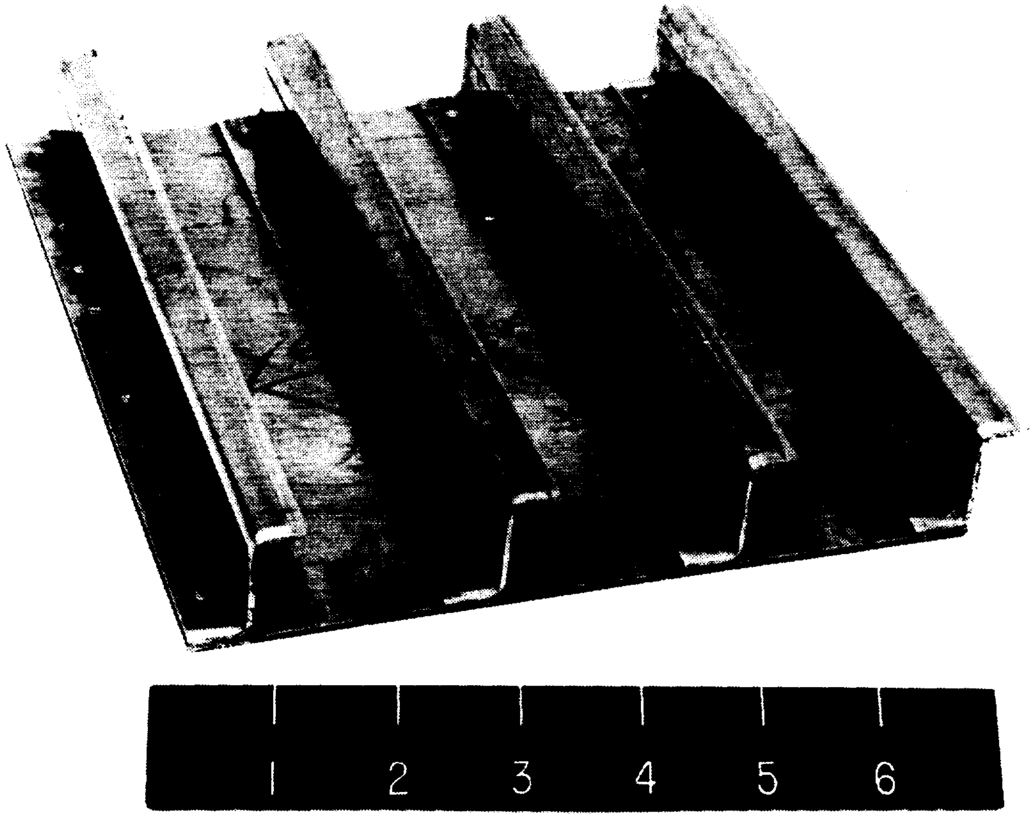

TGP-1105

Fig. 67 Riveted Panel: FVS 812 Alloy

The wavy as-received FVS 812 alloy sheet-Lot 340 (20 h degas) used for the panel skins were flattened by manually clamping the 1.6 mm (0.063 in.) sheet between stainless steel sheet and holding at 370°C (700°F) for 24 h. The 2024-T81 sheet used for the skin of the baseline riveted panel did not require flattening.

A cross-section from typical FVS812 stiffener at the 2.4 mm (0.090 in.) bend is shown in Fig. 69; the bend resulted in an approximate 4% thickness reduction.

***Testing.*** After fabrication, surface flatness and stiffener straightness measurements were made on each of the panels preparatory to testing. For flatness measurements, a grid of forty two measurement points were marked on each panel as shown in Fig. 70 (drawing number TGP-1104 Sheet 5). Each panel was supported at three points using ground, 2-in.- high, gage blocks, as shown in Fig. 71. The support blocks were positioned under

C-2

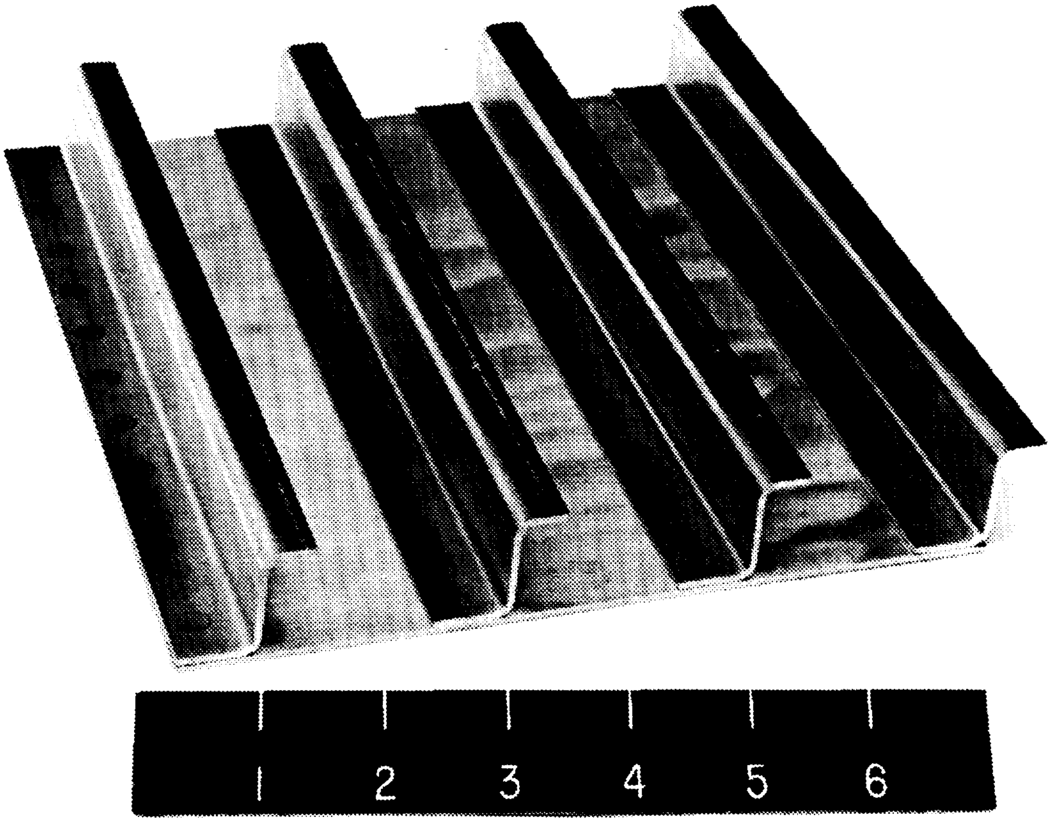

**Fig. 68 Resistance Spot-Welded Panel: FVS 812 Alloy**

points A1, G1, and E6. Heights were measured at each point with a Mitutoyo digital height gage by adjusting the height to a zero reading on the dial indicator, then reading the digital output on the height gage. Zero shift was checked by re-measuring point A1 at the end of each set of panel measurements. Repeatability of measurements was determined by measuring point D3 on panel TBP-1106 ten times. An average height of -0.03 mm (-0.0012 in.) was obtained, with a standard deviation of 0.01 mm (0.0004 in).

Each stiffener was measured for straightness at six points, corresponding to locations 1-6 of the panel flatness measurements. The stiffener measurements were made at a point 18.8 mm (0.74 in.) above the base of each stiffener as shown in Fig. 70. The panels were positioned vertically, and clamped lightly to a ground angle support as shown in Fig. 71. The same digital height gage and dial indicator setup was used for both the panel straightness and flatness measurements. For the stiffener straightness measurements, the height indicator was zeroed at point 1 on each stiffener, making the measurements reported for each stiffener relative to that point. Zero shift was checked by re-measuring point 1 on each stiffener at the end of each set of measurements. The results are presented in the appendix.

Preparations to test the panels at room temperature under compressive loading are in progress at the NASA Langley Research Center structural test facility.

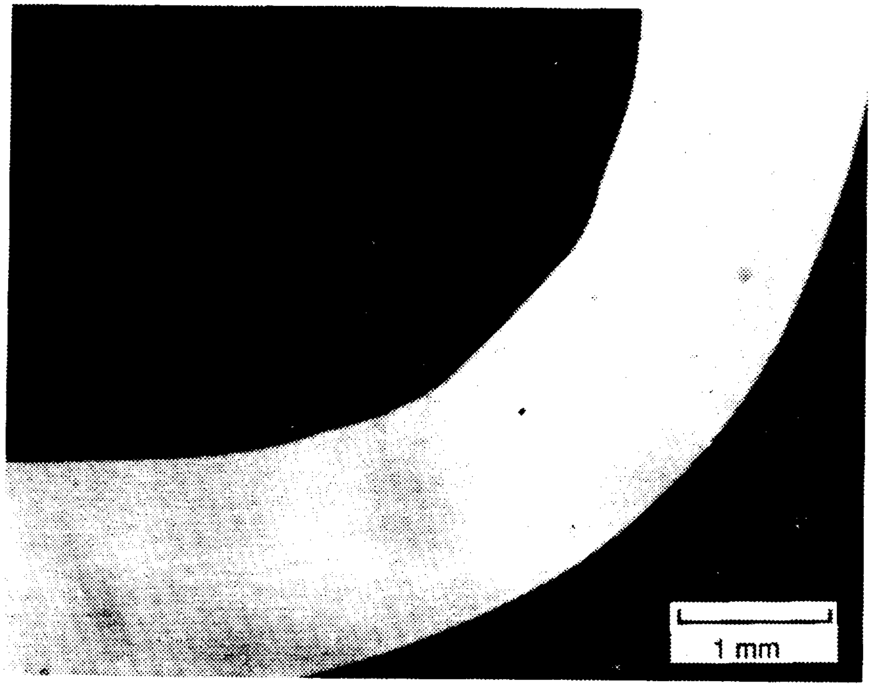

**Fig. 69 Typical Cross Section of FVS812 Zee Stiffener, 2.4 mm (0.090 in.) Bend Radius**

ORIGINAL PAGE
BLACK AND WHITE PHOTOGRAPH

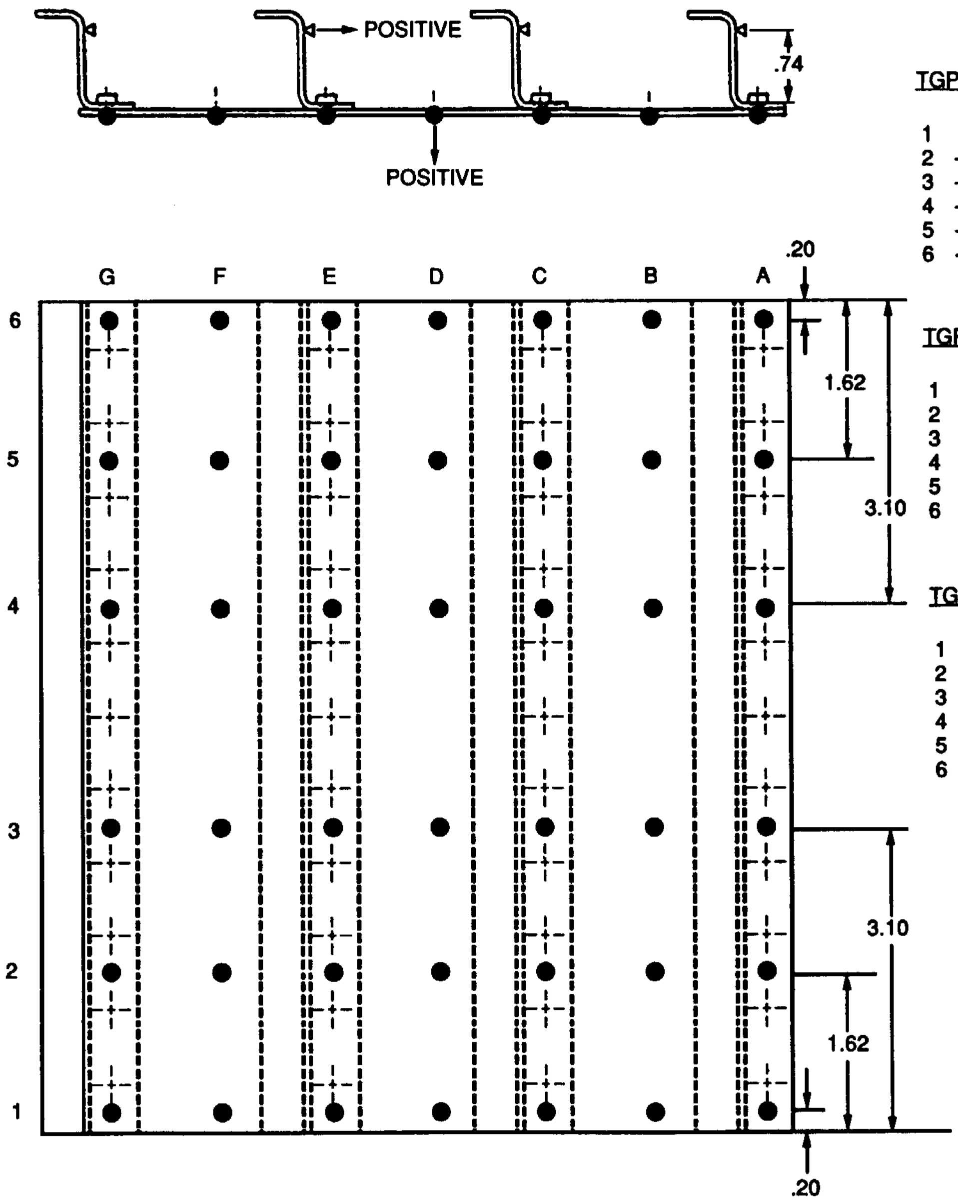

TGP-1104

| | FLATNESS MEASUREMENTS | | | | | | | STIFFENER FLATNESS MEASUREMENTS | | | |
|---|---|---|---|---|---|---|---|---|---|---|---|
| | A | B | C | D | E | F | G | A | C | E | G |
| 1 | .000 | .003 | .004 | .004 | .004 | .001 | -.003 | .000 | .000 | .000 | .000 |
| 2 | -.007 | -.002 | .001 | .004 | .004 | .004 | .002 | -.001 | -.001 | -.002 | -.003 |
| 3 | -.015 | -.008 | -.002 | .003 | .005 | .007 | .006 | -.002 | -.003 | -.003 | -.005 |
| 4 | -.024 | -.017 | -.008 | .000 | .006 | .009 | .011 | -.002 | -.003 | -.005 | -.005 |
| 5 | -.033 | -.022 | -.011 | -.003 | .004 | .007 | .011 | .000 | -.003 | -.006 | -.002 |
| 6 | -.042 | -.028 | -.016 | -.006 | .002 | .007 | .012 | .001 | -.002 | -.006 | -.000 |

TGP-1105

| | A | B | C | D | E | F | G | A | B | C | D |
|---|---|---|---|---|---|---|---|---|---|---|---|
| 1 | .000 | -.008 | -.013 | -.012 | -.008 | -.003 | .004 | .000 | .000 | .000 | .000 |
| 2 | -.005 | -.007 | -.007 | .000 | .006 | .012 | .018 | 000 | .003 | -.009 | -.004 |
| 3 | -.014 | -.012 | -.007 | .003 | .012 | .020 | .027 | -.002 | .006 | -.014 | -.005 |
| 4 | -.034 | -.023 | -.014 | .001 | .015 | .026 | .036 | -.004 | .011 | -.016 | -.007 |
| 5 | -.062 | -.037 | -.024 | -.007 | .009 | .024 | .036 | -.006 | .012 | -.016 | -.009 |
| 6 | -.070 | -.052 | -.034 | -.014 | .001 | .018 | .034 | -.010 | .016 | -.015 | -.013 |

TGP-1106

| | A | B | C | D | E | F | G | A | B | C | D |
|---|---|---|---|---|---|---|---|---|---|---|---|
| 1 | .000 | -.002 | -.010 | -.012 | -.014 | -.008 | .002 | .000 | .000 | .000 | .000 |
| 2 | .000 | -.001 | -.005 | -.005 | -.003 | .003 | 015 | .002 | -.007 | -.007 | -.002 |
| 3 | .000 | -.001 | -.002 | -.001 | .003 | .011 | .023 | .003 | -.015 | -.014 | -.005 |
| 4 | -.007 | -.006 | -.004 | .001 | .007 | .016 | .030 | .000 | -.026 | -.022 | -.010 |
| 5 | -.015 | -.011 | -.009 | -.003 | .003 | .014 | .034 | -.006 | -.036 | -.028 | -.011 |
| 6 | -.020 | -.014 | -.011 | -.005 | .003 | .016 | .035 | -.012 | -.047 | -.036 | -.012 |

◃ STIFFENER STRAIGHTNESS MEASURED POINT

● OUT-OF-PLANE MEASURED POINT

-┼- RIVET/SPOT WELD

ALL DIMENSIONS ARE IN INCHES.

Fig. 70 Compression Panel Flatness Measurements (Dwg. TGP-1104)

ORIGINAL PAGE
BLACK AND WHITE PHOTOGRAPH

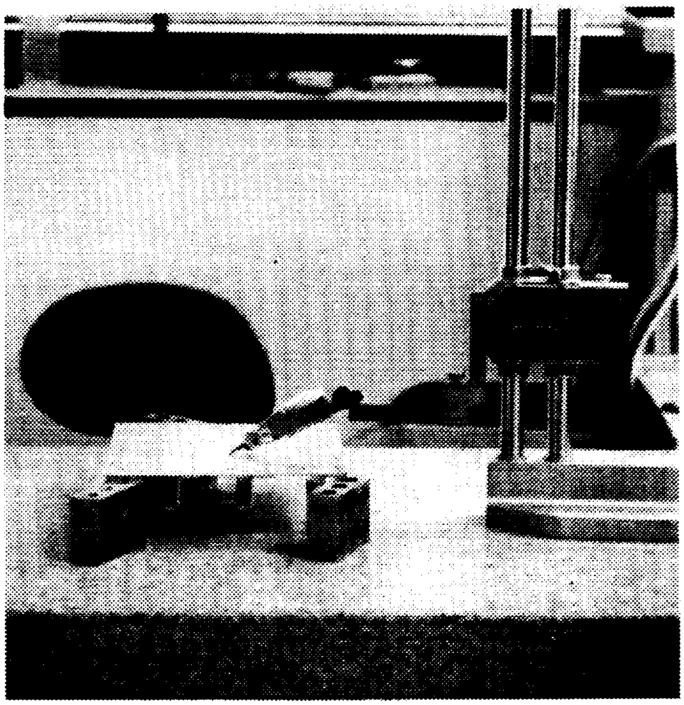

a) SURFACE FLATNESS

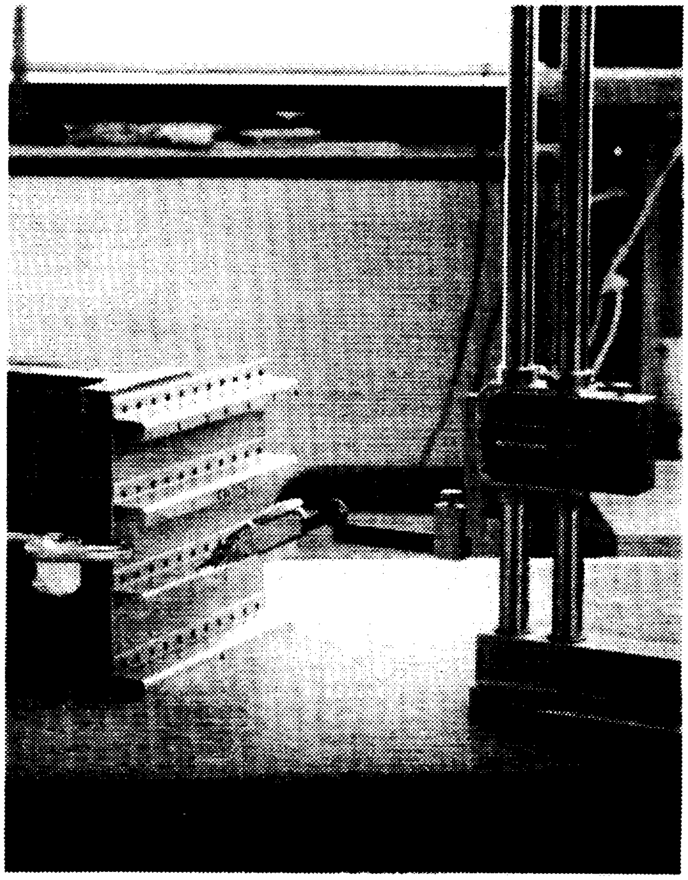

b) STIFFENER STRAIGHTNESS

**Fig. 71 Set-Up for Flatness and Straightness Measurements**

## 6. SUMMARY AND CONCLUSIONS

1. The FVS812 alloys exhibited excellent high-temperature strength stability. There was no significant effect on strength after thermal exposures up to 315°C (600°F) for 1000 h. Tensile ductility appeared to be sensitive to long-term thermal exposure; minimum values for all conditions ≥5% elongation. The apparent fluctuations in ductility, especially after thermal exposure, are not entirely explained and remain in need of further clarification, particularly if reliable design allowables are to be developed. The effects of dynamic strain aging on tensile ductility and other properties, such as toughness and fatigue crack initiation and growth, must be further explored.

2. The tear resistance of the FVS812 alloys were excellent compared with other aluminum alloys, particularly in the L-T direction. The lower T-L values were most likely associated with the low fracture resistance of prior ribbon particle boundaries. This characteristic must be carefully considered when developing structural design data. A minimum in unit propagation energy after thermal exposure at 200°C was observed in both lots of FVS812 and appears related to the reductions observed in tensile ductility after similar exposures.

3. S-N fatigue behavior for these alloys was comparable to that of 2024-T81 from the mid-life to high cycle range. Generally, very little difference existed between the L and T orientations, before and after thermal exposure. The 20 h degassed, as-received material had relatively higher fatigue strength at room temperature, than the 2 h degassed material. However, after thermal exposure at 100h/315°C (600°F), fatigue strength for the 2 h degassed alloy increased approximately 20% for both the L and T conditions. This effect is not explained and was not observed in the 20 h degassed alloy. At elevated temperature, fatigue life was satisfactory and consistent with other observations indicative of excellent dispersoid stability. There was no significant effect of sheet orientation on life at these temperatures. At 100,000 cycles, fatigue strength at 200°C (392°F) is reduced approximately 20% from the room temperature condition and, at 315°C (600°F), by approximately 38%.

4. The extended degassed alloy (20 h) appeared to have somewhat better tensile ductility, more consistent toughness and higher fatigue strength at room temperature. Weld porosity formation during fusion welding was clearly reduced in the 20 h degas alloy and weld porosity in the resistance spot welds was significantly lower than that of the 2 h alloy. The mechanism and effects of degassing are not clear, but are likely to involve hydrogen interactions as a result of billet degassing and subsequent evaporation and decomposition of other hydrogen containing species trapped in the microstructure.

5. Brake forming at temperatures ≥370°C (700°F) was readily accomplished. A minimum bend radius of 0.79 mm (1/32 in.) for 1.6 mm (0.063 in.) thick sheet was achieved without cracking for both degassed conditions and for the L and T orientations. The small bend radius offers excellent potential for the design of more efficient sheet-stiffened, built-up structure. The alloy has potential for hot forming more complex configurations.

6. FVS812 was readily resistance spot-welded and dispersoid coarsening during welding did not appear to seriously degrade strength. The average spot weld shear strength was approximately 80% that of the minimum average specified by MIL-W-6858D for comparable strength conventional aluminum alloys. Further weld parameter optimization should improve strength and consistency. In 20 h, extended-degassed material, weld porosity was reduced and strength was slightly increased compared with the standard 2 h degassed material. Static and fatigue strength of single-spot welds indicated good microstructural stability after testing at RT, 200°C (392°F), and 315 °C (600°F). Excellent resistance to deformation adjacent to the electrodes was exhibited, thereby allowing the use of a reduced minimum edge distance. Also, spot spacing was decreased because current shunting was reduced significantly, compared with conventional Al alloys. These characteristics are advantageous in the design of more efficient structure.

7. Gas-tungsten-arc or electron beam welding of these alloys was not feasible at this time. Although outgassing during welding was reduced in the extended-degassed alloy, extensive dispersoid coarsening and formation of primary intermetallic phases severely degraded weld strength and ductility. Gas content was too high to produce porosity free fusion welds. Improvements in material processing to further limit base metal gas content are necessary to increase weldability.

8. The manufacture of Z-stiffened riveted and resistance-spot-welded compression panels demonstrated the fabricability of this material using conventional methods.

# 7. RECOMMENDED FUTURE WORK

1. Determine the mechanism of billet degassing and its effect on hydrogen containing species and the effects of improved degassing procedures on mechanical properties and weld porosity formation.

2. Determine the mechanism and effects of dynamic strain aging (DSA) on notch toughness, fatigue crack initiation and fatigue crack growth for intermediate temperatures.

3. Determine mechanism and effect of intermediate temperature thermal exposure on mechanical properties.

4. Determine combined effects of DSA and low temperature exposure on mechanical properties.

5. Continue welding research and development with improved quality materials.

6. Continue hot forming research and development. Determine effect of forming on microstructure and properties.

7. Determine the effect of cold work and interference-fit fasteners on crack initiation behavior and crack growth at fastener holes.

8. Continue development and fabrication of structural test items for evaluation of elevated temperature applicability.

THIS PAGE INTENTIONALLY LEFT BLANK

## 8. REFERENCES

1. D. J. Chellman, *Elevated Temperature Aluminum Program (ETAP)*, LR 31519-11, Interim Report for Period April-June 1990, Lockheed Aeronautical Systems Co., Burbank, CA, June 1990.

2. Douglas Aircraft Co., *Study of High Speed Civil Transports* , NASA-CR-4235, Long Beach, CA , December 1989.

3. J. C. Eckvall, R. A. Rainen, and D. J. Chellman, *J. Aircraft*, **27**, 1990, pp. 836-843.

4. W. A. Frazier, E. W. Lee, M. E. Donnellan, and J. Thompson, *J. of Met.*, **41**, 1989, pp. 22-30.

5. S. L. Langenbeck, R.A. Rainen et al. *Elevated Temperature Aluminum Alloy Program*, Lockheed-California Co., Burbank, CA, AFWAL-TR-86-4027, May 1986.

6. E. Y. Ting and J. R. Kennedy, *Superplastic Forming and Diffusion Bonding Behavior of Rapidly Solidified, Dispersion Strengthened Al Alloys for Elevated Temperature Structural Applications* , Grumman Aerospace Corporation, Bethpage, NY 11714, NASA-CR 181849, September 1989.

7. A. K. Gogoa, P. V. Roa, and J. A. Sekhar, *J. Mat. Sci.* , **20**, 1985, p. 3091.

8. D. J. Skinner, R. L. Bye, D. Raybould, and A. M. Brown, *Scripta Met* , **20**, 1986, p. 867 .

9. D. J. Skinner, R. L. Bye, D. Raybould, A. M. Brown, and M. S. Zedalis, *Processing of Structural Metals by Rapid Solidification*, Eds. F. H. Froes, and S. J. Savages, ASM, Metals Park, OH, 1987, p. 291.

10. D. Munson, *J. Inst. Metals* , **95**, 1967, p.217 .

11. D. J. Skinner, *Dispersion Strengthened Aluminum Alloys*, Eds. Y.W. Kim and W. M. Griffith, TMS -Minerals, Metals & Materials Society, Warrendale, PA, Phoenix, AZ, 1988, p.181.

12. K. S. Chan, *Met. Trans.* , **20A**, 1989, pp. 2337-2344.

13. M. J. Mayo and W. D. Nix, *Superplasticity and Superplastic Forming* , Eds. C. H. Hamilton and N. E. Paton, TMS -Minerals, Metals & Materials Society, Warrendale, PA, Blaine, WA, 1988), pp. 21-25.

14. J. Weertman, *J. Appl. Phys.* , **28**, 1957, p. 362.

15. M. Zedalis, Private Communication, July 1991.

16. O. R. Singleton and R. M. Royster, *J. Metals* , November 1988, p. 40.

17. J. Kaufman and M. Holt, Pittsburg, PA, *Fracture Characteristics of Aluminum Alloys*, Alcoa Research Laboratories, Technical Paper No, 18, 1965.

18. J. G. Kaufman and A.H. Knoll, *Mat. Res. & Stand.* , April 1964, p. 151.

19. Grumman Corporation,*Test: Non-destructive Penetrant Method of Inspection*, GT-23A, Bethpage, NY, 1990.

20. P. Gilman and M. Zedalis, Private Communication. April 1991.

21. Y. W. Kim, *Dispersion Strengthened Aluminum Alloys*, Eds. Y.W. Kim and W.M. Griffith, TMS -Minerals, Metals & Materials Society, Warrendale, PA, Phoenix, AZ, 1988, p.p. 157-180.

22. W. C. Porr, Y. Leng, and R. P. Gangloff, *Elevated Temperature Fracture Toughness of P/M Al-Fe-V-Si* , University of Virginia, Unpublished Work, 1990.

23. D. J. Skinner, M. S. Zedalis, and P. Gilman, *Mat. Sci. & Eng.* , **A119**, 1989, pp. 81-86 .

24. D. J. Skinner, M. S. Zedalis, and J. Peltier, *Lightweight Alloys for Aerospace Applications*, Eds. E.W. Lee, E.H. Chia, and N.J. Kim, TMS-AIME, Warrendale, PA, 1989, pp. 71-78.

25. Y. Leng, W. C. Porr, and R. P. Gangloff, *Scripta Met* , **24**, 1990, pp. 2163-2168 .

26. S. Kalpakjian, *Manufacturing Processes of Engineering Materials* , Addison-Wesley, Reading, MA, 1984.

27. J. C. Lee, S. Lee, D. Y. Lee, and N. J. Kim, *Met. Trans.* , **22A**, 1991, pp. 853-858 .

28. H. H. Smith, D. J. Michel, and J. R. Reed, *Met. Trans.* **20A**, 1989, pp. 2425-2430 .

29. G. S. Murty and M. J. Koczak, *Unpublished Research* , 1990.

30. G. Sachs, *Principles and Methods of Sheet-Metal Fabricating* , Reinhold, New York, 1966.

31. D. Raybould, *Dispersion Strengthened Aluminum Alloys*, Eds. Y.W. Kim and W.M. Griffith, TMS-Minerals, Metals & Materials Society, Warrendale, PA, Phoenix, AZ, 1988, pp. 199-215.

32. S. Krishnaswamy and W. A. Baeslack, *Mat. Sci. and Eng.* ,**98**, 1988, pp. 137-141 .

33. G. E. Metzger, *Gas Tungsten Arc Welding of Al-10Fe-5Ce*, Air Force Wright Aeronautical Laboratories, AFWAL-TR-8784037, Wright-Patterson AFB, OH, February 1987.

34. H. Jones, *Mat. Sci. & Eng.* , **5**, 1969, pp. 1-18 .

35. W. A. Baeslack and K. S. Hagey, *Weld. J.*, **67**, 1988, pp. 139s-149s .

36. F. E. Bunce, *User's Manual for CURVPANL-The Analysis of Flat and Curved Stiffened Sheet Subjected to In-Plane Shear and Compressive Loads* , Grumman Corporation, Bethpage, NY, 1978.

THIS PAGE INTENTIONALLY LEFT BLANK

# APPENDIX A

# MECHANICAL PROPERTIES

**Table A-1 Effect of Thermal Exposure on Tensile Properties of FVS812 Alloy (Lot 96, 2 h Degas)**

| Alloy | Exposure | Direct. | Strain | Test Temp. | | 0.2 % Yield Strength | | Ultimate Strength | | Elong. | Modulus | |
|---|---|---|---|---|---|---|---|---|---|---|---|---|
| | | | Rate | °C (°F) | | ksi | (MPa) | ksi | (MPa) | (%) | 10^6 psi | (GPa) |
| Lot 96 | As-received | L | 0.001 | 20 (68) | | 64.9 | (448) | 68.4 | (471.9) | 6.6 | 11.3 | (77.8) |
| | | | | | | 66.0 | (455) | 68.6 | (472.9) | 6.7 | 11.8 | (81.6) |
| | | | | | *avg.* | *65.5* | (451) | *68.5* | (472.4) | *6.7* | *11.6* | (79.7) |
| | | T | | | | 62.3 | (429) | 67.3 | (464.2) | 14.2 | 12.6 | (86.5) |
| | | | | | | 60.9 | (420) | 66.9 | (460.9) | 13.3 | 12.1 | (83.2) |
| | | | | | *avg.* | *61.6* | (425) | *67.1* | (462.6) | *13.7* | *12.3* | (84.9) |
| | 100h/200°C | L | | | | 66.3 | (457) | 70.6 | (486.6) | 6.1 | 12.3 | (84.5) |
| | | | | | | 66.0 | (455) | 70.1 | (483.3) | 4.9 | 12.6 | (86.7) |
| | | | | | *avg.* | *66.2* | (456) | *70.3* | (485.0) | *5.5* | *12.4* | (85.6) |
| | | T | | | | 64.1 | (442) | 67.9 | (468.4) | 6.0 | 10.7 | (73.4) |
| | | | | | | 62.1 | (428) | 71.7 | (494.6) | 11.5 | 12.7 | (87.8) |
| | | | | | *avg.* | *63.1* | (435) | *69.8* | (481.5) | *8.8* | *11.7* | (80.7) |
| | 100h/315°C | L | | | | 67.5 | (466) | 69.3 | (477.5) | 6.3 | 8.4 | (57.8) |
| | | | | | | 64.0 | (441) | 69.3 | (477.6) | 6.8 | 11.9 | (82.1) |
| | | | | | *avg.* | *65.8* | (453) | *69.3* | (477.5) | *6.6* | *10.2* | (70.0) |
| | | T | | | | 67.4 | (465) | 70.9 | (488.6) | 6.3 | 8.7 | (60.1) |
| | | | | | | 62.2 | (429) | 69.8 | (481.3) | 6.1 | 12.2 | (84.1) |
| | | | | | *avg.* | *64.8* | (447) | *70.3* | (485.0) | *6.2* | *10.5* | (72.1) |
| | 1000h/200°C | L | | | | 64.3 | (443) | 69.3 | (478.0) | 5.4 | 11.8 | (81.3) |
| | | | | | | 62.6 | (431) | 69.0 | (476.0) | 5.8 | 13.1 | (90.5) |
| | | | | | *avg.* | *63.4* | (437) | *69.2* | (477.0) | *5.6* | *12.5* | (85.9) |
| | | T | | | | 60.8 | (419) | 68.6 | (472.7) | 6.8 | 13.4 | (92.0) |
| | | | | | | 60.3 | (416) | 68.1 | (469.2) | 7.4 | 12.1 | (83.2) |
| | | | | | *avg.* | *60.6* | (418) | *68.3* | (470.9) | *7.1* | *12.7* | (87.6) |
| | 1000h/315°C | L | | | | 62.5 | (431) | 68.4 | (471.7) | 6.3 | 12.3 | (84.5) |
| | | | | | | 60.0 | (414) | 68.7 | (473.8) | 7.0 | 16.1 | (111.2) |
| | | | | | *avg.* | *61.3* | (422) | *68.6* | (472.8) | *6.7* | *14.2* | (97.9) |
| | | T | | | | 64.6 | (445) | 71.4 | (492.1) | 11.3 | 12.6 | (86.9) |
| | | | | | | 64.0 | (441) | 70.5 | (486.1) | 8.1 | 12.6 | (86.7) |
| | | | | | *avg.* | *64.3* | (443) | *70.9* | (489.1) | *9.7* | *12.6* | (86.8) |

**Table A-2 Effect of Thermal Exposure on Tensile Properties of FVS812 Alloy (Lot 115)**

| Alloy | Exposure | Direct. | Strain Rate | Test Temp. °C (°F) | | 0.2 % Yield Strength ksi | (MPa) | Ultimate Strength ksi | (MPa) | Elong. (%) | Modulus 10^6 psi | (GPa) |
|---|---|---|---|---|---|---|---|---|---|---|---|---|
| Lot 115 (20 h Degas) | As-received | L | 0.001 | 20 (68) | | 63.3 | (436) | 66.6 | (458.9) | 12.3 | 12.3 | (84.8) |
| | | | | | | 60.9 | (420) | 67.2 | (463.1) | 11.5 | 14.2 | (97.9) |
| | | | | | *avg.* | *62.1* | (428) | *66.9* | (461.1) | *11.9* | *13.1* | (90.6) |
| | | T | | | | 56.8 | (391) | 64.5 | (445.0) | 12.2 | 13.9 | (95.8) |
| | | | | | | 60.2 | (415) | 65.7 | (453.0) | 12.2 | 11.6 | (80.1) |
| | | | | | *avg.* | *58.5* | (403) | *65.1* | (449.0) | *12.2* | *12.8* | (88.0) |
| | 100h/200°C | L | 0.001 | 20 (68) | | 61.9 | (427) | 68.3 | (471.0) | 7.7 | 13.9 | (95.5) |
| | | | | | | 64.6 | (446) | 68.8 | (474.2) | 9.7 | 11.5 | (79.0) |
| | | | | | *avg.* | *63.3* | (436) | *68.6* | (472.7) | *8.7* | *12.7* | (87.3) |
| | | T | | | | 63.7 | (439) | 68.2 | (470.1) | 10.7 | 11.0 | (75.9) |
| | | | | | | 62.5 | (431) | 68.1 | (469.8) | 11.5 | 11.0 | (75.5) |
| | | | | | *avg.* | *63.1* | (435) | *68.2* | (470.0) | *11.1* | *11.0* | (75.7) |
| | 100h/315°C | L | 0.001 | 20 (68) | | 64.1 | (442) | 68.4 | (471.8) | 14.6 | 11.0 | (75.7) |
| | | | | | | 62.3 | (429) | 69.0 | (475.6) | 9.8 | 12.8 | (88.3) |
| | | | | | *avg.* | *63.2* | (436) | *68.7* | (473.7) | *12.2* | *11.9* | (82.1) |
| | | T | | | | 61.5 | (424) | 69.1 | (476.2) | 9.8 | 12.0 | (82.5) |
| | | | | | | 61.2 | (422) | 68.9 | (474.9) | 11.9 | 12.9 | (89.2) |
| | | | | | *avg.* | *61.4* | (423) | *69.0* | (475.5) | *10.9* | *12.5* | (85.8) |
| | 1000h/200°C | L | 0.001 | 20 (68) | | 63.9 | (441) | 68.4 | (471.9) | 10.2 | 11.6 | (80.2) |
| | | | | | | 62.8 | (433) | 67.5 | (465.2) | 9.9 | 11.9 | (82.3) |
| | | | | | | 62.8 | (433) | 67.2 | (463.4) | 5.9 | 11.7 | (80.5) |
| | | | | | *avg.* | *63.2* | (436) | *67.7* | (466.9) | *8.7* | *11.8* | (81.0) |
| | | T | | | | 60.9 | (420) | 66.9 | (461.1) | 7.3 | 11.8 | (81.3) |
| | | | | | | 57.1 | (394) | 66.8 | (460.9) | 8.0 | 15.2 | (104.9) |
| | | | | | *avg.* | *59.0* | (407) | *66.9* | (461.0) | *7.6* | *13.5* | (93.1) |
| | 1000h/315°C | L | 0.001 | 20 (68) | | 62.2 | (429) | 67.8 | (467.2) | 12.6 | 12.0 | (82.9) |
| | | | | | | 61.0 | (420) | 67.5 | (465.1) | 6.6 | 12.6 | (86.9) |
| | | | | | *avg.* | *61.6* | (425) | *67.6* | (466.2) | *9.6* | *12.3* | (84.9) |
| | | T | | | | 64.1 | (442) | 68.4 | (471.3) | 8.8 | 10.1 | (69.4) |
| | | | | | | 60.6 | (418) | 64.9 | (447.6) | 6.7 | 13.1 | (90.4) |
| | | | | | *avg.* | *62.4* | (430) | *66.6* | (459.4) | *7.8* | *11.6* | (79.9) |
| Lot 115 (20 h Degas) | As-received | L | 0.001 | 315 (600) | | 21.8 | (150) | 29.5 | (203.2) | 13.4 | 8.8 | (60.3) |
| | | | | | | 25.7 | (177) | 29.8 | (205.7) | 11.5 | 4.4 | (30.4) |
| | | | | | *avg.* | *25.0* | (172) | *29.7* | (204.5) | *12.4* | *6.6* | (45.4) |
| | 100h/200°C | L | 0.001 | 315 (600) | | 26.2 | (181) | 31.0 | (213.5) | 11.4 | 5.8 | (39.9) |
| | | | | | | 27.0 | (186) | 31.7 | (218.3) | 16.9 | 5.1 | (35.0) |
| | | | | | *avg.* | *26.6* | (183) | *31.3* | (216.0) | *14.2* | *5.4* | (37.4) |
| | 100h/315°C | L | 0.001 | 315 (600) | | 27.7 | (191) | 28.3 | (195.1) | 28.6 | 2.1 | (14.5) |
| | | | | | | 26.6 | (183) | 29.6 | (204.4) | 15.6 | 7.5 | (51.8) |
| | | | | | *avg.* | *27.1* | (187) | *29.0* | (199.7) | *22.1* | *4.8* | (33.2) |
| | 1000h/200°C | L | 0.001 | 315 (600) | | 24.1 | (166) | 29.5 | (203.7) | 13.0 | 5.5 | (37.9) |
| | | | | | | 23.5 | (162) | 28.6 | (197.3) | 21.4 | 4.6 | (31.5) |
| | | | | | *avg.* | *23.8* | (164) | *29.1* | (200.5) | *17.2* | *5.0* | (34.7) |
| | 1000h/315°C | L | 0.001 | 315 (600) | | 27.5 | (190) | 30.1 | (207.6) | 18.6 | 4.7 | (32.3) |
| | | | | | | 27.6 | (190) | 30.7 | (211.5) | 15.1 | 4.0 | (27.7) |
| | | | | | *avg.* | *27.5* | (190) | *30.4* | (209.5) | *16.9* | *4.4* | (30.1) |

**Table A-3 Room Temperature Tensile Properties of FVS812 Lots 335 and 340, 2024-T81 and 2219-T62 Alloys**

| Alloy | Exposure | Direct. | Strain Rate | Test Temp. °C (°F) | | 0.2 % Yield Strength | | Ultimate Strength | | Elong. | Modulus | |
|---|---|---|---|---|---|---|---|---|---|---|---|---|
| | | | | | | ksi | (MPa) | ksi | (MPa) | (%) | 10^6 psi | (GPa) |
| Lot 335<br>(2 h Degas) | As-received | L | 0.001 | 20 (68) | | 65.8 | (454) | 68.8 | (474.5) | 10.1 | 12.0 | (82.5) |
| | | | | | | 65.8 | (453) | 68.6 | (473.2) | 8.9 | 11.3 | (77.6) |
| | | | | | *avg.* | *65.8* | (454) | *68.7* | (473.9) | *9.5* | *11.6* | (80.1) |
| | | T | | | | 63.7 | (439) | 70.3 | (484.7) | 10.4 | 12.5 | (86.0) |
| | | | | | | 64.2 | (442) | 69.6 | (479.7) | 13.1 | 11.8 | (81.0) |
| | | | | | *avg.* | *63.9* | (441) | *69.9* | (482.2) | *11.8* | *12.1* | (83.6) |
| Lot 340<br>20 h Degas) | As-received | L | 0.001 | 20 (68) | | 64.3 | (443) | 67.8 | (467.8) | 8.4 | 11.4 | (78.4) |
| | | | | | | 63.9 | (440) | 68.1 | (469.7) | 8.2 | 12.9 | (88.9) |
| | | | | | *avg.* | *64.1* | (442) | *68.0* | (468.7) | *8.3* | *12.1* | (83.7) |
| | | T | | | | 62.1 | (428) | 68.4 | (471.4) | 11.4 | 12.2 | (83.9) |
| | | | | | | 62.4 | (430) | 68.1 | (469.6) | 11.0 | 12.7 | (87.7) |
| | | | | | *avg.* | *62.3* | (429) | *68.2* | (470.5) | *11.2* | *12.5* | (85.8) |
| 2024-T81 | As-received | L | 0.001 | 20 (68) | | 67.6 | (466) | 73.5 | (506.6) | 8.9 | 10.2 | (70.0) |
| | | | | | | 67.6 | (466) | 73.2 | (505.0) | 9.4 | 8.8 | (60.7) |
| | | | | | *avg.* | *67.6* | (466) | *73.4* | (505.8) | *9.2* | *9.5* | (65.4) |
| | 100h/200°C | L | 0.001 | 20 (68) | | 50.2 | (346) | 62.9 | (433.9) | 11.0 | 10.3 | (71.3) |
| | | | | | | 56.2 | (387) | 62.6 | (431.8) | 10.7 | 9.7 | (67.1) |
| | | | | | | 50.4 | (348) | 62.6 | (431.3) | 11.4 | 10.4 | (71.4) |
| | | | | | *avg.* | 52.3 | (360) | 62.7 | (432.3) | 11.0 | 10.1 | (69.9) |
| | 100h/315°C | L | 0.001 | 20 (68) | | 22.8 | (157) | 34.9 | (240.5) | 19.1 | 8.4 | (57.8) |
| | | | | | | 17.8 | (123) | 35.0 | (241.0) | 19.3 | 5.9 | (40.5) |
| | | | | | | 17.0 | (117) | 35.2 | (242.6) | 22.5 | 7.5 | (51.9) |
| | | | | | *avg.* | *19.2* | (132) | *35.0* | (241.3) | *20.3* | *7.3* | (50.1) |
| 2219-T62 | As-received | L | 0.001 | 20 (68) | | 38.8 | (267) | 57.3 | (395.2) | 12.0 | 11.8 | (81.6) |
| | | | | | | 39.0 | (269) | 57.8 | (398.5) | 9.36* | 11.0 | (75.6) |
| | | | | | | 38.4 | (265) | 57.6 | (396.9) | 10.3 | 11.4 | (78.5) |
| | | | | | *avg.* | *38.7* | (267) | *57.6* | (396.9) | *10.6* | *11.4* | (78.5) |
| | 100h/200°C | L | 0.001 | 20 (68) | | 35.2 | (243) | 57.4 | (395.5) | 11.0 | 10.6 | (73.2) |
| | 100h/315°C | L | 0.001 | 20 (68) | | 23.7 | (164) | 46.9 | (323.3) | 13.7 | 10.3 | (70.7) |
| | | | | | | 23.9 | (165) | 46.7 | (321.7) | 13.1 | 9.6 | (65.9) |
| | | | | | *avg.* | *23.8* | (164) | *46.8* | (322.5) | *13.4* | *9.9* | (68.3) |

**Table A-4 Effect of Elevated Temperature on Tensile Properties of FVS812 Alloy (Lot 115, 20 h Degas)**

| Alloy | Exposure | Direct. | Strain Rate | Test Temp. °C (°F) | | 0.2 % Yield Strength | | Ultimate Strength | | Elong. | Modulus | |
|---|---|---|---|---|---|---|---|---|---|---|---|---|
| | | | | | | ksi | (MPa) | ksi | (MPa) | (%) | ks i | (MPa) |
| Lot 115<br>(20 h Degas) | as-received | L | 0.001 | 20 (68) | | 63.3 | (436) | 66.6 | (458.9) | 12.3 | 12.1 | (83.3) |
| | | | | | | 60.9 | (420) | 67.2 | (463.1) | 11.5 | 14.2 | (97.9) |
| | | | | | *avg.* | *62.1* | (428) | *66.9* | (461.1) | *11.9* | *13.1* | (90.6) |
| | | | | 80 (176) | | 46.5 | (320) | 57.1 | (393.4) | 5.0 | 10.4 | (72.0) |
| | | | | | | 53.6 | (369) | 57.9 | (399.3) | 5.2 | 7.3 | (50.5) |
| | | | | | *avg.* | *50.0* | (345) | *57.5* | (396.4) | *5.1* | *8.9* | (61.3) |
| | | | | 177 (351) | | 43.6 | (300) | 48.5 | (334.3) | 6.0 | 4.9 | (34.1) |
| | | | | | | 38.2 | (264) | 49.1 | (338.5) | 7.2 | 8.5 | (58.7) |
| | | | | | *avg.* | *40.9* | (282) | *48.8* | (336.4) | *6.6* | *6.7* | (46.4) |
| | | | | 200 (392) | | 44.1 | (304) | 46.4 | (319.7) | 7.1 | 5.4 | (37.5) |
| | | | | | | 42.2 | (291) | 46.4 | (319.7) | 9.0 | 7.8 | (53.4) |
| | | | | | *avg.* | *43.1* | (297) | *46.4* | (319.7) | *8.1* | *6.6* | (45.5) |
| | | | | 315 (600) | | 21.8 | (150) | 29.5 | (203.2) | 13.4 | 8.8 | (60.3) |
| | | | | | | 25.7 | (177) | 29.8 | (205.7) | 11.5 | 4.4 | (30.4) |
| | | | | | *avg.* | *25.0* | (172) | *29.7* | (204.5) | *12.4* | *6.6* | (45.4) |

**Table A-5 Effect of Strain Rate on Tensile Properties of FVS812 Alloy (Lot 115, 20 h Degas)**

| Alloy | Exposure | Direct. | Strain Rate | Test Temp. °C (°F) | | 0.2 % Yield Strength ksi | (MPa) | Ultimate Strength ksi | (MPa) | Elong. (%) | Modulus 10^6 psi | (GPa) |
|---|---|---|---|---|---|---|---|---|---|---|---|---|
| Lot 115 | As-received | L | 0.001 | 20 (68) | | 63.3 | (436) | 66.6 | (458.9) | 12.3 | 12.1 | (83.3) |
| (20 h Degas) | | | | | | 60.9 | (420) | 67.2 | (463.1) | 11.5 | 14.2 | (97.9) |
| | | | | | *avg.* | *62.1* | (428) | *66.9* | (461.1) | *11.9* | *13.1* | (90.6) |
| | | | 0.01 | | | 65.4 | (451) | 71.0 | (489.8) | 20.2 | 12.3 | (84.7) |
| | | | | | | 64.3 | (443) | 70.3 | (484.7) | 16.3 | 11.9 | (81.8) |
| | | | | | | 62.3 | (430) | 68.7 | (473.5) | 11.6 | 11.3 | (78.2) |
| | | | | | | 62.3 | (429) | 68.8 | (474.1) | *** | 12.3 | (85.0) |
| | | | | | *avg.* | *63.6* | (438) | *69.7* | (480.6) | *16.0* | *12.0* | (82.5) |
| | | | 0.1 | | | *** | *** | 73.9 | (509.7) | 11.1 | *** | *** |
| | | | | | | *** | *** | 75.0 | (516.9) | 7.8 | *** | *** |
| | | | | | | 65.1 | (449) | 73.8 | (509.1) | 11.0 | 12.3 | (85.1) |
| | | | | | *avg.* | *65.1* | (449) | *73.8* | (509.1) | *10.0* | *12.3* | (85.1) |
| | | | 1 | | | *** | *** | *** | *** | 9.0 | *** | *** |
| | | | | | | *** | *** | 74.4 | (512.7) | 8.8 | *** | *** |
| | | | | | *avg.* | *** | *** | *74.4* | (512.7) | *8.9* | *** | *** |
| | | | | | | | *** | | | | | *** |
| | | | 5 | | | *** | *** | 78.3 | (539.8) | 6.5 | *** | *** |
| | | | | | | *** | *** | 77.9 | (537.4) | 5.1 | *** | *** |
| | | | | | *avg.* | *** | *** | *78.1* | (538.6) | *5.8* | *** | *** |
| | | | 10 | | | 60.7 | (418) | 64.7 | (446.0) | 11.4 | 11.3 | (77.8) |
| | | | | | | *** | *** | *** | *** | 7.8 | *** | *** |
| | | | | | *avg.* | *60.7* | (419) | *64.7* | (446.0) | *9.6* | *11.3* | (77.8) |
| Lot 115 | As-received | L | 0.001 | 315 (600) | | 21.8 | (150) | 29.5 | (203.2) | 13.4 | 8.8 | (60.3) |
| (20 h Degas) | | | | | | 25.7 | (177) | 29.8 | (205.7) | 11.5 | 4.4 | (30.4) |
| | | | | | *avg.* | *25.0* | (172) | *29.7* | (204.5) | *12.4* | *6.6* | (45.4) |
| | | | 0.01 | | | 23.9 | (165) | 31.8 | (219.5) | 15.5 | 6.3 | (43.6) |
| | | | | | | 35.6 | (245) | 36.6 | (252.6) | 8.9 | 3.4 | (23.7) |
| | | | | | *avg.* | *29.8* | (205) | *34.2* | (236.1) | *12.2* | *4.9* | (33.7) |
| | | | 0.1 | | | 35.1 | (242) | 36.4 | (250.7) | 11.2 | 4.8 | (32.8) |
| | | | | | | 34.3 | (236) | 36.5 | (251.8) | 17.6 | 5.5 | (38.1) |
| | | | | | *avg.* | *34.7* | (239) | *36.4* | (251.3) | *14.4* | *5.1* | (35.4) |
| | | | 1 | | | *** | *** | 39.3 | (270.8) | 8.0 | *** | *** |
| | | | | | | *** | *** | 41.9 | (288.9) | 13.8 | *** | *** |
| | | | | | *avg.* | | | *40.6* | *(279.9)* | *10.9* | | |
| | | | | | | | | | | | | *** |
| | | | 5 | | | *** | *** | 42.5 | (293.2) | 10.0 | *** | *** |
| | | | | | | *** | *** | 41.6 | (287.1) | 10.9 | *** | *** |
| | | | | | *avg.* | *** | *** | *42.1* | (290.1) | *10.4* | *** | *** |

*continued next page*

**Table A-5 concluded**

| Alloy | Exposure | Direct. | Strain Rate | Test Temp. °C (°F) | | 0.2 % Yield Strength ksi | (MPa) | Ultimate Strength ksi | (MPa) | Elong. (%) | Modulus 10^6 psi | (GPa) |
|---|---|---|---|---|---|---|---|---|---|---|---|---|
| Lot 115 (20 h Degas) | As-received | L | 0.001 | 482 (900) | | 7.6 | (52) | 10.4 | (71.6) | 16.7 | 2.6 | (18.0) |
| | | | | | | 9.5 | (65) | 10.3 | (70.8) | 18.7 | 1.9 | (13.1) |
| | | | | | *avg.* | *8.5* | (59) | *10.3* | (71.2) | *17.7* | *2.3* | (15.6) |
| | | | 0.01 | | | 10.3 | (71) | 11.6 | (80.1) | 19.1 | 3.6 | (24.8) |
| | | | | | | 9.1 | (63) | 11.6 | (80.0) | 23.4 | 3.0 | (20.5) |
| | | | | | *avg.* | 9.7 | (67) | 11.6 | (80.1) | 21.2 | 3.3 | (22.7) |
| | | | 0.1 | | | 12.1 | (83) | 13.1 | (90.2) | 32.1 | 3.2 | (22.3) |
| | | | 0.1 | | | 11.1 | (76) | 13.6 | (93.5) | 25.3 | 3.9 | (27.0) |
| | | | | | *avg.* | *11.6* | (80) | *13.3* | (91.8) | *28.7* | *3.6* | (24.7) |
| | | | 1 | | | 14.6 | (101) | 16.7 | (115.4) | 28.2 | 3.2 | (22.1) |
| | | | | | | 14.6 | (100) | 16.5 | (113.4) | 29.1 | 5.2 | (36.1) |
| | | | | | | 16.5 | (113) | 17.4 | (119.8) | 27.4 | 3.8 | (26.1) |
| | | | | | *avg.* | *15.2* | (105) | *16.9* | (116.2) | *28.2* | *4.1* | (28.1) |
| | | | 5 | | | *** | *** | 24.5 | (169.1) | 49.6 | *** | *** |
| | | | | | | *** | *** | 17.7 | (121.7) | 26.2 | *** | *** |
| | | | | | | *** | *** | 18.4 | (126.6) | 26.8 | *** | *** |
| | | | | | *avg.* | *** | *** | *20.18* | (139.1) | *26.52* | *** | *** |

**** data not attainable*

## Table A-6 Effect of Short-Term (20 h) Thermal Exposure on Room Temperature Compression Properties of FVS812 Alloys

| Alloy | Exposure | Direction | | 0.2 % Yield Strength | | Modulus | |
|---|---|---|---|---|---|---|---|
| | | | | ksi | (MPa) | 10^6 psi | (GPa) |
| Lot 115 | As-received | L | | 45.4 | (313) | 11.3 | (77.9) |
| (20 h Degas) | | | | 45.2 | (312) | 11.5 | (79.3) |
| | | | *avg.* | *45.3* | *(312)* | *11.4* | *(78.6)* |
| | | T | | 55.7 | *(384)* | 12.6 | *(86.9)* |
| | | | | 52.4 | *(361)* | 11.7 | *(80.7)* |
| | | | *avg.* | *54.1* | *(373)* | *12.2* | *(84.1)* |
| | 20h/300°C | L | | 51.3 | (354) | 11.4 | (78.6) |
| | | T | | 60.7 | (419) | 11.5 | (79.3) |
| | 20h/400°C | L | | 53.8 | (371) | 12.2 | (84.1) |
| | | T | | 62.2 | (429) | 12.3 | (84.8) |
| | 20h/500°C | L | | 52.7 | (363) | 12.3 | (84.8) |
| | | | | 52.8 | (364) | 12.1 | (83.4) |
| | | | *avg.* | *52.8* | (364) | *12.2* | (84.1) |
| | | T | | 60.2 | (415) | 12.4 | (85.5) |
| | | | | 59.2 | (408) | 12.5 | (86.2) |
| | | | *avg.* | *59.7* | (412) | *12.5* | (86.2) |
| Lot 96 | As-received | L | | 49.0 | (338) | 11.9 | (82.1) |
| (2 h Degas) | | | | 51.0 | (352) | 12.4 | (85.5) |
| | | | *avg.* | *50.0* | *(345)* | *12.2* | *(84.1)* |
| | | T | | 59.2 | (408) | 12.3 | (84.8) |
| | | | | 56.3 | (388) | 12.2 | (84.1) |
| | | | *avg.* | *57.8* | *(399)* | *12.3* | *(84.8)* |
| | 20h/300°C | L | | 53.6 | (370) | 11.9 | (82.1) |
| | | T | | 60.5 | (417) | 11.9 | (82.1) |
| | 20h/400°C | L | | 56.9 | (392) | 11.8 | (81.4) |
| | | T | | 60.7 | (419) | 11.9 | (82.1) |
| | 20h/500°C | L | | 54.8 | (378) | 12.2 | (84.1) |
| | | | | 55.9 | (385) | 11.7 | (80.7) |
| | | | *avg.* | *55.4* | (382) | *12.0* | (82.7) |
| | | T | | 62.1 | (428) | 12.3 | (84.8) |
| | | | | 61.0 | (421) | 12.5 | (86.2) |
| | | | *avg.* | *61.6* | (425) | *12.4* | (85.5) |

Strain Rate: 0.005 s-1, Test Temperature: 20°C (68°F)

**Table A-7 Effect of Short-term(20h) Thermal Exposure on Room Temperature Tensile Properties of FVS812**

| Alloy | Exposure | Direct. | Strain Rate | Test Temp. °C (°F) | | 0.2 % Yield Strength ksi | (MPa) | Ultimate Strength ksi | (MPa) | Elong. (%) | Modulus 10^6 psi | (GPa) |
|---|---|---|---|---|---|---|---|---|---|---|---|---|
| Lot 115 | 20h/300°C | L | 0.001 | 20 (68) | | 63.6 | (438) | 67.2 | (463.3) | 9.3 | 10.2 | (70.2) |
| (20 h Degas) | | | | | | 63.1 | (435) | 67.4 | (464.6) | 8.4 | 10.3 | (70.7) |
| | | | | | *avg.* | *63.4* | (437) | *67.3* | (464.0) | *8.8* | *10.2* | (70.5) |
| | | T | | | | 60.8 | (419) | 68.0 | (469.0) | 10.8 | 12.3 | (85.1) |
| | | | | | | 59.0 | (407) | 67.1 | (462.3) | 8.1 | 12.3 | (85.0) |
| | | | | | *avg.* | *59.9* | (413) | *67.5* | (465.7) | *9.4* | *12.3* | (85.1) |
| | 20h/400°C | L | | | | 58.8 | (405) | 66.7 | (459.8) | 12.7 | 11.9 | (82.1) |
| | | | | | | 60.0 | (414) | 66.6 | (459.2) | 11.6 | 11.4 | (78.5) |
| | | | | | *avg.* | *59.4* | (410) | *66.7* | (459.6) | *12.2* | *11.7* | (80.3) |
| | | T | | | | 60.1 | (415) | 67.2 | (463.3) | 9.5 | 12.1 | (83.2) |
| | | | | | | 59.1 | (407) | 67.1 | (462.6) | 10.2 | 11.8 | (81.3) |
| | | | | | *avg.* | *59.6* | (411) | *67.2* | (463.0) | *9.8* | *11.9* | (82.3) |
| | 20h/500°C | L | | | | 56.5 | (390) | 66.0 | (455.3) | 8.9 | 12.5 | (85.9) |
| | | | | | | 58.2 | (401) | 66.7 | (460.0) | 13.2 | 11.4 | (78.5) |
| | | | | | *avg.* | *57.4* | (395) | *66.4* | (457.7) | *11.0* | *11.9* | (82.2) |
| | | T | | | | 59.8 | (412) | 68.3 | (470.8) | 8.5 | 11.4 | (78.5) |
| | | | | | | 58.7 | (404) | 68.3 | (470.8) | 8.7 | 12.0 | (82.9) |
| | | | | | *avg.* | *59.2* | (408) | *68.3* | (470.8) | *8.6* | *11.7* | (80.7) |
| Lot 96 | 20h/300°C | L | 0.001 | 20 (68) | | 61.5 | (424) | 67.0 | (462.1) | 11.2 | 11.3 | (77.8) |
| (2 h Degas) | | | | | | 60.5 | (417) | 67.4 | (464.8) | 11.9 | 12.4 | (85.6) |
| | | | | | *avg.* | *61.0* | (421) | *67.2* | (463.5) | *11.6* | *11.9* | (81.7) |
| | | T | | | | 61.5 | (424) | 69.0 | (475.4) | 9.2 | 11.7 | (80.5) |
| | | | | | | 61.1 | (422) | 68.9 | (475.1) | 9.4 | 12.2 | (84.3) |
| | | | | | *avg.* | *61.3* | (423) | *68.9* | (475.3) | *9.3* | *12.0* | (82.4) |
| | 20h/400°C | L | | | | 60.2 | (415) | 67.0 | (461.9) | 14.4 | 12.3 | (84.9) |
| | | | | | | 59.7 | (412) | 66.8 | (460.5) | 11.0 | 11.9 | (81.8) |
| | | | | | *avg.* | *60.0* | (413) | *66.9* | (461.2) | *12.7* | *12.1* | (83.4) |
| | | T | | | | 61.8 | (426) | 69.0 | (476.0) | 8.6 | 11.6 | (79.9) |
| | | | | | | 60.7 | (418) | 68.8 | (474.4) | 9.5 | 12.4 | (85.2) |
| | | | | | *avg.* | *61.3* | (422) | *68.9* | (475.2) | *9.0* | *12.0* | (82.6) |
| | 20h/500°C | L | | | | 58.1 | (400) | 66.4 | (457.7) | 6.3 | 12.1 | (83.3) |
| | | | | | | 59.2 | (408) | 67.0 | (461.8) | 7.2 | 11.6 | (79.7) |
| | | | | | *avg.* | *58.6* | (404) | *66.7* | (459.8) | *6.8* | *11.8* | (81.5) |
| | | T | | | | 59.2 | (408) | 68.6 | (473.1) | 7.0 | 12.3 | (84.9) |
| | | | | | | 60.6 | (418) | 69.7 | (480.4) | 7.6 | 12.1 | (83.5) |
| | | | | | *avg.* | *59.9* | (413) | *69.2* | (476.8) | *7.3* | *12.2* | (84.2) |

## Table A-8 Kahn Tear Test Results for FVS812 Alloy (Lot 115, 20 h Degas)

| Alloy | Exposure | Direction | | Tear Stress | | Yield Stress | | TS/YS | Initiation Energy | | Propagation Energy | | Total Energy | | Unit Propagation Energy (UPE) | |
|---|---|---|---|---|---|---|---|---|---|---|---|---|---|---|---|---|
| | | | | ksi | (MPa) | ksi | (MPa) | ratio | in.-lb | (J) | in.-lb | (J) | in.-lb | (J) | in-lb/in^2 | (kJ/mm^2) |
| Lot 115<br>(20 h Degas) | As-received | L-T | | 87.0 | (600) | | | | 37 | (4.2) | 85 | (9.6) | 122 | (13.8) | 1375 | (241) |
| | | | | 86.7 | (598) | | | | 36 | (4.0) | 81 | (9.1) | 117 | (13.2) | 1306 | (228) |
| | | | *avg.* | *86.8* | *(599)* | *61.8* | *(426)* | *1.40* | *36* | *(4.1)* | *83* | *(9.4)* | *119* | *(13.5)* | *1340* | *(235)* |
| | | T-L | | 86.6 | (597) | | | | 36 | (4.0) | 61 | (6.9) | 97 | (10.9) | 983 | (172) |
| | | | | 86.3 | (595) | | | | 30 | (3.4) | 66 | (7.5) | 96 | (10.8) | 1065 | (186) |
| | | | *avg.* | *86.5* | *(596)* | *59.6* | *(411)* | *1.45* | *33* | *(3.7)* | *63* | *(7.2)* | *96* | *(10.9)* | *1024* | *(179)* |
| | 100h/200°C | L-T | | 88.7 | (612) | | | | 34 | (3.9) | 83 | (9.4) | 117 | (13.3) | 1336 | (234) |
| | | | | 87.0 | (600) | | | | 34 | (3.8) | 78 | (8.8) | 112 | (12.6) | 1256 | (220) |
| | | | *avg.* | *87.9* | *(606)* | *64.4* | *(444)* | *1.36* | *34* | *(3.9)* | *80* | *(9.1)* | *115* | *(12.9)* | *1296* | *(227)* |
| | | T-L | | 86.6 | (597) | | | | 29 | (3.3) | 57 | (6.5) | 87 | (9.8) | 923 | (162) |
| | | | | 85.0 | (586) | | | | 27 | (3.1) | 56 | (6.3) | 83 | (9.4) | 899 | (157) |
| | | | *avg.* | *85.8* | *(592)* | *65.3* | *(450)* | *1.31* | *28* | *(3.2)* | *56* | *(6.4)* | *85* | *(9.6)* | *911* | *(159)* |
| | 100h/315°C | L-T | | 88.5 | (610) | | | | 33 | (3.7) | 75 | (8.5) | 108 | (12.2) | 1217 | (213) |
| | | | | 89.2 | (615) | | | | 34 | (3.9) | 75 | (8.5) | 110 | (12.4) | 1216 | (213) |
| | | | *avg.* | *88.8* | *(613)* | *62.9* | *(434)* | *1.41* | *33* | *(3.8)* | *75* | *(8.5)* | *109* | *(12.3)* | *1216* | *(213)* |
| | | T-L | | 84.5 | (582) | | | | 25 | (2.9) | 51 | (5.8) | 77 | (8.7) | 827 | (145) |
| | | | *avg.* | *84.5* | *(582)* | *63.1* | *(435)* | *1.34* | *25* | *(2.9)* | *51* | *(5.8)* | *77* | *(8.7)* | *827* | *(145)* |
| | 1000h/200°C | L-T | | 86.1 | (594) | | | | 33 | (3.8) | 76 | (8.5) | 109 | (12.3) | 1218 | (213) |
| | | | | 84.5 | (582) | | | | 31 | (3.5) | 77 | (8.8) | 109 | (12.3) | 1250 | (219) |
| | | | *avg.* | *85.3* | *(588)* | *62.5* | *(431)* | *1.36* | *32* | *(3.6)* | *76* | *(8.6)* | *109* | *(12.3)* | *1234* | *(216)* |
| | | T-L | | 86.4 | (596) | | | | 26 | (3.0) | 64 | (7.2) | 90 | (10.1) | 1026 | (180) |
| | | | | 85.8 | (592) | | | | 28 | (3.1) | 57 | (6.4) | 85 | (9.6) | 918 | (161) |
| | | | *avg.* | *86.1* | *(594)* | *59.5* | *(410)* | *1.45* | *27* | *(3.0)* | *60* | *(6.8)* | *87* | *(9.9)* | *972* | *(170)* |
| | 1000h/315°C | L-T | | 85.9 | (592) | | | | 29 | (3.3) | 82 | (9.3) | 111 | (12.6) | 1324 | (232) |
| | | | | 86.5 | (596) | | | | 32 | (3.6) | 81 | (9.2) | 113 | (12.7) | 1308 | (229) |
| | | | *avg.* | *86.2* | *(594)* | *62.6* | *(431)* | *1.38* | *30* | *(3.4)* | *82* | *(9.2)* | *112* | *(12.7)* | *1316* | *(230)* |
| | | T-L | | 85.0 | (586) | | | | 24 | (2.8) | 59 | (6.7) | 84 | (9.5) | 955 | (167) |
| | | | | 83.1 | (573) | | | | 26 | (2.9) | 52 | (5.9) | 78 | (8.8) | 844 | (148) |
| | | | *avg.* | *84.0* | *(579)* | *58.8* | *(405)* | *1.43* | *25* | *(2.8)* | *56* | *(6.3)* | *81* | *(9.1)* | *900* | *(157)* |

## Table A-9 Kahn Tear Test Results for FVS812 Alloy (Lot 96, 2 h Degas)

| Alloy | Exposure | Direction | | Tear Stress | | Yield Stress | | TS/YS | Initiation Energy | | Propagation Energy | | Total Energy | | Unit Propagation Energy (UPE) | |
|---|---|---|---|---|---|---|---|---|---|---|---|---|---|---|---|---|
| | | | | ksi | (MPa) | ksi | (MPa) | ratio | in.-lb | (J) | in.-lb | (J) | in.-lb | (J) | in-lb/in^2 | (kJ/mm^2) |
| Lot 96 | As-received | L-T | | 89.2 | (615) | | | | 36 | (4.1) | 97 | (11.0) | 134 | (15.1) | 1483 | (260) |
| (2 h Degas) | | | | 89.3 | (616) | | | | 37 | (4.2) | 88 | (10.0) | 126 | (14.2) | 1349 | (236) |
| | | | *avg.* | *89.3* | *(615)* | *65.5* | *(451)* | *1.36* | *37* | *(4.2)* | *93* | *(10.5)* | *130* | *(14.6)* | *1416* | *(248)* |
| | | T-L | | 89.8 | (619) | | | | 38 | (4.3) | 77 | (8.7) | 115 | (13.0) | 1175 | (206) |
| | | | | 86.1 | (594) | | | | 27 | (3.1) | 79 | (8.9) | 106 | (12.0) | 1205 | (211) |
| | | | *avg.* | *88.0* | *(607)* | *61.6* | *(425)* | *1.43* | *33* | *(3.7)* | *78* | *(8.8)* | *111* | *(12.5)* | *1190* | *(208)* |
| | 100h/200°C | L-T | | 88.2 | (608) | | | | 31 | (3.5) | 86 | (9.7) | 117 | (13.2) | 1308 | (229) |
| | | | | 88.2 | (608) | | | | 33 | (3.8) | 81 | (9.2) | 114 | (12.9) | 1240 | (217) |
| | | | *avg.* | *88.2* | *(608)* | *66.2* | *(456)* | *1.33* | *32* | *(3.6)* | *83* | *(9.4)* | *115* | *(13.0)* | *1274* | *(223)* |
| | | T-L | | 87.6 | (604) | | | | 28 | (3.2) | 62 | (7.1) | 91 | (10.3) | 954 | (167) |
| | | | | 84.6 | (584) | | | | 27 | (3.1) | 59 | (6.7) | 86 | (9.8) | 905 | (158) |
| | | | *avg.* | *86.1* | *(594)* | *63.1* | *(435)* | *1.37* | *28* | *(3.1)* | *61* | *(6.9)* | *89* | *(10.0)* | *930* | *(163)* |
| | 100h/315°C | L-T | | 85.0 | (586) | | | | 27 | (3.0) | 91 | (10.2) | 117 | (13.3) | 1382 | (242) |
| | | | | 85.4 | (589) | | | | 24 | (2.8) | 94 | (10.7) | 119 | (13.4) | 1439 | (252) |
| | | | *avg.* | *85.2* | *(588)* | *65.8* | *(453)* | *1.30* | *26* | *(2.9)* | *92* | *(10.4)* | *118* | *(13.3)* | *1410* | *(247)* |
| | | T-L | | 88.5 | (610) | | | | 30 | (3.4) | 63 | (7.1) | 93 | (10.5) | 959 | (168) |
| | | | | 81.2 | (560) | | | | 22 | (2.5) | 65 | (7.3) | 87 | (9.8) | 990 | (173) |
| | | | *avg.* | *84.8* | *(585)* | *64.8* | *(447)* | *1.31* | *26* | *(2.9)* | *64* | *(7.2)* | *90* | *(10.1)* | *975* | *(171)* |
| | 1000h/200°C | L-T | | 88.9 | (613) | | | | 36 | (4.1) | 80 | (9.0) | 116 | (13.1) | 1218 | (213) |
| | | | | 87.6 | (604) | | | | 36 | (4.1) | 80 | (9.1) | 116 | (13.2) | 1224 | (214) |
| | | | *avg.* | *88.2* | *(608)* | *62.6* | *(432)* | *1.41* | *36* | *(4.1)* | *80* | *(9.0)* | *116* | *(13.1)* | *1221* | *(214)* |
| | | T-L | | 87.9 | (606) | | | | 33 | (3.8) | 63 | (7.1) | 96 | (10.8) | 955 | (167) |
| | | | | 82.1 | (566) | | | | 25 | (2.9) | 65 | (7.4) | 91 | (10.2) | 995 | (174) |
| | | | *avg.* | *85.0* | *(586)* | *61.2* | *(422)* | *1.39* | *29* | *(3.3)* | *64* | *(7.2)* | *93* | *(10.5)* | *975* | *(171)* |
| | 1000h/315°C | L-T | | 84.0 | (579) | | | | 31 | (3.5) | 84 | (9.5) | 115 | (13.0) | 1285 | (225) |
| | | | | 90.3 | (622) | | | | 40 | (4.5) | 89 | (10.1) | 129 | (14.6) | 1359 | (238) |
| | | | *avg.* | *87.1* | *(601)* | *62.2* | *(429)* | *1.40* | *35* | *(4.0)* | *87* | *(9.8)* | *122* | *(13.8)* | *1322* | *(231)* |
| | | T-L | | 78.2 | (539) | | | | 21 | (2.3) | 60 | (6.8) | 81 | (9.1) | 915 | (160) |
| | | | | 85.8 | (592) | | | | 33 | (3.7) | 60 | (6.8) | 93 | (10.5) | 917 | (160) |
| | | | *avg.* | *82.0* | *(565)* | *63.6* | *(439)* | *1.29* | *27* | *(3.0)* | *60* | *(6.8)* | *87* | *(9.8)* | *916* | *(160)* |

## Table A-10 Kahn Tear Test Results for 2024-T81 and 2219-T62 Aluminum Alloy

| Alloy | Exposure | Direction | | Tear Stress | | Yield Stress | | TS/YS | Initiation Energy | | Propagation Energy | | Total Energy | | Unit Propagation Energy (UPE) | |
|---|---|---|---|---|---|---|---|---|---|---|---|---|---|---|---|---|
| | | | | ksi | (MPa) | ksi | (MPa) | ratio | in.-lb | (J) | in.-lb | (J) | in.-lb | (J) | in-lb/in^2 | (kJ/mm^2) |
| 2024-T81 | As-received | L-T | | 63.3 | (436) | | | | 8 | (0.9) | 10 | (1.1) | 17 | (2.0) | 151 | (26) |
| | | | | 69.9 | (482) | | | | 14 | (1.6) | 12 | (1.3) | 25 | (2.9) | 181 | (32) |
| | | | | 63.9 | (440) | | | | 10 | (1.1) | 9 | (1.0) | 19 | (2.1) | 134 | (23) |
| | | | | 65.3 | (450) | | | | 9 | (1.0) | 10 | (1.1) | 19 | (2.1) | 153 | (27) |
| | | | *avg.* | *65.6* | *(452)* | *67.6* | *(466)* | *0.97* | *10* | *(1.2)* | *10* | *(1.1)* | *20* | *(2.3)* | *155* | *(27)* |
| | 100h/200°C | L-T | | 65.6 | (452) | | | | 13 | (1.5) | 28 | (3.2) | 41 | (4.7) | 441 | (77) |
| | | | | 63.8 | (440) | | | | 13 | (1.5) | 13 | (1.4) | 26 | (2.9) | 197 | (35) |
| | | | | 62.2 | (429) | | | | 10 | (1.1) | 16 | (1.8) | 26 | (2.9) | 249 | (44) |
| | | | *avg.* | *63.9* | *(440)* | *52.3* | *(361)* | *1.22* | *12* | *(1.4)* | *19* | *(2.1)* | *31* | *(3.5)* | *295* | *(52)* |
| | 100h/315°C | L-T | | 38.4 | (265) | | | | 15 | (1.7) | 52 | (5.9) | 67 | (7.6) | 809 | (142) |
| | | | | 38.3 | (264) | | | | 15 | (1.7) | 45 | (5.1) | 60 | (6.8) | 702 | (123) |
| | | | | 37.1 | (256) | | | | 14 | (1.5) | 49 | (5.5) | 62 | (7.1) | 765 | (134) |
| | | | | 38.0 | (262) | | | | 14 | (1.5) | 36 | (4.0) | 49 | (5.6) | 556 | (97) |
| | | | *avg.* | *37.9* | (262) | *19.2* | *(132)* | *1.98* | *14* | *(1.6)* | *45* | *(5.1)* | *60* | *(6.7)* | *708* | *(124)* |
| 2219-T62 | As-received | L-T | | 62.9 | (434) | | | | 12 | (1.4) | 19 | (2.1) | 31 | (3.5) | 291 | (51) |
| | | | | 57.2 | (394) | | | | 12 | (1.4) | 16 | (1.8) | 28 | (3.2) | 253 | (44) |
| | | | *avg.* | *60.1* | *(414)* | *38.7* | *(267)* | *1.6* | *12* | *(1.4)* | *17* | *(1.9)* | *30.0* | *(3.4)* | *266* | *(46)* |
| | 100h/200°C | L-T | | 58.0 | (400) | | | | 12 | (1.4) | 18 | (2.1) | 31 | (3.4) | 286 | (50) |
| | | | | 57.6 | (397) | | | | 12 | (1.3) | 19 | (2.1) | 31 | (3.4) | 291 | (51) |
| | | | *avg.* | *57.8* | *(399)* | *35.2* | *(243)* | *1.64* | *12* | *(1.4)* | *19* | *(2.1)* | *31* | *(3.4)* | *289* | *(51)* |
| | 100h/315°C | L-T | | 54.2 | (374) | | | | 16 | (1.9) | 26 | (2.9) | 42 | (4.7) | 398 | (70) |
| | | | | 53.5 | (369) | | | | 18 | (2.0) | 27 | (3.0) | 45 | (5.0) | 420 | (74) |
| | | | *avg.* | *53.8* | *(371)* | *23.8* | *(164)* | *2.26* | *17* | *(1.9)* | *26* | *(3.0)* | *43* | *(4.9)* | *409* | *(72)* |

## Table A-11 Fatigue Results for FVS812 Alloy (Lot 96, 2 h Degas)

| Sample ID | Load Dir. | Exposure Cond. | Test Temp. °C | (°F) | Max. Test Stress ksi | MPa | Cycles to Failure |
|---|---|---|---|---|---|---|---|
| NF-5f | L | As-received. | 21 | (70) | 60.4 | 416.5 | 11,288 |
| NF-5g | | | | | 60.4 | 416.5 | 10,945 |
| NF-5h | | | | | 60.3 | 415.7 | 10,571 |
| NF-6e | | | | | 55.3 | 381.6 | 21,795 |
| NF-6f | | | | | 55.3 | 381.6 | 16,652 |
| NF-7a | | | | | 50.4 | 347.2 | 29,500 (1) |
| NF-7b | | | | | 50.4 | 347.2 | 44,530 |
| NF-33a | | | | | 45.3 | 312.4 | 32,437 |
| NF-34a | | | | | 40.3 | 277.7 | 3,664,968 |
| NF-34a2 | | | | | 40.3 | 277.7 | 266,630 |
| NF-35a | | | | | 35.2 | 243.0 | 9,562,400 |
| NF-17a | | | | | 30.2 | 208.3 | 1,487,010 (4) |
| NF-39a | | | | | 25.2 | 173.6 | 10,000,000 |
| NF-12a | L | 100h/315°C | 21 | (70) | 60.2 | 414.9 | 10,603 |
| NF-12b | | | | | 60.4 | 416.5 | 8,810 |
| NF-13a | | | | | 55.1 | 380.1 | 14,820 |
| NF-13b | | | | | 55.2 | 380.8 | 16,813 |
| NF-14a | | | | | 50.4 | 347.2 | 720 (2) |
| NF-14b | | | | | 50.4 | 347.2 | 17,430 |
| NF-36a | | | | | 45.3 | 312.4 | 35,090 |
| NF-37a | | | | | 40.3 | 277.7 | 70,223 |
| NF-38a | | | | | 35.2 | 243.0 | 779,709 |
| NF-18a | | | | | 30.2 | 208.3 | 13,607,800 |
| NF-5c | T | As-received. | 21 | (70) | 60.3 | 415.7 | 11,530 |
| NF-5d | | | | | 60.5 | 417.4 | 10,484 |
| NF-6c | | | | | 55.3 | 381.6 | 18,899 |
| NF-6d | | | | | 55.5 | 382.4 | 15,914 |
| NF-7c | | | | | 50.4 | 347.2 | 21,960 |
| NF-7d | | | | | 50.4 | 347.2 | 31,070 |
| NF-33b | | | | | 45.3 | 312.4 | 44,431 |
| NF-34b | | | | | 40.3 | 277.7 | 164,940 |
| NF-35b | | | | | 35.2 | 243.0 | 27,130 (6) |
| NF-17b | | | | | 30.2 | 208.3 | (7) |
| NF-17c | | | | | 30.2 | 208.3 | 323,880 |
| NF-39b | | | | | 25.2 | 173.6 | 10,000,000 |
| NF-12c | T | 100h/315°C | 21 | (70) | 60.5 | 417.4 | 8,682 |
| NF-12d | | | | | 60.4 | 416.5 | 11,947 |
| NF-13c | | | | | 55.3 | 381.6 | 16,464 |
| NF-13d | | | | | 55.5 | 382.4 | 15,935 |
| NF-14c | | | | | 50.4 | 347.2 | 22,160 |
| NF-14d | | | | | 50.4 | 347.2 | 19,070 |
| NF-36b | | | | | 45.3 | 312.4 | 38,428 |
| NF-37b | | | | | 40.3 | 277.7 | 289,010 |
| NF-38b | | | | | 35.2 | 243.0 | 3,690,069 (8) |
| NF-18b | | | | | 30.2 | 208.3 | 5,235,900 |

*continued on next page*

## Table A-11 concluded

| Sample ID | Load Dir. | Exposure Cond. | Test Temp. °C | (°F) | Max. Test Stress ksi | MPa | Cycles to Failure |
|---|---|---|---|---|---|---|---|
| NFT-16 | L | As-received. | 200 | (392) | 50.3 | 346.8 | 19,945 |
| NFT-15 | | | | | 40.4 | 278.6 | 55,320 |
| NFT-14 | | | | | 30.1 | 207.5 | 122,084 |
| NFT-19 | T | As-received. | 315 | (600) | 35.2 | 242.7 | 12,430 |
| NFT-17 | | | | | 25.0 | 172.4 | 204,622 |

(1) counter did not stop when specimen failed;
discovered at 29500
(2) machine overload
(3) premature failure due to inclusion repeated with NF-15b
(4) grip failure @ 891,500 cycles; re-gripped
w/fiberglass shims & re-run
(5) grip failure; specimen buckled when re-installed
replaced with spec. NF-15c
(6) bad test; bent specimen
(7) specimen buckled on setup; replaced with NF-17c
(8) grip failure
(9) test stopped
Note: Act. stress accounts for rounding of edges
due to polishing

## Table A-12 Fatigue Results for FVS812 Alloy (Lot 115, 20 h Degas)

| Sample | Load | Exposure | Test | Temp. | Max. Test Stress | | Cycles to |
|---|---|---|---|---|---|---|---|
| ID | Dir. | Cond. | °C | °F | ksi | MPa | Failure |
| NF-1a | L | As-received | 21 | (70) | 64.4 | 444.1 | 1,225 |
| NF-1b | | | | | 63.4 | 436.8 | 1,363 |
| NF-2a | | | | | 57.1 | 393.8 | 11,455 |
| NF-2b | | | | | 57.1 | 393.8 | 9,763 |
| NF-3a | | | | | 50.4 | 347.2 | 38,800 |
| NF-3b | | | | | 50.4 | 347.2 | 26,360 |
| NF-4a | | | | | 45.3 | 312.4 | 72,760 |
| NF-4b | | | | | 45.3 | 312.4 | 44,130 |
| NF-4e | | | | | 45.3 | 312.4 | 205,006 |
| NF-30a | | | | | 40.3 | 277.7 | 186,938 |
| NF-16a | | | | | 35.2 | 243.0 | 580,000 |
| NF-15a | | | | | 30.2 | 208.3 | 321,000 (3) |
| NF-15b | | | | | 30.2 | 208.3 | 209,720(5) |
| NF-15c | | | | | 30.2 | 208.3 | 10,000,000 |
| NF-8a | L | 100h/315°C(600°F) | 21 | (70) | 63.1 | 435.1 | 1,582 |
| NF-8b | | | | | 63.2 | 436.0 | 1,709 |
| NF-9a | | | | | 58.0 | 400.2 | 13,453 |
| NF-9b | | | | | 57.9 | 399.4 | 13,599 |
| NF-10a | | | | | 50.4 | 347.2 | 16,200 |
| NF-10b | | | | | 50.4 | 347.2 | 29,390 |
| NF-11a | | | | | 45.3 | 312.4 | 31,410 |
| NF-11b | | | | | 45.3 | 312.4 | 51,590 |
| NF-31a | | | | | 40.3 | 277.7 | 345,586 |
| NF-32a | | | | | 35.2 | 243.0 | 901,600 |
| NF-19a | | | | | 30.2 | 208.3 | 10,000,300 |
| NF-1c | T | As-received | 21 | (70) | 64.3 | 443.2 | 6,492 |
| NF-1d | | | | | 63.2 | 436.0 | 6,538 |
| NF-2c | | | | | 58.0 | 400.2 | 13,046 |
| NF-2d | | | | | 58.1 | 400.4 | 10,759 |
| NF-3c | | | | | 50.4 | 347.2 | 24,190 |
| NF-3d | | | | | 50.4 | 347.2 | 18,690 |
| NF-4c | | | | | 45.3 | 312.4 | 45,410 |
| NF-4d | | | | | 45.3 | 312.4 | 51,380 |
| NF-30b | | | | | 40.3 | 277.7 | 1,863,410(9) |
| NF-30b2 | | | | | 40.3 | 277.7 | 1,765,900(8) |
| NF-16b | | | | | 35.2 | 243.0 | 3,418,060 |
| NF-15d | | | | | 30.2 | 208.3 | 10,000,000 |

*continued on next page*

## Table A-12 concluded

| Sample ID | Load Dir. | Exposure Cond. | Test °C | Temp. °F | Max. Test Stress ksi | MPa | Cycles to Failure |
|---|---|---|---|---|---|---|---|
| NF-8c | T | 100h/315°C | 21 | (70) | 63.5 | 437.7 | 6,494 |
| NF-8d | | | | | 63.4 | 436.8 | 8,968 |
| NF-9c | | | | | 58.0 | 400.2 | 13,679 |
| NF-9d | | | | | 58.0 | 400.2 | 13,205 |
| NF-10c | | | | | 50.4 | 347.2 | 18,260 |
| NF-10d | | | | | 50.4 | 347.2 | 19,510 |
| NF-11c | | | | | 45.3 | 312.4 | 25,900 |
| NF-31b | | | | | 40.3 | 277.7 | 44,300 |
| NF-32b | | | | | 35.2 | 243.0 | 152,467 |
| NF-19b | | | | | 30.2 | 208.3 | 6,134,745 |
| NFT-22 | L | as-received | 200 | (392) | 50.2 | 346.1 | 9,912 |
| NFT-23 | | | | | 40.2 | 277.2 | 35,448 |
| NFT-24 | | | | | 30.0 | 206.9 | 210,764 |
| NFT-11 | T | as-received | 200 | (392) | 50.3 | 346.8 | 16,107 |
| NFT-20 | | | | | 45.1 | 311.0 | 16,406 |
| NFT-12 | | | | | 40.1 | 276.5 | 24,512 |
| NFT-13 | | | | | 30.2 | 208.2 | 138,140 |
| NFT-9 | L | as-received | 315 | (600) | 35.2 | 242.7 | 11,862 |
| NFT-7 | | | | | 30.2 | 208.2 | 99,302 |
| NFT-6 | | | | | 25.3 | 174.4 | 177,554 |
| NFT-10 | | | | | 25.0 | 172.4 | 236,758 |

(1) counter did not stop when specimen failed; discovered at 29500
(2) machine overload
(3) premature failure due to inclusion; repeated with NF-15b
(4) grip failure @ 891,500 cycles; re-gripped with w/fiberglass shims & re-run
(5) grip failure; specimen buckled when re-installed
replaced with spec. NF-15c
(6) bad test; bent specimen
(7) specimen buckled on setup; replaced with NF-17c
(8) grip failure
(9) test stopped
Note: Act. stress accounts for rounding of edges
due to polishing

## Table A-13 Fatigue Results for 2024-T81 Aluminum Alloy

| Sample ID | Load Dir. | Exposure Cond. | Test Temp. °C (°F) | Max. Stress ksi | Max. Stress MPa | Cycles to Failure | |
|---|---|---|---|---|---|---|---|
| NF-27a | L | As-received | 21 (70) | 65.5 | 451.3 | 9,559 | |
| NF-23a | | | | 60.4 | 416.6 | 22,285 | |
| NF-23b | | | | 60.4 | 416.6 | 24,816 | |
| NF-22a | | | | 55.4 | 381.9 | 21,914 | |
| NF-24a | | | | 50.4 | 347.2 | 51,719 | |
| NF-21a | | | | 45.3 | 312.4 | 80,920 | |
| NF-25a | | | | 40.3 | 277.7 | 110,523 | |
| NF-26a | | | | 35.2 | 243.0 | 209,000 | |
| NF-20a | | | | 30.2 | 208.3 | 9,038,469 | (a) |

(a) grip failure

THIS PAGE INTENTIONALLY LEFT BLANK

# APPENDIX B

# DETAILS OF ZEE-STIFFENED COMPRESSION PANELS

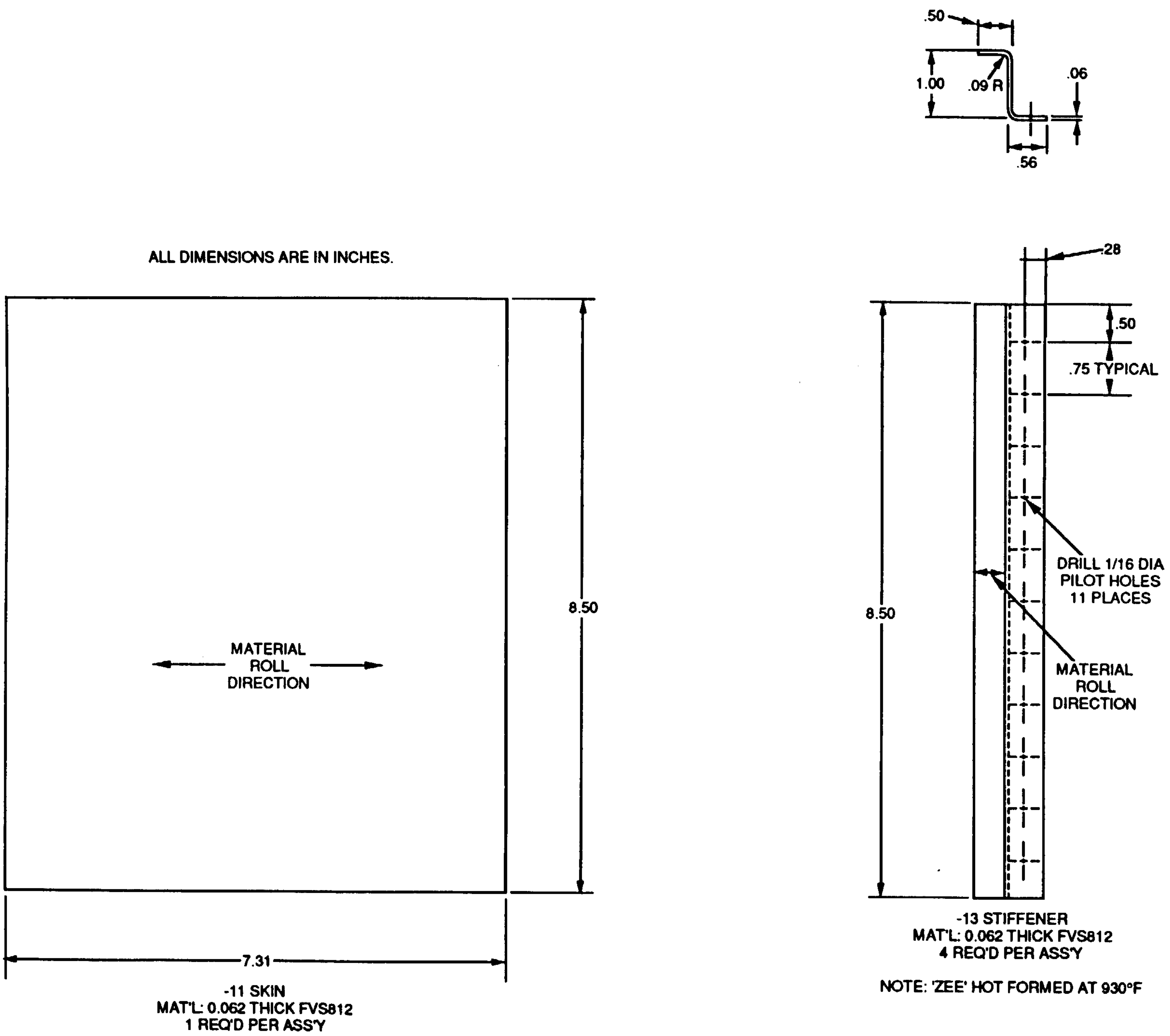

ALL DIMENSIONS ARE IN INCHES.

-11 SKIN
MAT'L: 0.062 THICK FVS812
1 REQ'D PER ASS'Y

-13 STIFFENER
MAT'L: 0.062 THICK FVS812
4 REQ'D PER ASS'Y

NOTE: 'ZEE' HOT FORMED AT 930°F

**Fig. B-1 FVS812 Aluminum Alloy Riveted Panel - Details (Dwg. TGP-1105)**

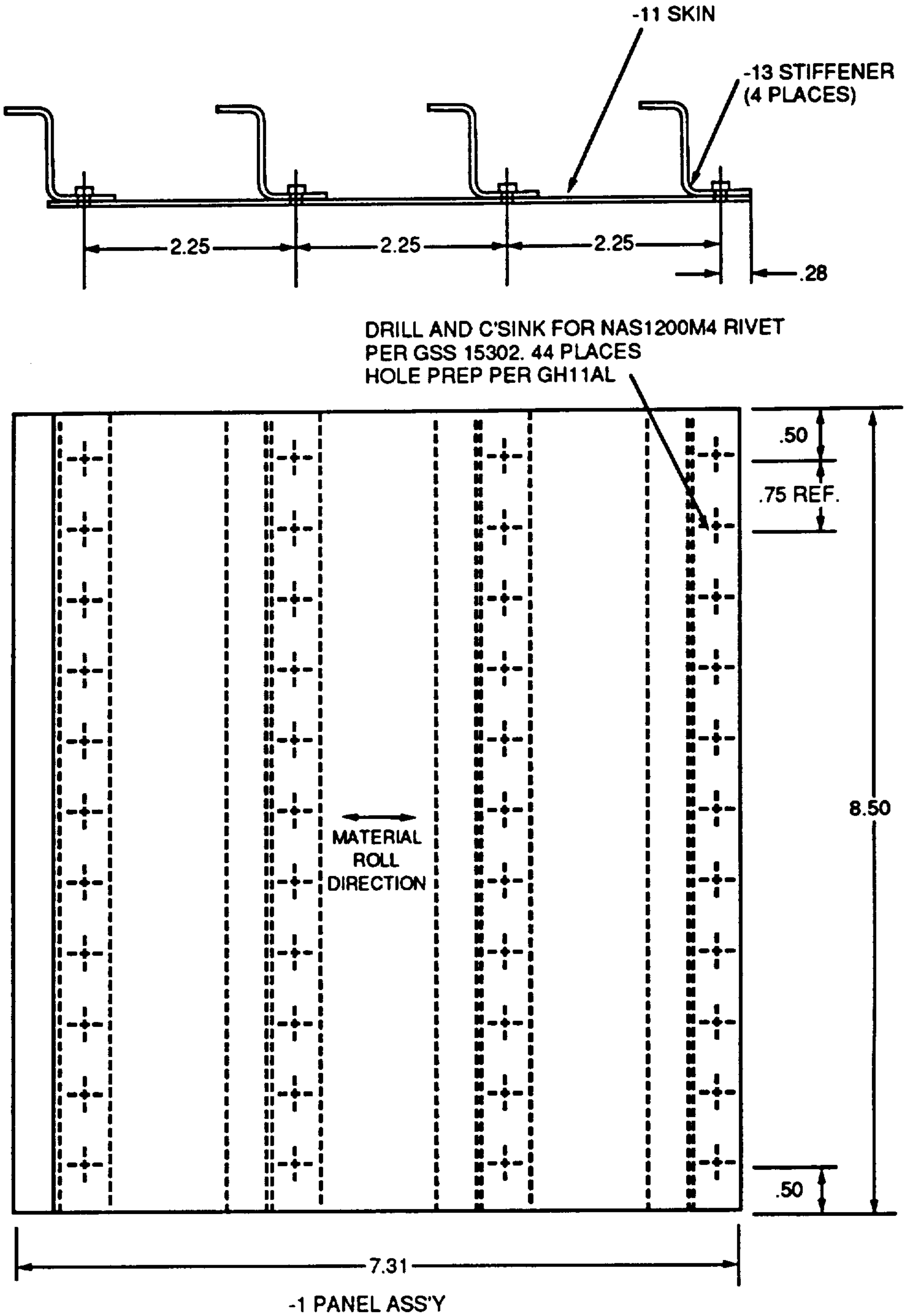

Fig. B-2 FVS812 Aluminum Alloy Rivets – Assy (Dwg. TGP-1105)

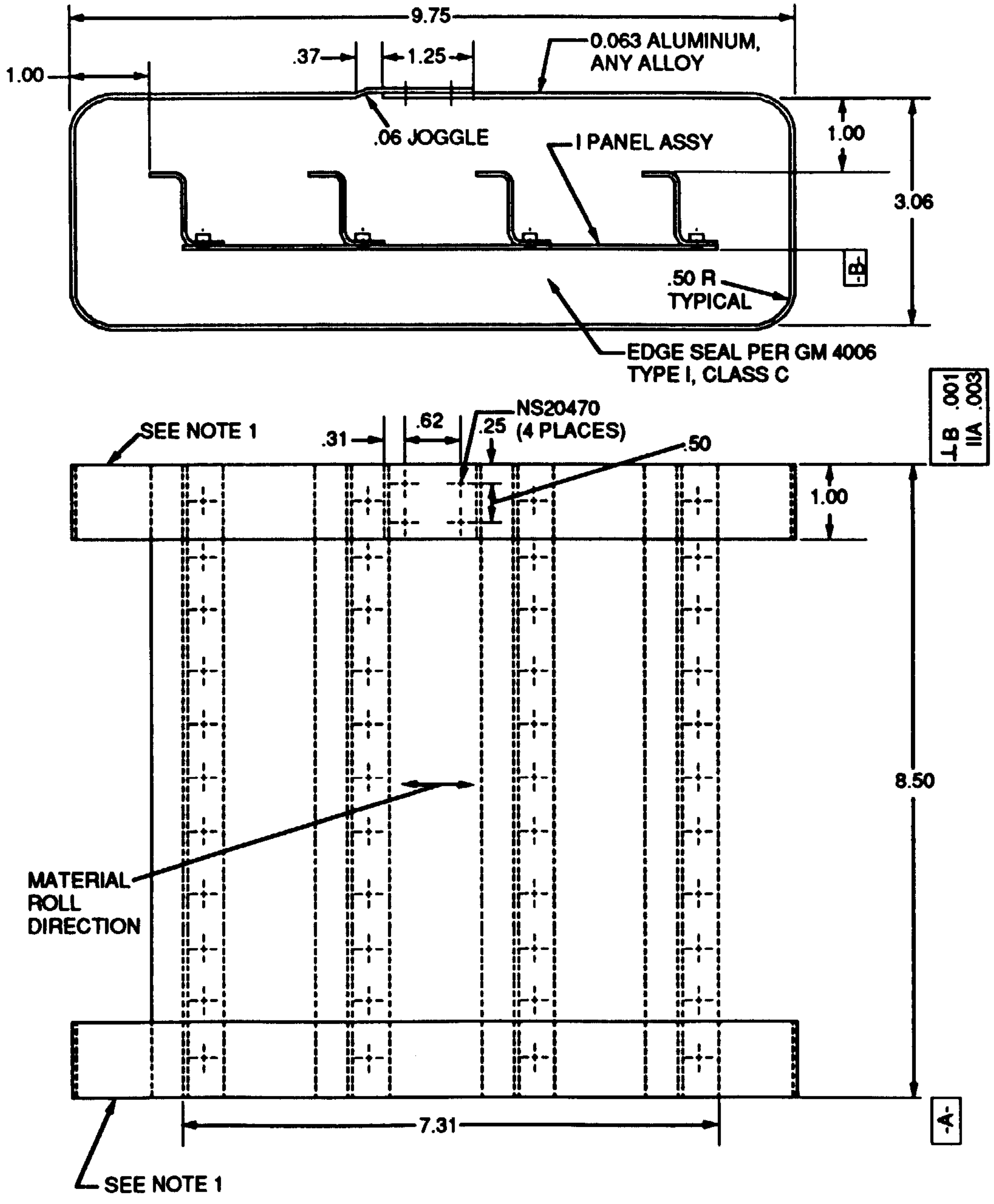

1) MACHINE EACH SURFACE TO ACHIEVE THE REQUIRED DIMENSION, PARALLELISM, AND PERPENDICULARITY. FULL CROSS SECTION OF -11 SKIN AND -13 STIFFENERS SHALL BE EXPOSED.

2) -11 SKIN AND -13 STIFFENERS SHALL NOT CONTAIN CRACKS, DENTS, OR OTHER IRREGULARITIES WHICH WOULD PROMOTE PREMATURE FAILURE DURING STATIC TESTING.

3) INSPECT ALL STIFFENERS AND SKINS:
   RECORD THICKNESS
   RECORD DIMENSIONS OF STIFFENERS

4) ALL DIMENSIONS ARE IN INCHES.

**Fig. B-3 FVS812 Aluminum Alloy Riveted Panel – End Potting (Dwg – TGP-1105)**

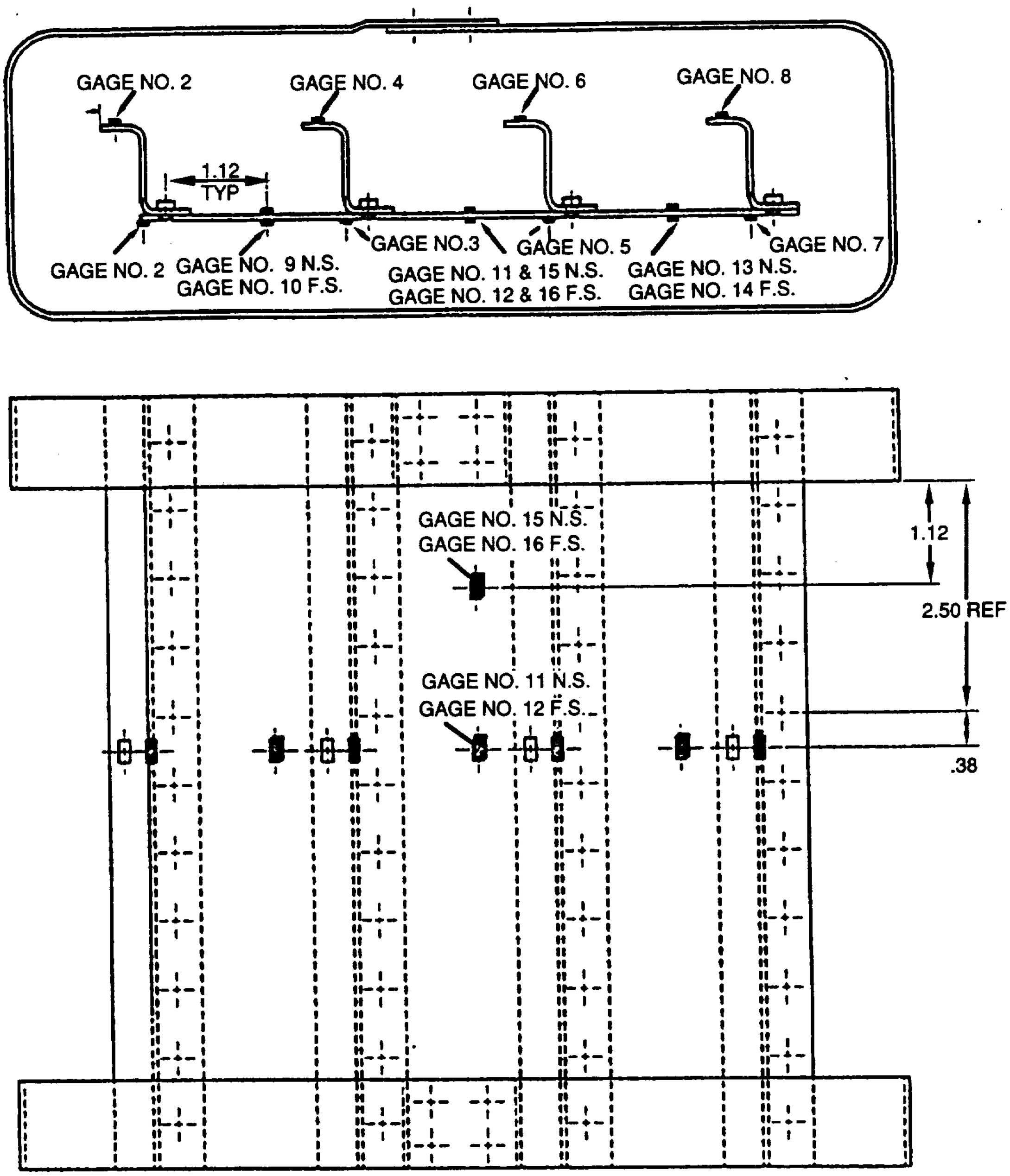

Fig. B-4 FVS 812 Aluminum Alloy Riveted Panel– Strain Gages

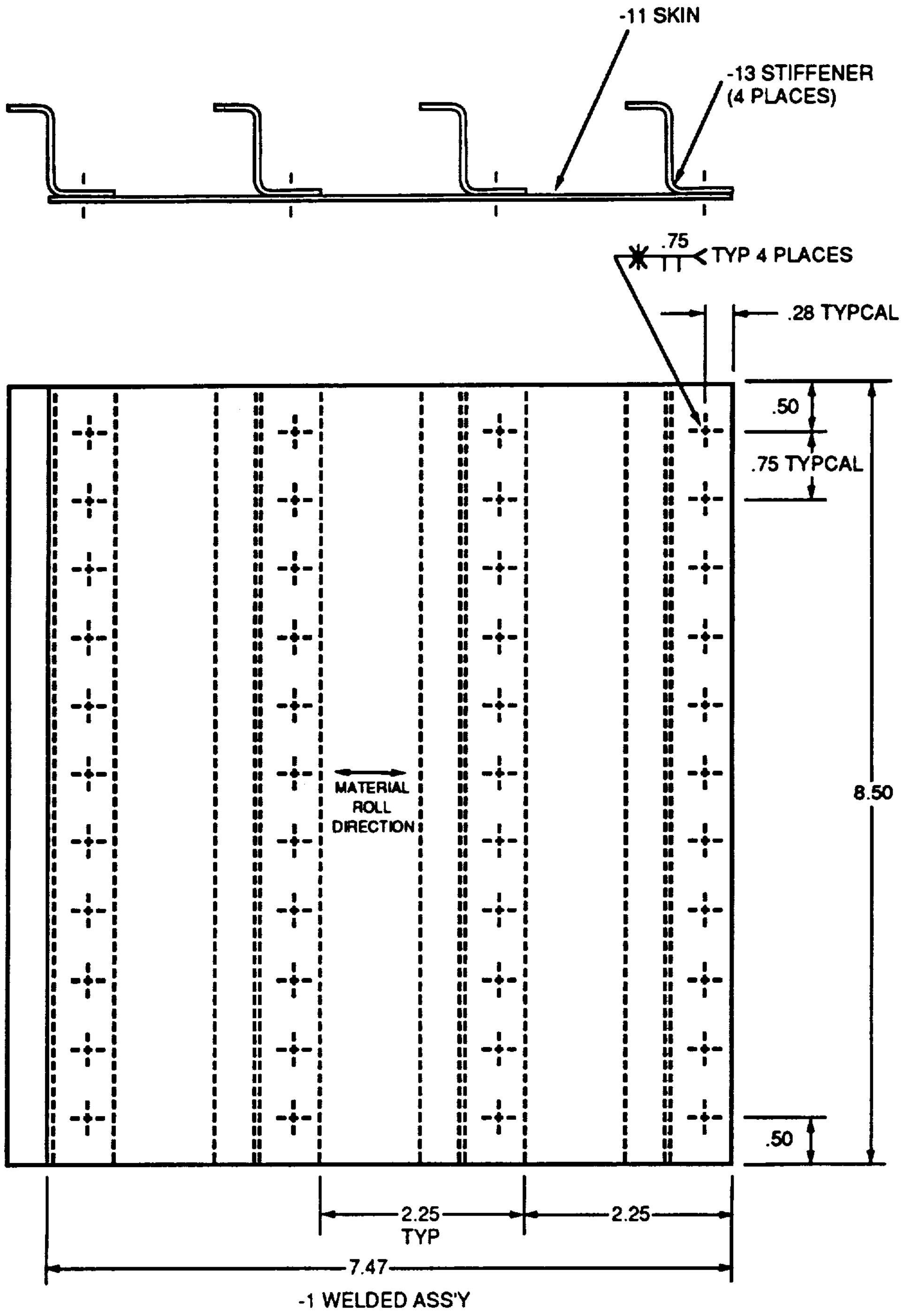

Fig. B-5 FVS812 Aluminum Alloy Spot-Welded Panel-Assy (Dwg. TGP-1106)

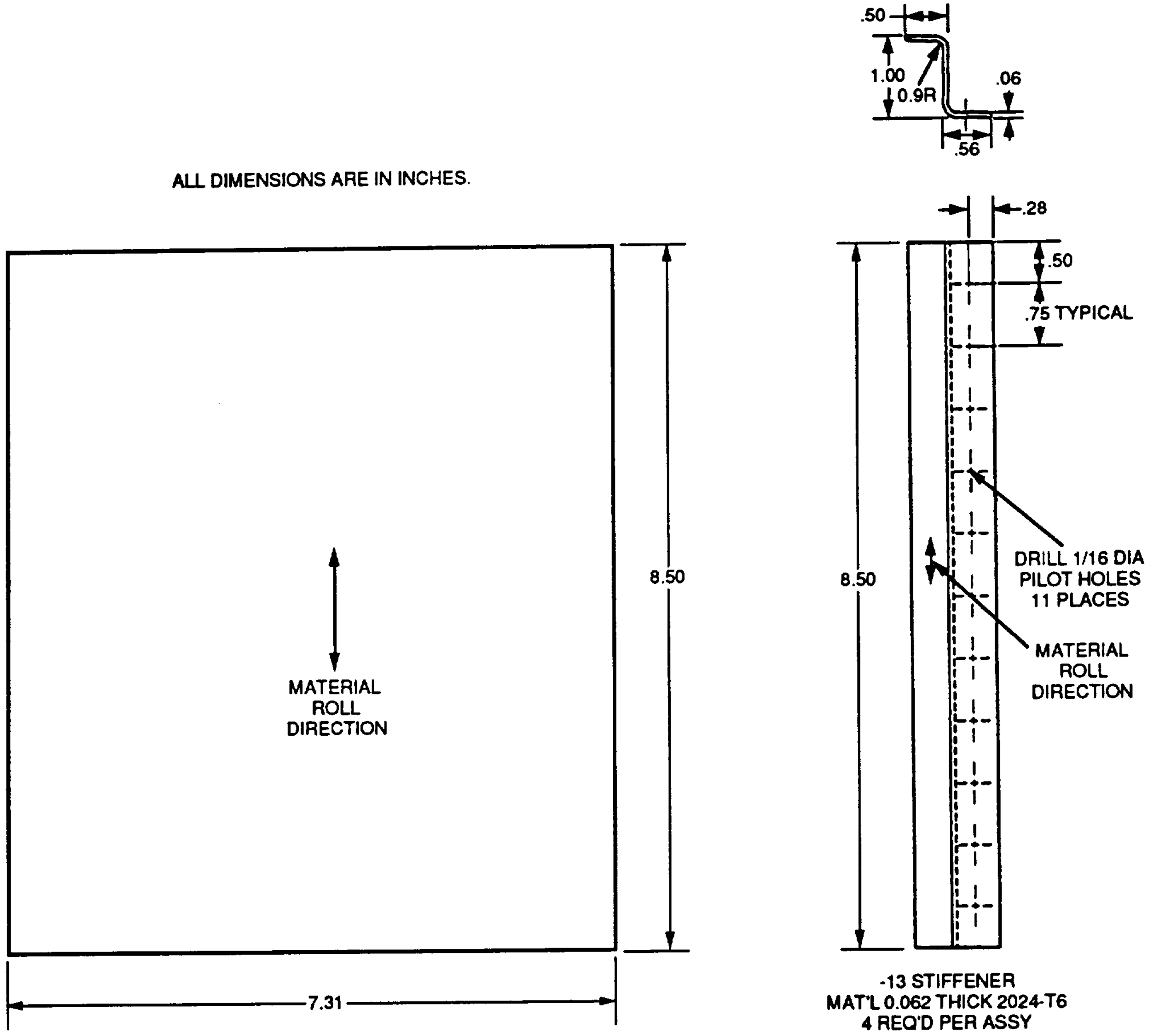

**Fig. B-6** 2024 Aluminum Alloy Riveted – Details (Dwg TGP-1104)

# Report Documentation Page

| | | |
|---|---|---|
| 1. Report No.<br>NASA CR-187575 | 2. Government Accession No. | 3. Recipient's Catalog No. |

| | |
|---|---|
| 4. Title and Subtitle<br>Effect of Thermal Exposure, Forming, and Welding on High-Temperature, Dispersion-Strengthened Aluminum Alloy: Al-8Fe-1V-2Si | 5. Report Date<br>August 1991 |
| | 6. Performing Organization Code |
| 7. Author(s)<br>J. R. Kennedy | 8. Performing Organization Report No.<br>RE- |
| | 10. Work Unit No.<br>505-63-50-02 |
| 9. Performing Organization Name and Address<br>Grumman Corporate Research Center<br>A02-26<br>Bethpage, NY, 11714 | 11. Contract or Grant No.<br>NAS1-18533 Extension |
| | 13. Type of Report and Period Covered<br>Contractor Report |
| 12. Sponsoring Agency Name and Address<br>National Aeronautics and Space Administration<br>Langley Research Center<br>Hampton, VA 23665-5225 | 14. Sponsoring Agency Code |

15. Supplementary Notes

Langley Technical Monitor: Dick Royster

Final Report Assistant Technical Monitor:

16. Abstract

The feasibility of applying conventional hot forming and welding methods to high-temperature aluminum alloy, Al-8Fe-1V-2Si (FVS812), for structural applications and the effect of thermal exposure on mechanical properties were determined. FVS812 (AA8009) sheet exhibited good hot forming and resistance welding characteristics. It was brake formed to 90° bends (0.5T bend radius) at temperatures ≥390°C (730°F), thus indicating the feasibility of fabricating basic shapes, such as angles and zees. Hot forming of simple contoured-flanged parts was demonstrated. Resistance spot welds with good static and fatigue strength at room and elevated temperatures were readily produced. Extended vacuum degassing during billet fabrication reduced porosity in fusion and resistance welds. However, electron beam welding was not possible because of extreme degassing during welding, and gas-tungsten-arc welds were not acceptable because of severely degraded mechanical properties. The FVS812 alloy exhibited excellent high-temperature strength stability after thermal exposures up to 315°C (600°F) for 1000 h. Extended billet degassing appeared to generally improve tensile ductility, fatigue strength, and notch toughness. But the effects of billet degassing and thermal exposure on properties need to be further clarified. The manufacture of zee-stiffened, riveted, and resistance-spot-welded compression panels was demonstrated.

| | |
|---|---|
| 17. Key Words (suggested by Author(s))<br>Dispersion Strengthened, Al-Fe-V-Si Alloys, Forming, Fusion Welding, Resistance Welding, Thermal Exposure | 18. Distribution Statement<br>Unclassified- Unlimited<br>Subject Category 26 |

| | | | |
|---|---|---|---|
| 19. Security Classif. (of this report)<br>Unclassified | 20. Security Classif. (of this page)<br>Unclassified | 21. No. of pages<br>138 | 22. Price |